Pulsed Fiber Lasers Employing Diverse Saturable Absorbers and Chirped Pulse Amplification Technique

Thesis submitted in partial fulfilment of the requirement for the Degree of Doctor of Philosophy (Ph.D.) in Science

by

Uttam Kumar Samanta

Index No.: 58/20/Phys./27

Registration No.: SOPHY1105820 dated 09.11.2020

Department of Physics
Jadavpur University
Kolkata, India – 700 032

2024

Certificate from the Supervisor

This is to certify that the thesis entitled **"Pulsed Fiber Lasers Employing Diverse Saturable Absorbers and Chirped Pulse Amplification Technique"** Submitted by **Uttam Kumar Samanta** who got his name registered on **09.11.2020** for the award of Ph. D. (Science) degree of Jadavpur University, is absolutely based upon his own work under the supervision of **Dr. Mukul Chandra Paul** and that neither this thesis nor any part of it has been submitted for either any degree / diploma or any other academic award anywhere before.

Mukul Chandra Paul 1.5.2021

Dr. Mukul Chandra Paul
मुख्य वैज्ञानिक / Chief Scientist
सीएसआईआर - केन्द्रीय कांच एवं सिरामिक अनुसंधान संस्थान
CSIR - CENTRAL GLASS & CERAMIC RESEARCH INSTITUTE
वैज्ञानिक तथा औध्योगिक अनुसंधान परिषद
Council of Scientific & Industrial Research
196, राजा एस. सी. मल्लिक रोड, कोलकाता- 700 032
196, Raja S.C. Mullick Road, Kolkata - 700 [illegible]

(Signature of the Supervisor(s) date with official seal)

Acknowledgements

I acknowledge CSIR-Central Glass and Ceramics Research Institute (CGCRI), Kolkata, the institute which afforded me an outstanding opportunity to advance my professional career and undertake Ph.D. research in the domains of ultrafast fiber lasers. The Fiber Optics and Photonics Division houses world-class facilities, facilitating cutting-edge advancements in fiber development. In addition to the research environment, CGCRI provided me the chance to discover my interests through participation in a variety of extracurricular activities, including sports, cultural events, and more. I express my heartfelt gratitude to the Director of CGCRI & the head of the Fiber Optics and Photonics Division for providing a dynamic research environment to us.

I am sincerely grateful to my former PhD supervisor, Late Dr. Mrinmay Pal who gave me the opportunity to be a part of his research team. I am immensely grateful to Dr. Mukul Chandra Paul, who welcomed me in his team following the unexpected passing of my previous mentor, and supported me consistently throughout my entire PhD journey. His comprehensive skill and calmness in challenging situation has taught me lot to navigate research complexities.

Alongside my supervisor, I am very much thankful to Dr. Atasi Pal, Dr. Debashri Ghosh and Dr. Anirban Dhar for their kind guidance to improve comprehensive skill and thoughtful discussions on various topics covering fiber fabrication to cutting-edge laser technologies. I am sincerely thankful to Dr. Sourav Das Chowdhury, who guided me in the field of ultrafast lasers and helped me to improve my manuscript writing skill and presentation skill. I am also grateful to Dr. Debasish Pal and Nishant Kumar Shekhar who provided their insightful thoughts to overcome several problems.

I extend my thankfulness to my fellow lab mates Shubhranil Maity, Vincent Akash Gomes, Sajib Chowdhury, Debparna Majumdar, Nilotpal Chowdhury, Aruna Ghosh, and Abdul Malek Mallick for their invaluable assistance during experiments, informative discussions on various topics, and for all the joyful moments we shared. I am also thankful to my long-time friends and roommates Sourav and Sumanta for their constant support in solving the challenges of daily life.

Finally, I am very much thankful to DST-INSPIRE, India for providing me the financial support (IF180796) throughout my tenure.

Uttam Kr. Samanta, 15/05/2024

Dedicated to my Parents, Rai & Mum

Thesis title: Pulsed Fiber Lasers Employing Diverse Saturable Absorbers and Chirped Pulse Amplification Technique

Index No: 58/20/Phys./27

Abstract

This thesis contains the performance of four distinct saturable absorbers to generate stable femtosecond pulse maintaining an all fiber configuration. Out of four, two are physical saturable absorbers (fiber saturable absorber (FSA) & semiconductor saturable absorbing mirror (SESAM)) and other two are artificial saturable absorbers (nonlinear amplifying loop mirror (NALM) & Mamyshev regenerator). During the experiment, depending on the dispersion map of the architecture several types of stable pulses are observed such as stable Q-switched, all normal dissipative soliton, dispersion managed dissipative soliton. Beside the stable solution, quasi-stable state like noise-like pulse (NLP), unequal multi-pulse states are also observed. Few states are diagnosed which are far away from stable region, contains extreme pulsation, in literature they are named chaotic states. All these states are captured and characterized in detail by performing dispersive Fourier transform (DFT), relative intensity noise (RIN). In case of NALM based laser, dual gain segment based figure-9 architecture is explored and a novel pulse dynamics of NLP is captured. A new architecture of Mamyshev oscillator is proposed where an all-fiber Lyot filter is utilized as one of the spectral filter. The efficiency of the proposed cavity is checked numerically by solving generalized non-linear Schrodinger equation (GNLSE). At the end, the output from most stable state is considered for amplification via chirped pulse amplification (CPA) technique. For this, two different architectures are implemented. The first setup is capable to deliver sub-300 fs pulses with 160 nJ of pulse energy. In the second architecture, the repetition rate is reduced by incorporating a pulse-picking setup. final It can deliver pulses of 2.2 μJ at 1.09 MHz of repetition rate.

List of acronyms

ANDi: All normal dispersion

AOM: Acuosto-optic modulator

ASE: Amplified spontaneous emission

Bi: Bismuth

BPF: Band pass filter

BW: Bandwidth

CBC: Coherent beam combination

CFBG: Chirped fiber Bragg grating

CMS: Cladding mode stripper

CNTs: Carbon nano tubes

CPA: Chirped pulse amplification

CQGLE: Cubic-quintic Ginzburg Landau equation

Cr: Chromium

CS: Conventional soliton

CW: Continuous wave

DFT: Dispersive Fourier transform

DMS: Dispersion managed soliton

DS: Dissipative soliton

DSR: Dissipative soliton resonance

EDFA: Erbium doped fiber amplifier

EFSA: Erbium fiber saturable absorber

EOM: Electro optic modulator

Er: Erbium

FBG: Fiber Bragg grating

FFT: Fast Fourier transform

FSA: Fiber saturable absorber

FSR: Free spectral range

FWHM: Full width half maxima

FWM: Four wave mixing

GNLSE: Generalized nonlinear Schrodinger equation

GVD: Group velocity dispersion

Ho: Holmium

HR-FBG: High reflective FBG

LF: Lyot filter

LMA: Large mode area

LR-FBG: Low reflective FBG

MASER: Microwave amplification by stimulated emission of radiation

MCVD: Modified chemical vapor deposition

MMF: Multi mode fiber

MMI: Multimodal interference

MM-LD: Multimode laser diode

MO: Mamyshev oscillator

NAbLM: Nonlinear absorbing loop mirror

NALM: Nonlinear amplifying loop mirror

NCD: Net cavity dispersion

Nd: YAG: Neodymium-doped yttrium aluminum garnet

NLP: Noise like pulse

NLSE: Nonlinear Schrodinger equation

NOLM: Nonlinear optical loop mirror

NPE: Nonlinear polarization evolution

NPR: Nonlinear polarization rotation

OCT: Optical coherence tomography

OSA: Optical spectrum analyzer

OSC: Oscilloscope

PC: Polarization controller

PCF: Photonic crystal fiber

PD: Photodiode

PMF: Polarization maintaining fiber

RF: Radio frequency

RI: Refractive index

RIN: Relative intensity noise

RSA: Reverse saturable absorption

RWs: Rouge waves

SA: Saturable absorber

SBS: Stimulated Brillouin scattering

SESAM: Semiconductor saturable absorbing mirror

SIB: Stress induced birefringence

Sm: Samarium

SMF: Single mode fiber

SM-LD: Single mode laser diode

SNR: Signal-to-Noise ratio

SPM: Self phase modulation

SRS: Stimulated Raman scattering

SSG: Small signal gain

TBP: Time bandwidth product

Tm: Thulium

TMDs: Transition metal di-chalcogenides

TPA: Three photon absorption

VOA: Variable optical attenuator

VPD: Vapor phase deposition

WDM: Wavelength Division Multiplexture

WGN: White Gaussian noise

XPM: Cross phase modulation

Yb: Ytterbium

YDFA: Ytterbium doped fiber amplifier

ZDW: Zero dispersion wavelength

List of Figures

Chapter: 01

Chapter: 02

Chapter: 03

Chapter: 04

Chapter: 05

Chapter: 06

List of Tables

Contents

Chapter: 03

State transition SESAM-based mode-locked fiber lasers at 1064 nm

Chapter: 04

Rectangular pulses in dual gain segment based figure-9 laser

Chapter: 01

Introduction

Abstract

In this chapter, fundamentals of fiber lasers, popular techniques of constructing a pulsed laser such as Q-switching, mode-locking have been briefed. The effect of dispersion, non-linearity on the ultra-short pulse propagation in a nonlinear medium is discussed. Importance of saturable absorbers to produce pulsed output, types of saturable absorbers, their working principle is also presented. At the end chapter wise organization of the thesis is detailed.

1.1. Introduction: Since the very first discovery of laser in 1960 by T. H. Maiman relied on the theory of MASER (Charles Towens, 1953) [1], fundamental research and commercialization of lasers have been flourishing because of their numerous fascinating traits in photonics research field. But the main reason behind this rapid growth is the application of lasers in several sectors; material industry, astronomical research, defense and most importantly the medical fields [2-7]. Depending on the types of applications, lasers with several emitting wavelengths have been developed. The global market value of laser technology has crossed the value of 15 Billion in the year 2023 and is expected to cross 32 Billion in 2032 [8]. A laser can be classified into four main groups depending on the type of gain medium used to form the laser, such as i) solid-state laser ii) gas laser iii) semiconductor laser iv) dye laser. Nd: YAG and CO_2 lasers are commonly used in the material industry due to their emission wavelengths, which are readily absorbed by a wide range of materials. Ti: Sapphire lasers find applications in research fields such as spectroscopy, because of their high gain bandwidth and the ability to produce very short-duration pulses [9-11]. Although these lasers are serving well in their respective fields by their performance, fiber lasers have started to replace them because of their robustness, low maintenance, ease of thermal management and smaller footprints. A fiber laser fits into the category of solid-state laser as a rare earth element doped silica fiber is used as the gain medium.

Modern day's advancement of optical fiber started to flourish after the development of low-loss silica fiber by Charles Kao [12]. Although the very first laser is invented at 1961 where an Nd-doped fiber used as gain medium, development of low loss silica fiber, Erbium (Er) doped fiber amplifier [13-14] gave a kick start to optical fiber based long-haul communication. The development other rare-earth doped optical fibers like Ytterbium (Yb), Thulium (Tm), Holmium (Ho) and various optical fiber based components like fiber Bragg gratings (FBGs) [15], wavelength division multiplextures (WDM), faraday isolators, couplers etc. open a new avenue to compact, alignment-free fiber laser system. Besides that, various inherent optical properties of optical fibers like dispersion, nonlinearity, birefringence makes fiber laser interesting in the ultrafast domain.

A particular field of application might rely on one or multiple laser parameters such as emission wavelength, average power, repetition rate, pulse duration, peak power, and pulse energy. For examples, Yb-doped fiber laser is mostly utilized in material processing industry for the reason most metals have efficient energy absorption at 1064 nm [16]. High-precision engraving on ceramics, metals are done by lasers with ns to fs duration [17]. Fs-laser at 1064

nm is used as the pump source to generate super-continuum out of photonic crystal fiber (PCF) which have a specific application on optical coherence tomography (OCT) [18-19]. Yb-doped fiber laser is also useful in imaging of biological samples via multiphoton microscopy [20-21].

Er-doped fiber laser and amplifier with its emission at the telecommunication wavelength (1550 nm) are used in high speed data transmission [22]. Besides, these lasers are also exploited in developing different type of sensors like stress-sensor, vibration-sensor, and hazardous chemical sensor [23-25]. Due to pronounced water absorption at 1.9 microns, Tm-doped fiber lasers play a significant role in meeting the needs of the surgical industry [26-27]. Recently, research on bismuth (Bi) –doped optical fiber has also flourished because of its large emission bandwidth covering 1100-1650 nm which would greatly enhanced the transmission bandwidth in near future [28]. Research on optical fibers with different host material other than silica glass (e.g. chalcogenide, telluride, fluoride glass) is also being expanded for MID-IR generation [29-31]. Along with that, various materials, including transition metals like chromium [32], noble metals such as silver and gold [33-34], as well as several combinations of multiple rare earth elements [35-36] are incorporated into the core of optical fibers to achieve specific desired properties and constantly thriving the research field of 'Specialty optical fibers'.

Construction of ultrafast laser requires a method called saturable absorption in the cavity by which the cavity supports ultra-short pulse. Moreover, a stable pulsing operation requires a balance between parameters like dispersion, nonlinearity, gain, linear & nonlinear loss etc. [37-40]. A slight perturbation from a range of parameters leads the laser to any quasi-stable, unstable, chaotic state from the stable state which opens up a direction to study the pulse dynamics [41-44]. Moreover, inherent properties of optical fiber dispersion, Kerr-nonlinearity and these properties induced phenomenon self-phase modulation (SPM), stimulated Raman scattering (SRS), cross phase modulation (XPM), four wave mixing (FWM) comes into play when an optical fiber is exposed to an ultra-short pulse [45-47]. Although these phenomenon sometimes limit the performance of a system for a particular application, they lead to fascinating optical pulse attributes which make optical fiber interesting to study 'nonlinear pulse dynamics'.

The ultimate goal of this thesis is to build an ultrafast laser system capable of producing pulses with single pulse energy in the micro-joule range. Aiming to this, a significant amount of work has been carried out in constructing a suitable seed oscillator and studying their pulse

dynamics. Performance of four different type of saturable absorbers are studied extensively. Out of four saturable absorbers, three saturable absorbers are utilized in making a suitable oscillator in distinct cavity architecture maintaining an all fiber architecture. The performance of the last SA is checked numerically. During the seed development process various types of pulse state have been observed such as: stable Q-switched pulse, dissipative solitons (DS), dispersion managed solitons (DMS), Noise like pulse (NLP) etc. Alongside these stable state, state transition to a complete chaotic state have also been observed. The roundtrip-to-roundtrip spectral instability of the chaotic state is characterized by performing dispersive Fourier transform (DFT); comparison of relative intensity noise (RIN) between stable and chaotic state is also done. A novel cavity architecture of 'Mamyshev oscillator' is proposed and its pulse dynamics are investigated by solving GNLSE numerically. A tunable 'Lyot filter' in combination with a Gaussian filter is used to form the cavity and 'amplifier similariton' is diagnosed as the stable state which is compressible to its transform-limited duration.

The end part contains two distinct designs of CPA set up where a stable mode-locked laser delivering stable DMS featuring high spectral bandwidth is considered as the seed source. The first architecture delivers sub-300 fs pulses at a repetition rate of 17.65 MHz with single pulse energy of 160 nJ. The later one delivers 2 μJ pulses with nearly 150 ps of pulse duration.

From the next section, basics of pulsed fiber lasers, effects of dispersion and non-linearity pulse propagation through optical fiber, process of saturable absorption and spectral filtering and CPA method is described.

1.2. Basics of fiber laser: Construction of any laser requires a suitable gain medium pumped inside resonator. In case of fiber laser, the gain medium is a rare-earth (RE) material (Nd, Yb, Er, Tm,) doped fiber pumped by semiconductor laser diodes; the pump is launched through free-space coupling or through WDM or pump combiners. Pigtailed fibers Bragg gratings (FBGs) or free space wavelength specific mirrors are used to form the resonators. In table-1.1, absorption and emission band of different RE-doped fibers are shown. Schematic of two simplest fiber laser cavity is shown in figure 1.1. Figure 1.1(a) is a linear configuration, in contrast figure, 1.1(b) is the ring configuration; these architectures form the resonator by sustaining standing and travelling wave respectively and are frequently employed by researchers with up-gradation/modification.

Table – 1.1 Popular Absorption and emission band of different rare earth doped materials

RE-material	Absorption band	Emission band
Neodymium (Nd^{3+})	800 nm	1030–1100 nm, 900–950 nm, 1320–1350 nm
Ytterbium (Yb^{3+})	915 nm, 976 nm	1020 – 1080 nm
Erbium (Er^{3+})	976 nm, 1480 nm	1520 – 1600 nm
Thulium (Tm^{3+})	793 nm, 1620 nm	1700–2100nm
Holmium(Ho^{3+})	1950 nm, 1125 nm	2100 nm, 2900 nm

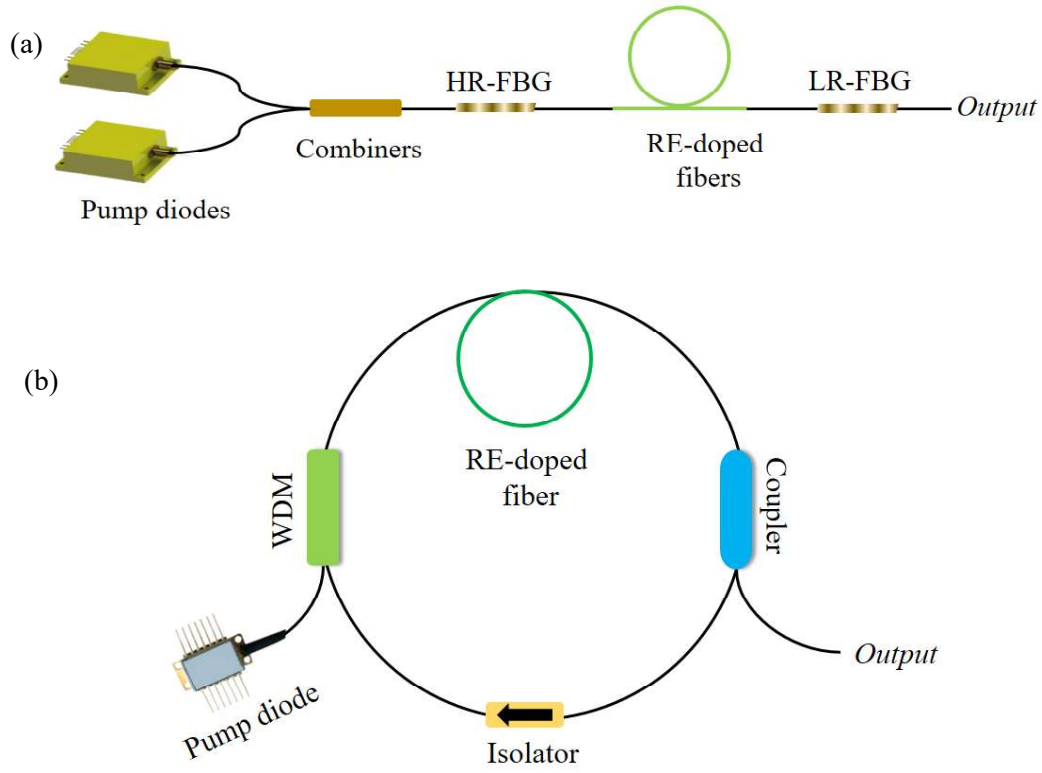

Figure 1.1: Schematic of simplest fiber laser cavity (a) Linear configuration (b) ring configuration

1.2.1 Modes of operation: Relying on the time dependency of output power, lasers are grouped into two broad groups; One is which gives continuous-wave output in time, known as a CW laser and the other class is called pulsed laser which provides output in a repetitive form. Figure 1.2 shows the output power variation of a CW laser (above) and pulsed laser (below) with time. As the output of a CW laser is not dependent on time, the average power is same as the peak power. But in case of pulsed laser, peak power is different from the average

power and calculated by the formula, $Peak\ power = \frac{Average\ power}{Repetition\ rate * Pulse\ width}$. Repetition rate of a laser is the measurement of number of pulses produced per second and the pulse width is time interval between leading and training edge of a pulse. As the formula of peak power says, a pulsed laser produces pulses of higher peak power which make them advantageous in lot of applications like material processing, waveguide inscription, nonlinear optics etc. Lasers with femtosecond time span is used to look into ultra-short natural phenomenon like molecular transition in spectroscopy. To obtain pulsed output, few additional techniques are adopted over a CW laser. There are four adopted methods to get pulsed output of distinct pulse duration; such as i. Quasi-cw (ms); ii. Gain switching (ms- ns); iii. Q-switching (µs-ns); iv. Mode-locking (ns-fs). Each technique has their own advantages and disadvantages over others and chosen upon the requirements of any particular application.

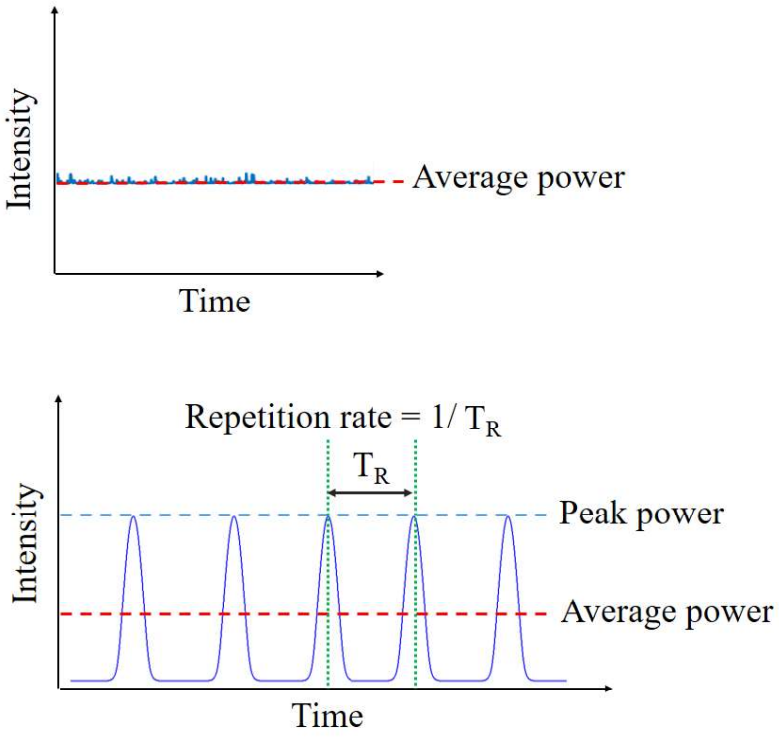

Figure 1.2: Time variation of output of CW and pulsed laser. CW laser (above) and pulse laser (below).

Quasi-CW and gain-switching are the processes where the pump in other term the gain is modulated periodically. In Quasi-CW the pump is kept switched on for enough time such that the laser goes to the steady CW state then the pump is switched off; which allows the system to thermally cool down. However, in gain-switching the pump is switched on for short time,

which don't allow the laser to transit to steady state, delivering shorter duration pulse than Quasi-CW process [48]. Both Q-switching and mode-locking can be done by an active and a passive way. However, Q-switching and mode-locking are two distinct mechanism discussed in the subsequent sections. In the active method, an AOM or EOM is used in the cavity which is controlled from outside via additional electronics. In the passive method, a component named 'saturable absorber' is incorporated in the cavity which supports large intensity fluctuation in the cavity and suppresses lower intensity part; the fluctuation then shapes into a stable pulse over roundtrips [49-50].

1.2.1.A. Q-switching: By modulating the cavity loss periodically Q-switched pulses can be obtained. In this method a shutter is introduced inside the cavity which works as a periodic gate; when the shutter remains closed no feedback is provided to develop stimulated emission and in this interval a high population inversion is achieved. Then the shutter is suddenly opened to start the oscillation, as a result a large number of photons develops inside the cavity and the cavity delivers a high energy pulse. The Q-factor of a cavity is defined as $2\pi \frac{\text{energy stored}}{\text{energy loss per cycle}}$. When cavity loss is high (shutter is closed), then the cavity has a low Q-factor. The Q-factor switches to a higher value as the cavity loss reduces. In figure 1.3, a schematic of buildup process of a Q-switched pulse is shown. Initially, an artificially high amount of loss is considered. The number of upper state population grows by following the equation

$$N_2(t) = R_p \tau_2 \left(1 - e^{-\frac{t}{\tau_2}}\right) \qquad \text{\_\_\_\_\_} eqn.(1.1)$$

This equation is obtained by solving the rate equation of an excited state atom and cavity photon numbers [51]. R_p is the pumping rate and τ_2 is the excited state life time. To get a Q-switched pulse, the pumping time should be comparable to the decay time of the excited state atoms; a longer pumping time reduces the efficiency as the excited state population degrades after an interval τ_2. Solid-state gain medium with higher excited state life time generates more efficient Q-switched pulse in contrast to gas lasers having shorter excited state life time. Referring to figure 1.3, at a constant pump level, at time T0 although the upper level population crosses the threshold value (N_{th}), the number of photons remain low because there is no chance of stimulated emission. At T1, as the shutter opens, the cavity loss decreases; at this moment the number of stimulated photons starts to grow rapidly and consequently population of upper level starts reducing. When N_2 becomes less then $N_{th,}$ (at

T2) then the number of photons falls again to zero at a comparatively slower rate and the cavity is ready for another buildup process. The pulse duration and the pulse shape can be controlled by optimizing the cavity length and loss modulating curve.

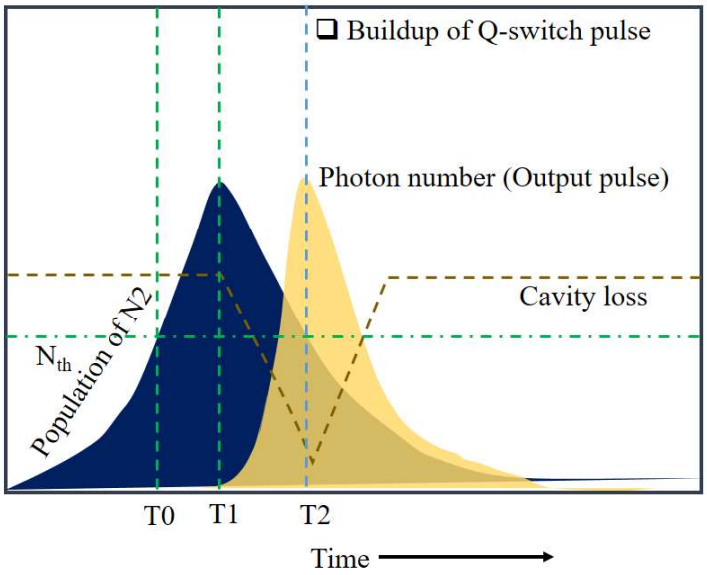

Figure 1.3: Schematic of the buildup process of a Q-switched pulse

Active Q-switching: In case of active Q-switching, an electronically controlled modulator such as AOM/EOM are incorporated inside the cavity as the loss modulators [52-53]. EOM or AOM are made of materials like crystalline quartz, tellurium oxide. By this method, nanosecond to microsecond duration is achievable with MHz to kHz repetition rate which is controlled by a function generator.

Passive Q-switching: In contrast to active method, passively Q-switched lasers do not require any type of electronically controlled modulators. In this method, a material with nonlinear transmission property is utilized in the cavity such that when the optical intensity grows in the cavity the transmission automatically reduces and let the cavity delivers short duration pulse. These materials are called saturable absorbers (SA), can be thin films, specialty optical fibers [54-56] with suitable parameters. Detail of saturable absorbers are discussed in **section 1.4.**

1.2.1.B. Mode-locking: The mode-locking mechanism is the best and commonly adopted method to obtain pulses of ultra-short duration and the pulse attributes are totally different from a Q-switched pulse. As the name suggests, the excited longitudinal modes in a cavity

are locked in phase to generate short pulse. In a Fabry-Perot cavity the frequency gap between two consecutive excited modes is '$\delta\nu = \delta\nu_{m+1} - \delta\nu_m = c/2nL$' where c is the speed of light, n is the refractive index of the medium and L is the length of the cavity. This frequency gap ($\delta\nu$) is known as free spectral range (FSR) which becomes equal to the fundamental repetition rate of the laser once mode-locking is achieved. For a ring configuration the formula changes to 'c/nL' [57]. Mathematically, the electric field of an m^{th} longitudinal mode is represented as

$$E_m(t) = A_m * \exp[j(\phi_m - 2\pi\nu_m t)] \qquad \text{Eqn. (1.2)}$$

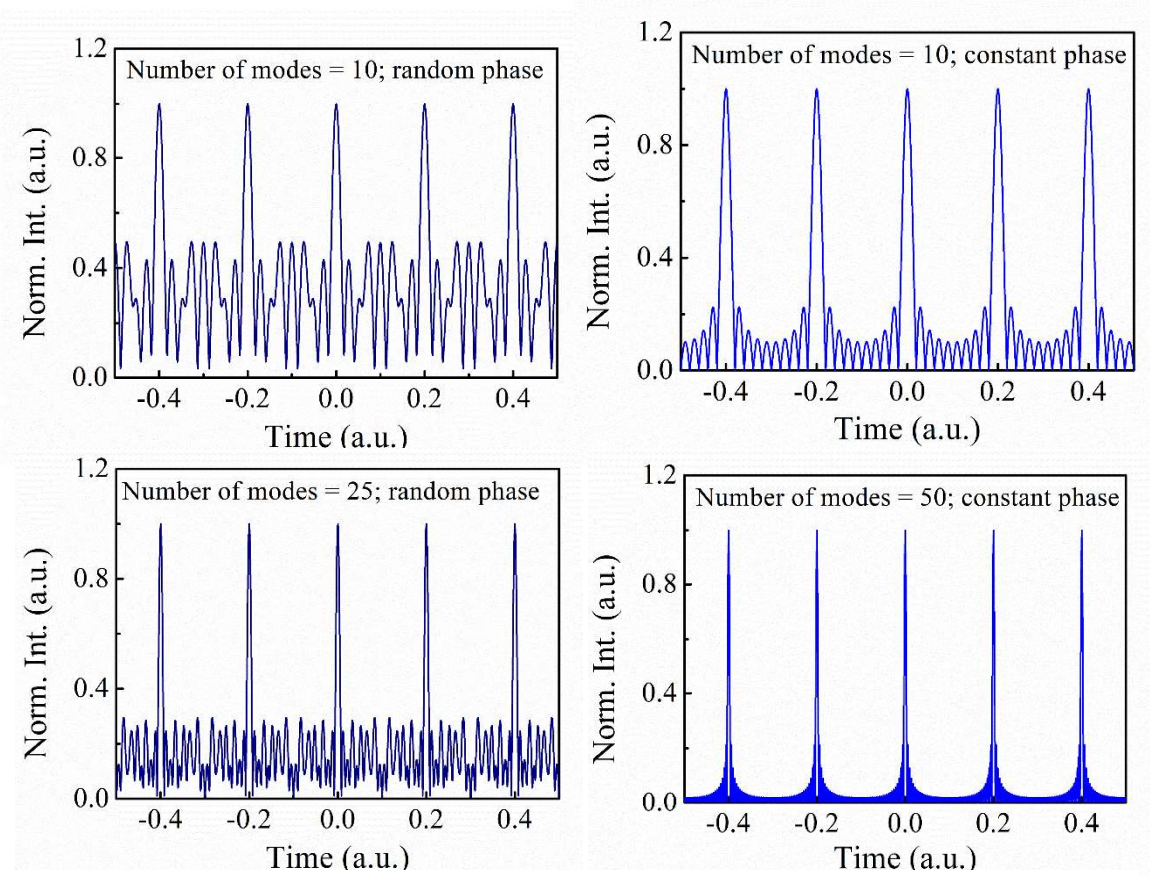

Figure 1.4: Superposition of multiple modes with random and constant phase. (a) 10 modes with random phase relation. (b) 25 modes with random phase relation (c) 10 modes with constant phase relation (d) 50 modes with constant phase relation

A_m, ϕ_m and ν_m are the amplitude, phase and carrier frequency of the corresponding modes. Considering total (2N +1) number of excited modes, the net electric field becomes

$$E(t) = \sum_{-N}^{N} A_m * \exp[j(\phi_m - 2\pi\nu_m t)] \qquad \text{\_\_\_\_\_} Eqn.(1.3)$$

If the relative phases among the excited modes are locked among the excited modes such that $\phi_{m+1} - \phi_m = \Delta\phi = constant$, the intensity of the electric field transform to

$$[E(t)]^2 = I_0 \left\{ \frac{sin[\pi(2N+1).\delta\nu.t]}{\sin(2\pi.\delta\nu.t)} \right\}^2 \qquad \text{\_\_\_\_\_} Eqn.(1.4)$$

In figure 1.4(a) and 1.4(b), intensity profile of 10 superposed modes with a constant phase relation and random phase relations are shown respectively. It could be noticed that a constant phase relation among the excited modes suppresses the noisy side-bands. Figure 1.4(c) and 1.4(d) present the comparison of 50 and 100 modes in a constant phase relation. The figures interpret that with the increment of number of excited modes, the pulse duration decreases. This is the reason behind the requirement of broader spectrum (larger number of excited modes) to obtain shorter pulse duration. In mathematics the frequency bandwidth is obtained by performing Fourier transform of a single pulse with the complex information. The product of time bandwidth and frequency bandwidth which is known as time bandwidth product (TBP) are different for different shape of pulses. For a Gaussian pulse it is 0.44 but for a Secant Hyperbolic pulse TBP is 0.318. For a square pulse this value becomes 0.886 [58]. The minimum pulse duration obtained from a certain amount of frequency bandwidth is known as transform limited duration, is also related to the TBP. Generally, a mode-locked laser does not deliver transform limited pulse because of inherent dispersion and non-linearity-induced chirp acquired while travelling through the medium; however, the pulse duration can be reduced by minimizing the chirp outside the cavity by adding dispersive elements. A brief discussion on the effect dispersion and non-linearity on the ultra-short pulse is presented in **section 1.3**.

Active mode-locking: Similar to the active Q-switching an intensity modulator is used to build an actively mode-locked cavity. Only difference is that the external modulator is used to provide selective gain to the phase locked modes by driving the modulator at the mode-spacing frequency of the particular cavity. For a cavity with certain length the modulation frequency is fixed for active mode-locking [59,60].

Passive mode-locking: Different from the active mode-locking, passive mode-locking does not require any external controlling system to generate pulses. Analogous to the passive Q-switching method, a saturable absorber is incorporated inside the cavity which allows high

intensity fluctuations to transmit through and suppresses the low intensity noise. Upon appropriate feedback that allowed fluctuations shaped into a stable single pulse and circulates in the cavity. While circulating the short duration pulse experiences dispersion and non-linearity of the medium which affects both on the pulse and spectrum. Under a suitable condition when the pulse can survive after experiencing all these pulse shaping affect, the laser delivers stable mode-locked pulse train. Compared to active mode-locking, passive mode-locking mechanism generates pulses of shorter duration and broader spectrum. As many parameters comes into play in passive mode-locking, various interesting pulse dynamics are also observed. Understanding the root of these non-linear pulse dynamics and finding a way to apply them in various applications have become a great field of research [61-63].

1.3. Ultra-short pulse propagation in an optical fiber: Mathematically, a Gaussian pulse is expressed as

$$A\,(w,T) = P * e^{-(1+iC)\frac{t^2}{T_0^2}} * e^{i*w_0*t} \qquad \text{Eqn. (1.5)}$$

In equation (1.5), P is the peak power, w_0 is the carrier frequency and T_0 is the pulse width. C is the chirp parameter. Chirp is defined as the instantaneous frequency, C>0 means the up-chirp i.e., instantaneous frequency increases linearly from the leading edge to trailing edge; and C<0 means the opposite. Sometimes C can be a function of time which corresponds to the nonlinear chirp. When an ultra-short pulse propagates through an optical fiber, dispersion and Kerr-nonlinearity are two main factors that affects the pulse shaping.

The pulse propagation through an optical fiber can be studied by solving nonlinear Schrodinger equation (NLSE) described as

$$\frac{\partial A}{\partial z} = \frac{\alpha}{2}A + \frac{i\,\beta_2}{2}\frac{\partial^2 A}{\partial T^2} - i\,\gamma|A|^2 A \qquad \text{Eqn. (1.6)}$$

A is the slowly varying amplitude of the pulse envelope, α is the linear loss, β_2 is the second order dispersion, γ is the non-linear coefficient. The NLSE is derived from well-known Maxwell equations [64].

1.3.1 Effect of dispersion: As the refractive index of any material depends on the optical frequency, light of each frequency component travels with a different phase velocity. The waveguide structure also affects the effective refractive index of the guided modes. So, in

optical fiber material dispersion and waveguide dispersion are two main contributors of the chromatic dispersion.

Material dispersion: If a pulse with certain width propagates through a medium of and refractive index $n(\omega)$, then time taken by the pulse to traverse L distance is $\tau = \frac{L}{v_g}$ where v_g is the group velocity and $1/v_g$ can be written as $\frac{dk}{d\omega}$. k is the propagation constant and represented as $k = \frac{\omega}{c}\, n(\omega)$; So,

$$\frac{1}{v_g} = \frac{dk}{d\omega} = \frac{1}{c}\left[n(\omega) + \omega\frac{dn}{d\omega}\right] \qquad \text{\_\_\_\_}Eqn.\,(1.7)$$

Rewriting the above equation in terms of wavelength gives

$$\frac{1}{v_g} = \frac{1}{c}\left[n(\lambda_0) - \frac{1}{\lambda_0}\frac{dn}{d\lambda_0}\right] \qquad \text{\_\_\_\_}Eqn.\,(1.8)$$

Now, if the spectral width of corresponding optical pulse is $\Delta\lambda_0$, then each spectral component will travel with a different group velocity and as a result the pulse broadens. The broadening is given by

$$\Delta\tau = \frac{d\tau}{d\lambda_0}\,\Delta\lambda_0 = -\frac{L}{c}\frac{\Delta\lambda_0}{\lambda_0}\left[\lambda_0^2\frac{d^2n}{d\lambda_0^2}\right] \qquad \text{\_\_\_\_\_}Eqn.\,(1.9)$$

The material dispersion is defined as the amount of pulse broadening per unit length of propagation per wavelength interval. $D_m = \frac{\Delta\tau}{L\,\Delta\lambda_0}$ and the unit is ps/km.nm. For silica based or other type of optical fibers, variation of refractive index with the wavelength is given by Sellemeier's equation. The wavelength where $\frac{d^2n}{d\lambda_0^2}$ becomes zero is known as zero dispersion wavelength (ZDW) and for pure silica based fiber ZDW is 1.27 micron.

Waveguide dispersion: Considering refractive index of core (n_0) and cladding (n_1) independent of the wavelengthλ_0, the normalized propagation constant for a particular mode is given by

$$b = \frac{\frac{\beta^2}{k_0^2} - n_1^2}{n_0^2 - n_1^2} \qquad \text{\_\_\_\_\_}Eqn.\,(1.10)$$

Where b is the function of V number of the optical fiber. The V number of an optical fiber of core radius a is defined as

$$V = \frac{2\pi}{\lambda_0}\, a\, sqrt(n_0^2 - n_1^2) \qquad \text{_____}Eqn.(1.11)$$

After a few steps of calculation the inverse of group velocity becomes

$$\frac{1}{v_g} = \frac{d\beta}{d\omega} = \frac{n_2}{c} + \frac{n_1 - n_2}{c}\left[\frac{d(bV)}{dV}\right] \qquad \text{_____}Eqn.(1.12)$$

The broadening of pulse after propagating L distance is given by

$$\Delta\tau_w = \frac{d\tau_w}{d\lambda_0}\,\Delta\lambda_0 \approx -\frac{L}{c}(n_0 - n_1)\frac{\Delta\lambda_0}{\lambda_0}\left(V\frac{d^2(bV)}{dV^2}\right) \qquad \text{_____}Eqn.(1.13)$$

Now, similar to the material dispersion, waveguide dispersion is defined as $D_w = \frac{\Delta\tau_w}{L\,\Delta\lambda_0}$. Consequently the total dispersion of an optical fiber becomes sum of D_w and D_m.

$$D = D_w + D_m \qquad \text{_____}Eqn.(1.14)$$

D is known as dispersion parameter. The second order group velocity dispersion can be calculated from dispersion parameter from the formula

$$\beta_2 = -\frac{\lambda_0^2}{2\pi c}\, D \qquad \text{_____}Eqn.(1.15)$$

It is evident from the definition of waveguide dispersion that by altering core radius and refractive index of core, D_w can be changed in other words total dispersion and ZDW can be modified. The second-order chromatic dispersion parameter (β2) for a standard single-mode fiber operating at a wavelength of 1064 nm (Corning, HI1060) is measured at 22.28 ps²/km. In contrast, for another standard single-mode fiber designed for operation at 1550 nm, SMF-28, the corresponding β2 value is determined to be -17.6 ps²/km. These distinct β2 values signify the differential chromatic dispersion characteristics exhibited by these fibers at their respective operational wavelengths.

To analyze the effect of dispersion on an optical pulse while propagating down an optical fiber, equation 1.6 can be solved by setting linear loss and nonlinear parameter at zero.

$$i\,\frac{\partial A\,(z,T)}{\partial z} = \frac{\beta_2}{2}\frac{\partial^2 A(z,T)}{\partial T^2} \qquad \text{_____}Eqn.(1.16)$$

Where,

$$A(z,T) = \frac{1}{2\pi}\int_{-\infty}^{\infty} \widetilde{A(z,\omega)}\exp(-i\omega T)\, dT$$

Solution of the equation is given by

$$\widetilde{A(z,\omega)} = \widetilde{A(0,\omega)}\exp(\frac{i\,\beta_2\omega^2 z}{2})$$

This indicates while propagating through an optical fiber, each frequency component experiences a certain phase shift which depends on the distance travelled and the frequency itself. Although it does not affect the spectrum shape but modifies the pulse shape in temporal

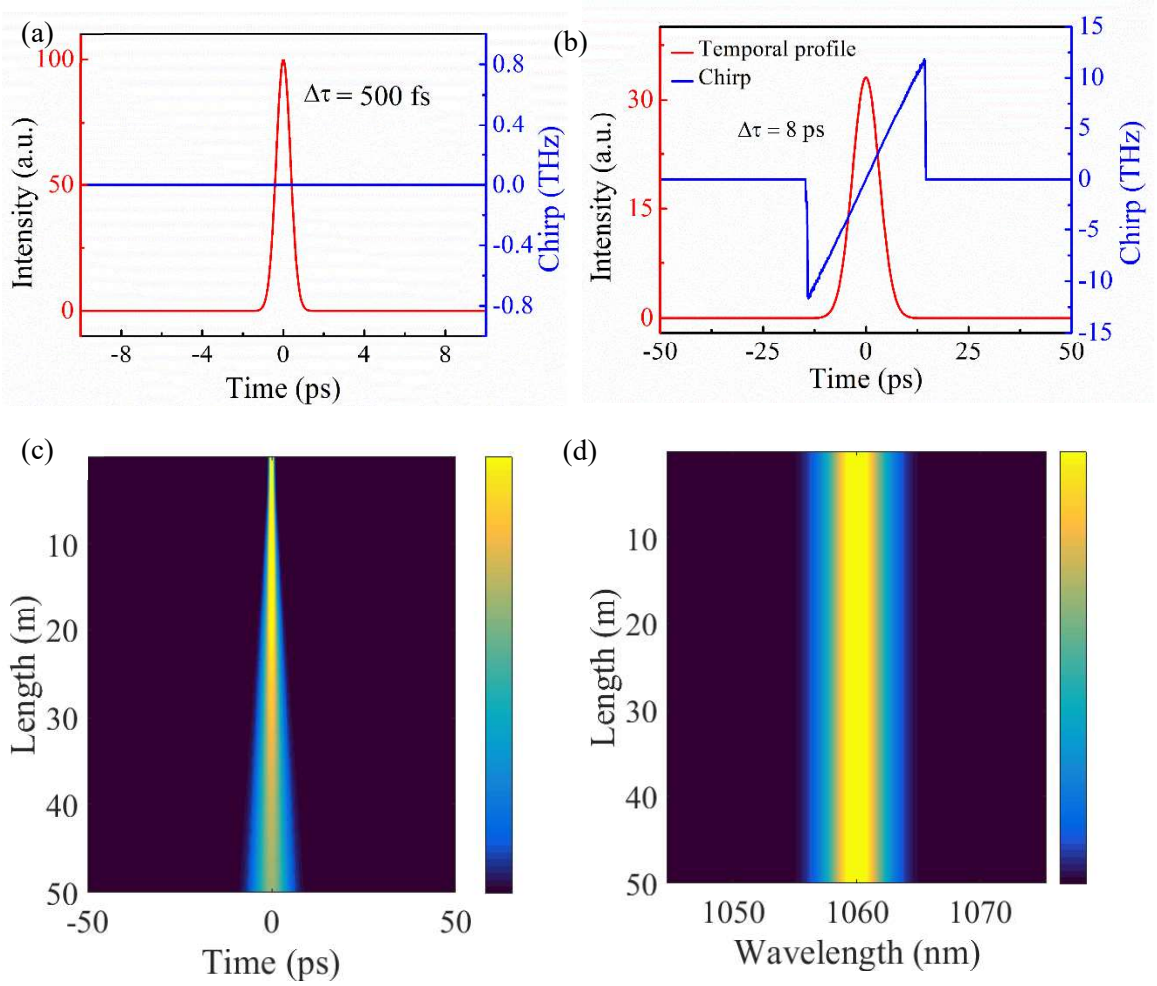

Figure 1.5: Effect of dispersion on the pulse propagation. (a) Initial pulse and chirp profile (b) Final pulse and associated chirp (c) variation of pulse (d) variation of corresponding optical spectrum along the length.

domain. After propagating a distance z, the equation of pulse becomes

$$A(z,T) = \frac{1}{2\pi}\int_{-\infty}^{\infty} \widetilde{A(z,\omega)}\exp(\frac{i\,\beta_2\omega^2 z}{2})\exp(-i\omega T)\,dT \qquad \text{Eqn. (1.17)}$$

A Gaussian pulse of duration T_0 can be expressed as $A\,(0,T) = \exp(-\frac{T^2}{T_0^2})$.After propagating a distance of z through an optical fiber it becomes

$$A(z,T) = \frac{T_0}{sqrt(T_0^2 - i\beta_2 z)}\; exp\left[-\frac{T^2}{(T_0^2 - i\beta_2 z)}\right] \qquad \text{Eqn. (1.18)}$$

Which signifies although a Gaussian pulse can maintain its shape the duration increases to $T_0[1 + (\frac{z\,|\beta_2|}{T_0^2})^2]^2$. But if the input pulse is initially chirped, then the final duration depends on the initial chirp properties and sign of β_2. By doing some calculations it is found that the chirp, $\delta\omega(T) = -\frac{\partial\varphi}{\partial T} \propto sgn(\beta_2)$. When the pulse propagates through a normal dispersion medium, the final pulse is linearly up-chirped that means lower frequency lights travel faster and accumulate at the leading edge. The exact opposite things happen when a pulse travels through a medium with anomalous dispersion [65].

Considering an optical pulse of certain spectral bandwidth around angular frequency w0, the propagation constant b(W) can be expanded by Taylor series expansion as

$$\beta\,(\omega) = \beta_0 + (\omega - \omega_0)\frac{\partial\beta}{\partial\omega} + (\omega - \omega_0)^2\frac{\partial^2\beta}{\partial\omega^2} + (\omega - \omega_0)^3\frac{\partial^2\beta}{\partial\omega^3} + \qquad \text{Eqn. (1.19)}$$

Figure 1.5 represents the evolution of a transform limited Gaussian pulse (central wavelength = 1060 nm, FWHM = 500 fs, Peak power = 100 W) while propagating through a fiber of length 50 meter in normal dispersion (HI1060). Figure 1.5(a) is the temporal profile and associated chirp of the input pulse whereas figure 1.5(b) depicts the final temporal profile and its associated chirp. As the figures interpret, the pulse duration broadens to 8 ps and it acquires an up-chirp during propagation. Figure 1.5(c) and 1.5(d) show the evolution of the pulse and corresponding optical spectrum along the length. The spectrum remains uniform as dispersion does not create new frequencies akin to non-linearity.

1.3.2. Effect of nonlinearity: The refractive index of any material changes nonlinearly when it is exposed to intense electromagnetic field. In case of silica based optical fiber, the modified refractive index becomes

$$n = n_0 + n_2|E|^2 \qquad \text{_____}Eqn.(1.20)$$

n is the linear index and n_2 is non-linear index coefficient which depends on the third order dielectric susceptibility. The nonlinear parameter of an optical fiber at a particular frequency is given by $= \frac{\omega_0 n_2}{cA_{eff}}$, ω_0 is the carrier frequency, A_{eff} is the mode-field area. To look into the effect of nonlinearity on the pulse propagation, equation 1.6 could be solved by assuming a

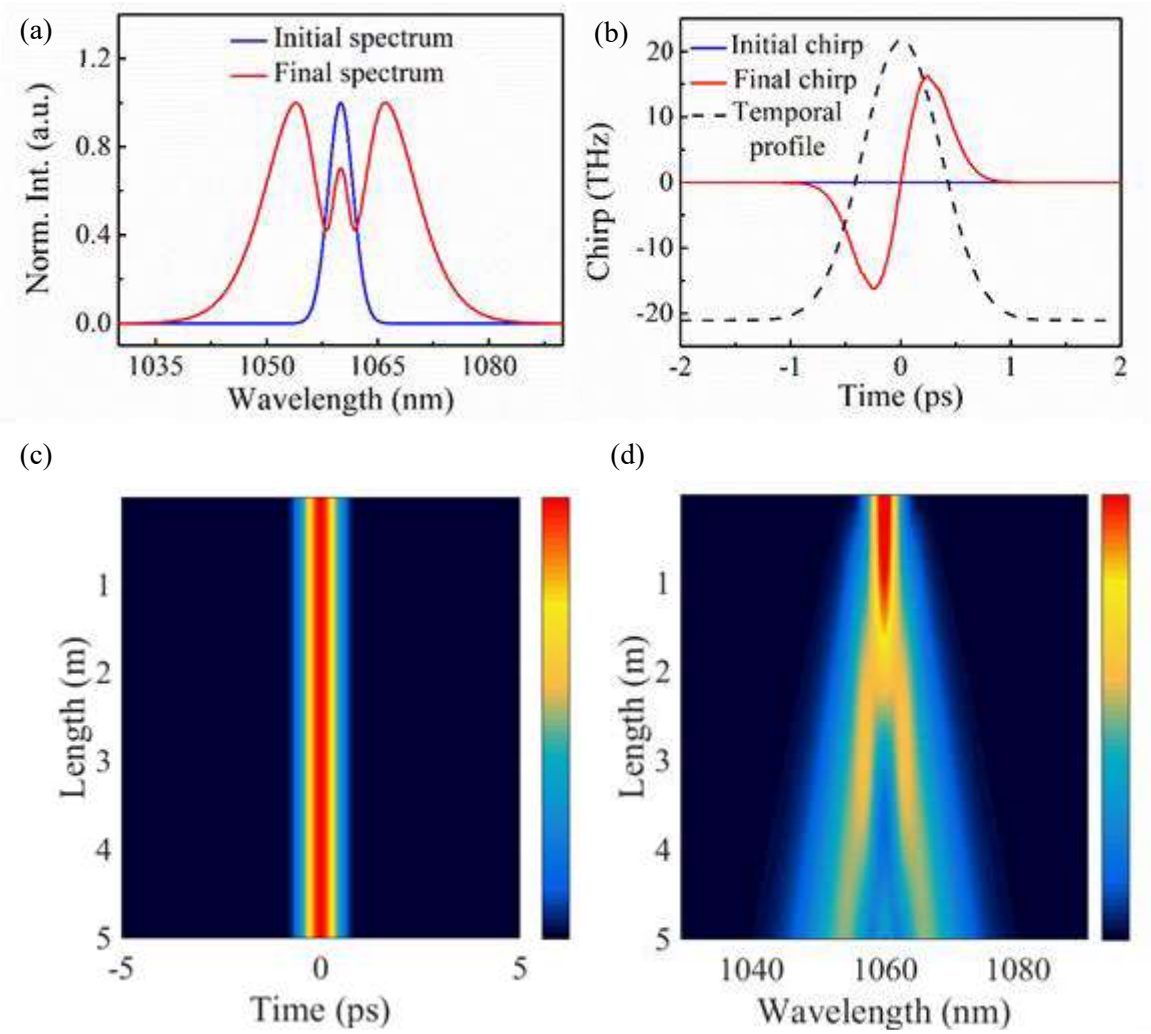

Figure 1.6: Effect of non-linearity on ultra-short pulse propagation (a) Initial and final spectrum (b) Initial and final chirp with temporal intensity profile (c) Evolution of optical spectrum & (d) pulse along the length of the fiber

dispersion less and lossless medium. It is noticed that an additional phase term includes with the pulse envelope as, $A\,(z,T) = A(0,T)exp(i * |A(0,T)|^2 * z)$. This phase term is called nonlinear phase $\varphi_{NL}$and as the phase modulates because of its own intensity the process is known as SPM. By calculating chirp (which is the first order time derivative of the nonlinear phase in this case) $\delta\omega(T) = -\frac{\partial\varphi_{NL}}{\partial T} = -z * \frac{\partial|A(0,T)|^2}{\partial T}$, we see that SPM induced chirp increases as the pulse propagates down the fiber, what this means is new frequency components generates continuously as the pulse propagates. As a result, we can notice a broadening in the corresponding optical spectrum keeping the pulse shape unaltered, which is generally known as SPM-induced spectrum broadening. Near the leading edge of the pulse, $\delta\omega(T)$ is negative which means light of higher wavelength accumulates near the leading edge and opposite happens at trailing edge. The effect is similar to the case of positive dispersion. So, when an optical pulse travels through a normal dispersive nonlinear medium, there is no chance of chirp cancellation. But is case of negatively dispersive medium, dispersion induced linear chirp and SPM induced non-linear chirp could get cancelled in appropriate condition and as a result the pulse can propagate without altering its shape both in temporal and spectral domain, which is known as optical soliton [64-65]. Figure 1.6 shows the effect of nonlinearity on the spectrum of an optical pulse of 500 fs duration and 30 W peak power. While propagating through 5 meter of HI1060. Figure 1.6(a) is the comparison between initial and final spectrum which indicates the optical spectrum broadens during propagation due to SPM-induced new frequencies. Figure 1.6(b) presents the initial and final chirp with corresponding temporal profile. Figure 1.6(c) and 1.6(d) shows the variation of temporal profile and spectrum along the length. As nonlinearity modifies complex phase in the electric field, the temporal profile remains unaltered, only the spectrum gets broaden [64-65].

1.4. Saturable absorbers: Saturable absorbers are a kind of optical components which transmits light of higher intensity by absorbing low intensity components. Figure 1.7 shows the effect of saturable absorber on a pulse with noisy background. These components are used to favor higher intensity light inside a cavity to promote pulsed operation. The transmittance of a SA varies in a non-linear fashion with the intensity of the light. Alongside the dispersion engineering and non-linearity, few parameters of a SA are also responsible for pulse shaping

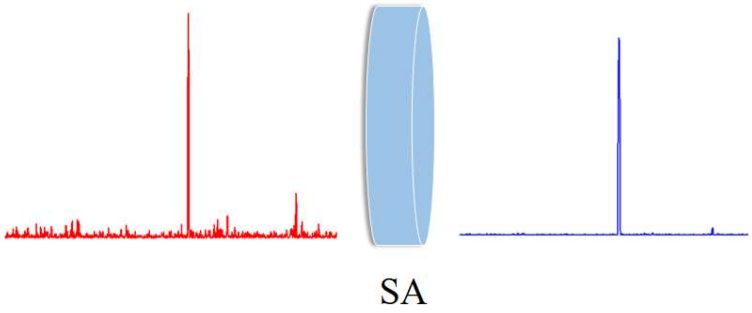

Figure 1.7: Effect of a SA on a noisy pulse.

and distinct pulse dynamics. The transmission function of a typical SA is given by the following equation [66]

$$T(I) = 1 - \frac{\alpha_0}{1 + \frac{I}{I_{sat}}} - \beta I - \alpha_{ns} \qquad \text{_____} Eqn.(1.21)$$

α_0 is the modulation depth, defined as the difference between maximum and minimum transmittance. I_{sat} is the saturation intensity defined as the intensity where the transmittance becomes 1/e time of the maximum value. A linear loss is always present which could not be suppressed anyhow and limits the transmittance; known as non-saturable loss, presented as α_{ns} in the equation 1.21. Another important phenomenon like inverse/reverse saturable absorption can happen in a SA by which the transmittance can reduce after a certain intensity

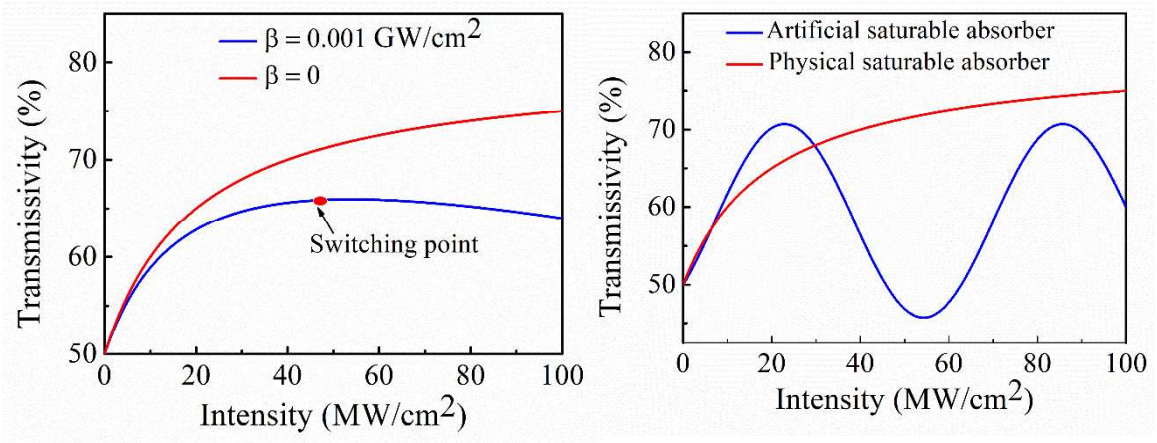

Figure 1.8: (a) Transmission curve of a SA with and without reverse saturation effect
(b) Transmission curve of an artificial and physical saturable absorber

[67-68]. Several nonlinear process like two photon absorption and three photon absorption are responsible for this mechanism. In the equation of transmissivity, β is reverse saturation coefficient. The point from where the transmission starts reducing is called the switching

point. In figure 1.8(a), the transmission function of two SAs are plotted, of which only one have the RSA effect. Other parameters are same for both the SAs; $I_{sat} = 20\ MW/cm\hat{}2$, α_0 = 30 %, α_{ns} = 0.2;

SAs can be categorized into two class depending on their working principle. The first class is named physical SA which are mainly made of materials in form of thin films, semiconductor hetero structures, quantum dots, nano-powders, specialty optical fibers doped with suitable materials etc. As physical SAs are made of materials, these are wavelength specific. The mechanism of physical SAs can be explained by looking into the inter-band transition of the material. The electrons of valance band absorb photons of appropriate energy and accumulates at the conduction band. Initially few electrons decay back to the valance band through recombination with material defects. Although the light of low intensity gets absorbed the conduction band remains unsaturated. For high intensity light electrons fills the higher energy states and the absorption saturates, consequently the material becomes transparent for a pulse with short duration. After a certain time, the absorption recovers by recombination process. Beside these process materials can possesses two photon absorption (TPA) which can induce reverse saturable absorption phenomenon also that can influence the pulse dynamics [69].

The other class is called artificial SAs which are not really absorbers that absorbs light of certain wavelength but architectures which also show non-linear transmittance relying on various optical properties of light i.g., polarization, spatial modal distributions, interference etc [70-72]. In case of optical fiber based artificial SAs, nonlinear optical loop mirrors (NOLM), nonlinear amplifying loop mirrors (NALM), nonlinear absorbing loop mirrors (NAbLM) and their combinations are relied on non-spatial interference effects. Working principle of Nonlinear polarization evolution (NPE), nonlinear polarization rotation (NPR) relies on the polarization of optical field. Multimodal interference (MMI) is also an all fiber architecture, working principle of which is based on spatial modal interference. In contrast to physical SAs, artificial SAs possesses a transmission curve, transmittance of which varies periodically (sinusoid) with the intensity i.e. it has the property of reverse saturable absorption by default. However, by modifying cavity parameters like length, polarization state, the switching point can be altered. This particular property makes artificial SAs more versatile than its counterpart to explore various pulse dynamics in a single cavity. Another advantage of artificial SAs is that these can handle much more intra-cavity power that physical SAs due to high damage threshold. Although in terms of stability, demand of physical

SAs is higher as the performance of artificial SAs are prone to environmental perturbations. In recent times, better stability has been achieved from artificial SA based lasers by adopting all polarization maintaining fiber architecture [73,74]. Comparison of transmission function of physical and artificial SAs is shown in figure 1.8(b).

1.5. Spectral filter: The purpose of a spectral filter is to allow a portion of the optical spectrum for particular use. Although it seems trivial, but in case of ultrafast laser in normal dispersion regime, spectral filter becomes an important component to obtain/maintain stable state. As in normal dispersion regime, there is no chance of balancing between dispersion and nonlinearity induced chirp, by chopping off a part of the spectrum in each roundtrip, a spectral filter manages the chirp of the pulse and prevent excessive nonlinear phase accumulation [75]. A spectral filter can be present in a cavity in various forms such as FBGs [76,77], fiber coupled band-pass filter [78,79], birefringent filter [80,81], interferometric filter [82,83] etc. Dispersive elements like gratings are also used as tunable spectral filters[84,85]. The limited gain bandwidth of the active medium can also play the role of a spectral filter in certain conditions [86,87].

1.6. Chirped pulse amplification: Amplification of ultra-short pulse was limited by optical wave-breaking and pulse degradation by SRS till the invention of CPA technique [88]. In this method, the peak power of the pulse from a *'seed'* laser is reduced initially by increasing the pulse duration to increase the threshold of SRS and reduce SPM-induced phase accumulation. This is done by traversing the pulse through a dispersive media and the stage is called '*stretcher*'. Following pulse stretching, the pulse is amplified in single of multiple *'amplifier'* stage. In the amplification stage, LMA gain fibers are adopted often to avoid nonlinearity [89,90]. After the amplification, the pulse is compresses again by suitable dispersion engineering which is known as '*compressor*'. A schematic of complete method is shown in figure 1.9. Even after adequate stretching, sometimes the non-linearity could not be avoided during amplification to higher average power; which requires an additional electronic setup to reduce the repetition rate of the oscillator systematically. This is known as *'pulse picking'*.

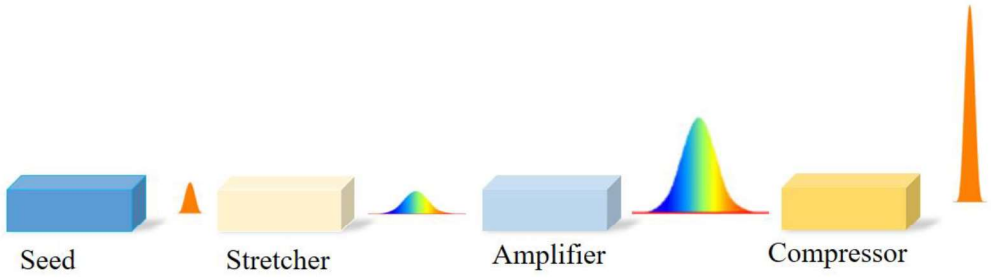

Figure 1.9: A schematic of the CPA technique.

1.7. Organization of thesis:

This thesis explores the ability, advantages, and disadvantages of four distinct saturable absorbers in producing stable pulses of ultra-short duration. Out of these four saturable absorbers, two are physical saturable absorbers [fiber saturable absorbers (FSA), Semiconductor saturable absorber mirror (SESAM)] and two are artificial saturable absorbers [non-linear amplifying loop mirror (NALM) & Mamyshev regenerator]. It is evident that the pulse dynamics observed in these four types of saturable absorbers based lasers are different from each other. At last, output from the most stable oscillator is amplified via CPA technique. The thesis contains six chapters after this introductory chapter, each chapter presenting the outcomes along with possible reasons of different cavity architectures. In each chapter, working principle, current literatures and the state-of-the-art of the related topic is discussed. The following is a concise overview of each chapter.

Chapter: 02. Aiming to an all-fiber architecture, a fiber saturable absorber is fabricated by MCVD method. This chapter contains details of fiber fabrication process and important fiber characterizations including linear and nonlinear absorption measurement. The fiber is utilized as a saturable absorber in a cavity where an Er/Yb-doped fiber is used as the gain medium. It is shown that the FSA has the ability to produced stable Q-switched pulses of microsecond duration from the cavity but at a sufficient pump power the cavity does not transit to the mode-locked state. The performance of the laser is checked by varying the length of the FSA. Possible reasons behind the incapability of the FSA to not producing mode-locked pulse have also been discussed.

Chapter: 03. In this chapter, performance of SESAMs are checked in two different dispersion region (all normal dispersion, net normal dispersion managed) at 1064 nm region. The cavities are made in linear configuration and a CFBG is utilized for dispersion management as well as output coupler. It is observed that SESAMs are capable to deliver stable mode-

locked state with pico-second pulse duration. Alongside the stable single pulse state, unequal multipulse, unstable harmonic and complete chaotic state have been observed from a single cavity by influencing the pump power only. Detail characterization of these states are done to check spectral and temporal stability. The dispersion managed seed is considered for further amplification via CPA technique which is shown in a following chapter.

Chapter: 04. This chapter contains mode-locked pulse dynamics at nanosecond time scale. In a figure-9 cavity the mode-locked has been achieved by utilizing a NALM as an artificial saturable absorber; as a new inclusion the cavity contains two amplifiers one in the NALM loop and another one in the arm. It is found that both the spectral and temporal properties behave oppositely with the pumping strength of the amplifiers. The autocorrelation trace confirms the state as an NLP state. No fundamental mode-locked state is obtained from this cavity. Possible reasons and solutions are discussed accordingly.

Chapter: 05. A new architecture of a MO has been proposed where a tunable Lyot filter is used as one of the spectral filter. Outcomes of a numerical investigation have been presented by solving GNLSE to check the ability of the architecture to generate ultra-short pulse. Other types of pulsing states along with the single pulse state have been observed and the attributes of each pulsing state has been discussed.

Chapter: 06. Considering the DMS state as the suitable state, the output power/energy is amplified via CPA method. Two different architecture have been adopted in this scheme. In the first architecture, the pulse energy is amplified to 160 nJ via two stage amplification, then the pulse duration is compressed to 295 fs. Second architecture contains 3 stage amplifier and a pulse picking scheme which reduces the repetition rate to 1.09 MHz. Pulse compression is not done in this architecture. Pulse energy obtained after the final amplifier is 2 μJ.

Chapter: 07. This chapter contains the possible future outlooks related to the work done.

{Bibliography}

1. Maiman, Theodore H. "Stimulated optical radiation in ruby." (1960): 493-494.
2. Kannatey-Asibu Jr, Elijah. *Principles of Laser Materials Processing: Developments and Applications*. John Wiley & Sons, 2023.
3. Emiliani, Esteban, Andres Kanashiro, and OriolAngerri. "Lasers for stone lithotripsy: advantages/disadvantages of each laser source." *Current Opinion in Urology* 33, no. 4 (2023): 302-307.
4. Rehman, Zia Ur, Fei Yang, Mengmeng Wang, and Tong Zhu. "Fundamentals and advances in laser-induced transfer." *Optics & Laser Technology* 160 (2023): 109065.
5. Li, Can, Yue Tao, Man Jiang, Pengfei Ma, Wei Liu, Rongtao Su, Jiangming Xu, JinyongLeng, and Pu Zhou. "High-power single-frequency fiber amplifiers: progress and challenge." *Chinese Optics Letters* 21, no. 9 (2023): 090002.
6. Phillips, Katherine C., Hemi H. Gandhi, Eric Mazur, and S. K. Sundaram. "Ultrafast laser processing of materials: a review." *Advances in Optics and Photonics* 7, no. 4 (2015): 684-712.
7. Lee, Hyub, Chin Huat Joel Lim, Mun Ji Low, Nicholas Tham, VadakkeMathamMurukeshan, and Young-Jin Kim. "Lasers in additive manufacturing: A review." *International Journal of Precision Engineering and Manufacturing-Green Technology* 4 (2017): 307-322.
8. Website: https://www.mordorintelligence.com/industry-reports/lasers-market
9. Liu, Han, Sijia Sun, Li Zheng, Geyang Wang, Wenlong Tian, Dacheng Zhang, Hainian Han, Jiangfeng Zhu, and Zhiyi Wei. "Review of laser-diode pumped Ti: sapphire laser." *Microwave and Optical Technology Letters* 63, no. 8 (2021): 2135-2144.
10. Duley, Wi. "CO2 lasers effects and applications." (2012).
11. Dumitras, Dan C., ed. *Nd YAG Laser*. BoD–Books on Demand, 2012.
12. Kao, Charles K. *Optical fiber systems: technology, design, and applications*. New York: McGraw-Hill, 1982.
13. Stone, J., and C_A Burrus. "Neodymium-doped silica lasers in end-pumped fiber geometry." *Applied Physics Letters* 23, no. 7 (1973): 388-389.
14. Laming, Richard I., Michael N. Zervas, and David N. Payne. "Erbium-doped fiber amplifier with 54 dB gain and 3.1 dB noise figures." *IEEE photonics technology letters* 4, no. 12 (1992): 1345-1347.
15. Hill, Kenneth O., Y. Fujii, Derwyn C. Johnson, and Brian S. Kawasaki. "Photosensitivity in optical fiber waveguides: Application to reflection filter fabrication." *Applied physics letters* 32, no. 10 (1978): 647-649.
16. Hubeatir, Kadhim A., Mohanned M. Al-Kafaji, and Hadeel J. Omran. "A review: Effect of different laser types on material engraving process." *J. Mater. Sci* 6, no. 4 (2018): 210-217.
17. Chmielewska, D., R. Gebel, K. Szamałek, Andrzej Olszyna, Joanna Marczak, Antoni Sarzyński, and Marek Strzelec. "Application of laser radiation in decoration and marking of ceramic products." In *Laser Technology 2012: Applications of Lasers*, vol. 8703, pp. 131-139. SPIE, 2013.
18. Lim, Hyungsik, Yi Jiang, Yimin Wang, Yu-Chih Huang, Zhongping Chen, and Frank W. Wise. "Ultrahigh-resolution optical coherence tomography with a fiber laser source at 1 μm." *Optics letters* 30, no. 10 (2005): 1171-1173.
19. Trifanov, Irina, Paulo Caldas, LiviuNeagu, Rosa Romero, Martin O. Berendt, José R. Salcedo, Adrian GH Podoleanu, and António B. Lobo Ribeiro. "20-mW 70-nm bandwidth ASE fibre optic source at

1060-nm wavelength region for optical coherence tomography." In *Fiber Lasers VII: Technology, Systems, and Applications*, vol. 7580, pp. 164-172. SPIE, 2010.

20. Kong, Cihang, Christian Pilger, Henning Hachmeister, Xiaoming Wei, Tom H. Cheung, Cora SW Lai, Thomas Huser, Kevin K. Tsia, and Kenneth KY Wong. "Compact fs ytterbium fiber laser at 1010 nm for biomedical applications." *Biomedical optics express* 8, no. 11 (2017): 4921-4932.
21. Kim, Dong Uk, Hoseong Song, Woosub Song, Hyuk-Sang Kwon, Miae Sung, and Dug Young Kim. "Two-photon microscopy using an Yb 3+-doped fiber laser with variable pulse widths." *Optics express* 20, no. 11 (2012): 12341-12349.
22. Ivanovs, G., V. Bobrovs, S. Olonkins, A. Alsevska, L. Gegere, R. Parts, P. Gavars, and G. Lauks. "Application of the erbium-doped fiber amplifier (EDFA) in wavelength division multiplexing (WDM) transmission systems." *Int. Journal of Physical Sciences* 9, no. 5 (2014): 95-101.
23. Liu, Haochong, Wei He, Yumin Zhang, Xinyi Chen, Zhihan Li, Shaode Li, and Lianqing Zhu. "Erbium-doped fiber laser based on intermodal interference between single-mode fiber and suspended core fiber for strain and temperature sensing." *Optical Fiber Technology* 75 (2023): 103203.
24. Li, Yuan, Cheng Zhou, Jiajun Tian, Shaobo Ji, and Yong Yao. "An all-fiber multi-channel ultrasonic sensor using a switchable fiber Bragg gratings filter in erbium-doped fiber laser." *Journal of Lightwave Technology* 37, no. 17 (2019): 4330-4339.
25. Gao, Liang, Long Huang, Lin Chen, and Xiangfei Chen. "Simultaneous measurement of strain and temperature with a multi-longitudinal mode erbium-doped fiber laser." *Optics Communications* 297 (2013): 98-101.
26. Gu, Runyan, Zhilong Li, Cheng Lei, Sheng Li, Du Wang, and Xinghuan Wang. "Thulium-Doped Fiber Laser and Its Application in Urinary Lithotripsy." *Journal of Medical and Biological Engineering* 43, no. 4 (2023): 351-361.
27. Pal, Debasis, Aditi Ghosh, Ranjan Sen, and Atasi Pal. "Continuous-wave and quasi-continuous wave thulium-doped all-fiber laser: implementation on kidney stone fragmentations." *Applied Optics* 55, no. 23 (2016): 6151-6155.
28. Bufetov, I. A., and E. M. Dianov. "Bi-doped fiber lasers." *Laser physics letters* 6, no. 7 (2009): 487.
29. Zhu, Xiushan, Gongwen Zhu, Chen Wei, Leonid Vasilyevich Kotov, Junfeng Wang, Minghong Tong, Robert A. Norwood, and N. Peyghambarian. "Pulsed fluoride fiber lasers at 3 μm." *JOSA B* 34, no. 3 (2017): A15-A28.
30. Sanghera, Jas S., L. Brandon Shaw, and Ishwar D. Aggarwal. "Chalcogenide glass-fiber-based mid-IR sources and applications." *IEEE Journal of selected topics in quantum electronics* 15, no. 1 (2009): 114-119.
31. Cui, Shuo, RadwanChahal, Catherine Boussard-Plédel, VirginieNazabal, Jean-Louis Doualan, Johann Troles, Jacques Lucas, and Bruno Bureau. "From selenium-to tellurium-based glass optical fibers for infrared spectroscopies." *Molecules* 18, no. 5 (2013): 5373-5388.
32. Yeh, Szu-Ming, Sheng-Lung Huang, Yi-Jen Chiu, HidenoriTaga, Pi Ling Huang, Yi-Chung Huang, Yu-Kuan Lu et al. "Broadband chromium-doped fiber amplifiers for next-generation optical communication systems." *Journal of lightwave technology* 30, no. 6 (2012): 921-927.
33. Chattopadhyay, Rik, ArindamHaldar, Mukul C. Paul, and Shyamal K. Bhadra. "Noble metal doped optical fiber for specialty light source." In *Advances in Optical Science and Engineering: Proceedings of the Third International Conference, OPTRONIX 2016*, pp. 95-105. Springer Singapore, 2017.

34. Rivera, V. A. G., F. A. Ferri, and E. Marega Jr. "Localized surface plasmon resonances: noble metal nanoparticle interaction with rare-earth ions." *Plasmonics-Principles and Applications* 1, no. 11 (2012): 283-312.
35. Cheo, P. K., and G. G. King. "Clad-pumped Yb, Ercodoped fiber lasers." *IEEE Photonics Technology Letters* 13, no. 3 (2001): 188-190.
36. Chang, Jun, Qing-Pu Wang, and Gang-Ding Peng. "Optical amplification in Yb3+-codoped thulium doped silica fiber." *Optical Materials* 28, no. 8-9 (2006): 1088-1094.
37. Chong, Andy, William H. Renninger, and Frank W. Wise. "Environmentally stable all-normal-dispersion femtosecond fiber laser." *Optics letters* 33, no. 10 (2008): 1071-1073.
38. Baumgartl, Martin, B. Ortaç, J. Limpert, and A. Tünnermann. "Impact of dispersion on pulse dynamics in chirped-pulse fiber lasers." *Applied Physics B* 107 (2012): 263-274.
39. Wang, Zhiqiang, Li Zhan, Xiao Fang, and Hao Luo. "Spectral filtering effect on mode-locking regimes transition: similariton-dissipative soliton fiber laser." *JOSA B* 34, no. 11 (2017): 2325-2333.
40. Jeon, Jinwoo, Junsu Lee, and Ju Han Lee. "Numerical study on the minimum modulation depth of a saturable absorber for stable fiber laser mode locking." *JOSA B* 32, no. 1 (2015): 31-37.
41. Gupta, Bhaswar Dutta, Sourav Das Chowdhury, DevnathDhirhe, and Mrinmay Pal. "Intermittent events due to spectral filtering induced multi-pulsing instability in a mode-locked fiber laser." *JOSA B* 37, no. 8 (2020): 2278-2286.
42. Churkin, D. V., S. Sugavanam, N. Tarasov, S. Khorev, S. V. Smirnov, S. M. Kobtsev, and S. K. Turitsyn. "Stochasticity, periodicity and localized light structures in partially mode-locked fibre lasers." *Nature communications* 6, no. 1 (2015): 7004.
43. Runge, Antoine FJ, Neil GR Broderick, and Miro Erkintalo. "Dynamics of soliton explosions in passively mode-locked fiber lasers." *JOSA B* 33, no. 1 (2016): 46-53.
44. Akhmediev, Nail, Jose M. Soto-Crespo, and Graham Town. "Pulsating solitons, chaotic solitons, period doubling, and pulse coexistence in mode-locked lasers: Complex Ginzburg-Landau equation approach." *Physical Review E* 63, no. 5 (2001): 056602.
45. Aguergaray, Claude, Antoine Runge, Miro Erkintalo, and Neil GR Broderick. "Raman-driven destabilization of mode-locked long cavity fiber lasers: fundamental limitations to energy scalability." *Optics letters* 38, no. 15 (2013): 2644-2646.
46. Gao, Lei, Tao Zhu, Min Liu, and Wei Huang. "Cross-phase modulation instability in mode-locked laser based on reduced graphene oxide." *IEEE Photonics Technology Letters* 27, no. 1 (2014): 38-41.
47. Kim, Bok Young, Jae K. Jang, Yoshitomo Okawachi, Xingchen Ji, Michal Lipson, and Alexander L. Gaeta. "Synchronization of nonsolitonic Kerr combs." *Science Advances* 7, no. 43 (2021): eabi4362.
48. Karen, X. Z., Logan G. Wright, Paul JL Webster, and James M. Fraser. "Deep nonlinear ablation of silicon with a quasi-continuous wave fiber laser at 1070 nm." *Optics letters* 38, no. 11 (2013): 1799-1801.
49. Zhao, Heng, Gai-Ming Ma, Xiang-Yue Li, Ti-Jian Li, Hu Cui, Meng Liu, Ai-Ping Luo, Zhi-Chao Luo, and Wen-Cheng Xu. "Buildup dynamics in an all-polarization-maintaining Yb-doped fiber laser mode-locked by nonlinear polarization evolution." *Optics Express* 28, no. 17 (2020): 24550-24559.
50. Wang, Zhiqiang, K. Nithyanandan, AurélienCoillet, Patrice Tchofo-Dinda, and Philippe Grelu. "Buildup of incoherent dissipative solitons in ultrafast fiber lasers." *Physical Review Research* 2, no. 1 (2020): 013101.

51. Lasers by Siegman, Anthony E. (1986) Hardcover; Revised ed. Edition, ISBN-13: 978-0935702118, ISBN-10: 0935702113

52. Barmenkov, Yuri O., Alexander V. Kir'yanov, Jose L. Cruz, and Miguel V. Andres. "Pulsed regimes of erbium-doped fiber laser Q-switched using acousto-optical modulator." *IEEE Journal of Selected Topics in Quantum Electronics* 20, no. 5 (2014): 337-344.

53. Wang, Yunzheng, Weichun Huang, Cong Wang, JiaGuo, Feng Zhang, Yufeng Song, Yanqi Ge et al. "An all-optical, actively Q-switched fiber laser by an antimonene-based optical modulator." *Laser & photonics reviews* 13, no. 4 (2019): 1800313.

54. Wang, Gaozhong, Aidan A. Baker-Murray, and Werner J. Blau. "Saturable absorption in 2D nanomaterials and related photonic devices." *Laser & Photonics Reviews* 13, no. 7 (2019): 1800282.

55. Ma, Chunyang, Cong Wang, Bo Gao, Jordan Adams, Ge Wu, and Han Zhang. "Recent progress in ultrafast lasers based on 2D materials as a saturable absorber." *Applied Physics Reviews* 6, no. 4 (2019).

56. Kurkov, A. S. "Q-switched all-fiber lasers with saturable absorbers." *Laser Physics Letters* 8, no. 5 (2011): 335-342.

57. Lasers: Fundamentals and Applications - K. Thyagarajan, AjoyGhatak

58. Principles of lasers, Orazios Velto, **Publisher:** Plenum Press, New York-London, 1977, **ISBN Code:** 0306310449

59. Haus, Herman A. "Mode-locking of lasers." *IEEE Journal of Selected Topics in Quantum Electronics* 6, no. 6 (2000): 1173-1185.

60. Han, Ying, YubinGuo, Bo Gao, Chunyang Ma, Ruohan Zhang, and Han Zhang. "Generation, optimization, and application of ultrashort femtosecond pulse in mode-locked fiber lasers." *Progress in Quantum Electronics* 71 (2020): 100264.

61. Woodward, Robert I. "Dispersion engineering of mode-locked fibre lasers." *Journal of Optics* 20, no. 3 (2018): 033002.

62. Lau, K. Y., and D. Hou. "Recent research and advances of material-based saturable absorber in mode-locked fiber laser." *Optics & Laser Technology* 137 (2021): 106826.

63. Jiang, Tian, Ke Yin, Cong Wang, Jie You, Hao Ouyang, Runlin Miao, Chenxi Zhang et al. "Ultrafast fiber lasers mode-locked by two-dimensional materials: review and prospect." *Photonics Research* 8, no. 1 (2020): 78-90.

64. Introduction to fiber optics, By Ajoy Ghatak_ and K. Thyagarajan , **ISBN: 978-1316644010** publisher: **Cambridge University Press, 2017.**

65. Nonlinear fiber optics by Govind P. Agrawal, Sixth Edition • 2019, ISBN: 978-0-12-817042-7, Academic Press, Elsevier

66. Ma, Chunyang, Xiaojian Tian, Bo Gao, and Ge Wu. "Numerical simulations on influence of the saturable absorber in Er-doped fiber laser." *Optics Communications* 410 (2018): 941-946.

67. Du, Wenxiong, Heping Li, Junwen Li, Pinghe Wang, Shangjian Zhang, and Yong Liu. "Mechanism of dissipative-soliton-resonance generation in fiber laser mode-locked by real saturable absorber." *Optics Express* 26, no. 16 (2018): 21314-21323.

68. Cheng, Zhaochen, Huihui Li, Hongxing Shi, Jun Ren, Quan-Hong Yang, and Pu Wang. "Dissipative soliton resonance and reverse saturable absorption in graphene oxide mode-locked all-normal-dispersion Yb-doped fiber laser." *Optics Express* 23, no. 6 (2015): 7000-7006.
69. Hongzhi, Yang. "Saturable absorption and two-photon absorption in graphene." (2012).
70. Qi, Yaoyao, Mengyuan Liu, Nannan Luan, Song Yang, Zhenxu Bai, Bingzheng Yan, Ding Jie, Yulei Wang, and Zhiwei Lu. "Recent research progress of nonlinear multimode interference mode-locking technology based on multimode fibers." *Infrared Physics & Technology* 121 (2022): 104017.
71. Han, Ying, YubinGuo, Bo Gao, Chunyang Ma, Ruohan Zhang, and Han Zhang. "Generation, optimization, and application of ultrashort femtosecond pulse in mode-locked fiber lasers." *Progress in Quantum Electronics* 71 (2020): 100264.
72. Smirnov, S. V., S. Sugavanam, O. A. Gorbunov, and D. V. Churkin. "Generation of spatio-temporal extreme events in noise-like pulses NPE mode-locked fibre laser." *Optics Express* 25, no. 19 (2017): 23122-23127.
73. Chen, Feihong, QiangHao, and Heping Zeng. "Optimization of an NALM mode-locked all-PM Er: fiber laser system." *IEEE Photonics Technology Letters* 29, no. 23 (2017): 2119-2122.
74. Bowen, Patrick, Harman Singh, Antoine Runge, Richard Provo, and Neil GR Broderick. "Mode-locked femtosecond all-normal all-PM Yb-doped fiber laser at 1060 nm." *Optics Communications* 364 (2016): 181-184.
75. Chong, Andy, William H. Renninger, and Frank W. Wise. "Properties of normal-dispersion femtosecond fiber lasers." *JOSA B* 25, no. 2 (2008): 140-148.
76. Litago, IñakiAporta, Daniel Leandro, MaríaÁngelesQuintela, Rosa Ana Pérez-Herrera, Manuel López-Amo, and Jose Miguel López-Higuera. "Tunable SESAM-based mode-locked soliton fiber laser in linear cavity by axial-strain applied to an FBG." *Journal of Lightwave Technology* 35, no. 23 (2017): 5003-5009.
77. Boulanger, Vincent, Michel Olivier, Félix Guilbert-Savary, François Trépanier, Martin Bernier, and Michel Piché. "All-fiber Mamyshev oscillator enabled by chirped fiber Bragg gratings." *Optics Letters* 45, no. 12 (2020): 3317-3320.
78. Kim, Dohyun, Shuangyou Zhang, Dohyeon Kwon, Ruoyu Liao, Yifan Cui, Zhigang Zhang, Youjian Song, and Jungwon Kim. "Intensity noise suppression in mode-locked fiber lasers by double optical bandpass filtering." *Optics Letters* 42, no. 20 (2017): 4095-4098.
79. Ouyang, Chunmei, Ping Shum, Honghai Wang, JiaHaur Wong, Kan Wu, Songnian Fu, Ruoming Li, E. J. R. Kelleher, A. I. Chernov, and E. D. Obraztsova. "Observation of timing jitter reduction induced by spectral filtering in a fiber laser mode locked with a carbon nanotube-based saturable absorber." *Optics letters* 35, no. 14 (2010): 2320-2322.
80. Zou, Meng, Yanli Ran, Jie Hu, Zhikun Xing, Zhijun Yan, Chen Liu, Qizhen Sun, and Deming Liu. "Multiwavelength mode-locked fiber laser based on an all fiber Lyot filter." *IEEE Photonics Technology Letters* 32, no. 22 (2020): 1419-1422.
81. Luo, Xing, Tong Hoang Tuan, Than Singh Saini, HoaPhuocTrung Nguyen, Takenobu Suzuki, and YasutakeOhishi. "Tunable and switchable all-fiber dual-wavelength mode locked laser based on Lyot filtering effect." *Optics Express* 27, no. 10 (2019): 14635-14647.

82. Wu, Peng, Qiang Zhou, Yueqi Wang, Guangwei Deng, Yunru Fan, Si Shen, Qiang Xu, Yunxiang Wang, Haizhi Song, and You Wang. "Wavelength-tunable passively mode-locked all-fiber laser at 1.5 μm." *Applied Optics* 58, no. 19 (2019): 5143-5147.
83. Ahmad, Harith, F. D. Muhammad, M. Z. Zulkifli, and SulaimanWadi Harun. "Graphene-based mode-locked spectrum-tunable fiber laser using Mach–Zehnder filter." *IEEE Photonics Journal* 5, no. 5 (2013): 1501709-1501709.
84. Ma, Chunyang, AnkitaKhanolkar, YiminZang, and Andy Chong. "Ultrabroadband, few-cycle pulses directly from a Mamyshev fiber oscillator." *Photonics Research* 8, no. 1 (2020): 65-69.
85. Liu, Zhanwei, Zachary M. Ziegler, Logan G. Wright, and Frank W. Wise. "Megawatt peak power from a Mamyshev oscillator." *Optica* 4, no. 6 (2017): 649-654.
86. Renninger, William H., Andy Chong, and Frank W. Wise. "Pulse shaping and evolution in normal-dispersion mode-locked fiber lasers." *IEEE Journal of Selected Topics in Quantum Electronics* 18, no. 1 (2011): 389-398.
87. Zhao, L. M., D. Y. Tang, and J. Wu. "Gain-guided soliton in a positive group-dispersion fiber laser." *Optics letters* 31, no. 12 (2006): 1788-1790.
88. Strickland, Donna. "Nobel Lecture: Generating high-intensity ultrashort optical pulses." *Reviews of Modern Physics* 91, no. 3 (2019): 030502.
89. Yilmaz, Tolga, Laurent Vaissie, MehmetcanAkbulut, David M. Gaudiosi, Lowell Collura, Timothy J. Booth, Jayesh C. Jasapara et al. "Large-mode-area Er-doped fiber chirped-pulse amplification system for high-energy sub-picosecond pulses at 1.55 μm." In *Fiber Lasers V: Technology, Systems, and Applications*, vol. 6873, pp. 330-337. SPIE, 2008.
90. Krylov, Alexander, Andrey Senatorov, Alexey Gladyshev, YuryYatsenko, Alexey Kosolapov, Anton Kolyadin, Maxim Khudyakov, Mikhail Likhachev, and Igor Bufetov. "10-μJ-level femtosecond pulse generation in the erbium CPA fiber source with microstructured hollow-core fiber assisted delivery and nonlinear frequency conversion." *Applied Optics* 62, no. 21 (2023): 5745-5754.

Chapter: 02

Fiber saturable absorber based Q-switched laser at 1550 nm

Abstract

This chapter delves into the fabrication and characterization process of a specialty fiber as well as working principle of different type of fiber saturable absorbers. We have fabricated an erbium-doped fiber by modified chemical vapor deposition (MCVD) process in combination with solution doping technique where erbium is incorporated inside the core via solution doping process. Different important characterization of the erbium doped fiber including linear and non-linear absorptions are shown and discussed. Finally, the fabricated erbium doped fiber is used as a saturable absorber in a cavity where the gain medium is an Er/Yb co-doped double clad optical fiber. Performance of the developed Q-switched laser is shown in detail by altering pump power and with different length of fiber saturable absorber.

2.1. Introduction: To achieve high energy pulses directly from an oscillator, Q-switching is the most adopted technique [1-2]. Although Q-switched pulses are achievable via both an active method and a passive method, researchers tend to avoid the active method owing to its design complexity such as the requirements of an acousto-optic modulator (AOM) and additional electronic setup to run the AOM [3]. In the passive Q-switching method, a material-based saturable absorber (SA) is inserted inside the cavity which modulates the cavity loss periodically as the transmission of the SA depends on the intra-cavity power in a nonlinear fashion [4-5]. The thin film-based SA's such as 2D-TMDs, Graphenes, CNTs, black phosphorus, and topological insulators [6-11] are widely adopted because of their easy fabrication process and good performance. Although researchers have achieved good quality pulses by using these materials, use of these materials is limited by their low damaged threshold to generate high energy pulses. With that performance of these material-based SAs also tends to degrade with time due to oxidation and exposure to heat during performance [12]. A great alternative to materials-based SAs are specialty optical fiber-based SAs, which have higher damaged thresholds and also they are easier to incorporate inside a cavity to maintain all fiber structure which makes the laser more robust in nature [13]. A fiber saturable absorber (FSA) is nothing but a single/multi-mode fiber doped with suitable material inside its core such that the fiber possesses both linear and non-linear loss at the working wavelength regime. The incorporation of such fiber inside a cavity modulates the cavity loss periodically which generates repetitive output.

2.2. Working principle of Fiber saturable absorbers: The main criteria for a fiber to work as a SA is to have an absorption band at the emission band of the gain medium that is used to form the laser. To work as a superior SA, the absorption cross-section of the FSA should be greater than the emission cross-section of the gain fiber [13]. The first ever FSA-based Q-switched laser was built at 1084 nm where an Nd^{3+} doped fiber was used as the gain fiber and a Cr^{4+} doped fiber was utilized as the SA element [13]. It is reported that the absorption cross-section of the Cr-doped fiber is 5 times larger than the emission spectrum of Nd^{3+} doped fiber at 1084 nm. There are few processes act in the fiber which determines the dynamical behavior of the FSAs.

2.2.1. High ion pair concentration: During the fabrication of rare-earth doped silica fibers if the concentration of active ion goes high, they can appear in a clustered form inside the core. This ion pair can exchange energy upon excitation. Upon excitation of the pump, one of the ion goes to the excited and another losses energy and decays to ground state which is

known as up-conversion; as a result, effectiveness of one ions is lost. Although this process limits the performance of the laser or amplifier, these fibers can affect the pulse dynamics of the laser due to its unique loss property. In study it is found that heavily doped Er-doped fiber and Ho-doped fiber laser shows a self-pulsing behavior [14]. Tm-doped fiber with high concentration has been utilized as a SA in an Er-doped fiber laser as the Tm-doped fiber has an absorption band at 1550 nm region [15].

***2.2.2.* Fiber saturable absorber with non-radiative and radiative transition from excited state:** As the rare-earth doped fibers have their absorption and radiative emission bandwidth at the same wavelength range, they all can be used as a SA at respective wavelength range. However, as the absorption band of the rare-earth doped fibers also corresponds to the radiative transition, the excited state life-time is expected to be in millisecond region which increases the Q-switched pulse duration as a consequence. To overcome the problem an interesting method has been adopted where the FSA is placed inside a sub-resonator to reduce its lifetime by inducing stimulated emission. In an Yb-doped fiber laser (1050-1080 nm) a segment of Bi-doped fiber has been placed by making a sub cavity at resonance wavelength 1160 nm [16]. Similar configuration is exploited for a Ho-doped FSA; in a laser of Yb-doped gain medium lasing at 1125 nm the FSA is placed in another resonator of resonance wavelength 2050 nm [17].

Beside that some rare-earth materials and most transition metal relax back to ground state by non-radiative transition to the host material silica. The process of relaxing is fast in this case and fiber containing these ions can perform as SA. Transition metal such a Cr [18], and Sm [19] doped fiber has been utilized as SA in Nd and Yb-doped cavity respectively.

***2.2.3.* Multi-modal interference**: A typical multi-modal interference (MMI) based SA contains a passive multimode fiber (MMF) of a particular length spliced between two SMF [20]. However new configurations such as introducing graded index MMF or an all-core fiber have been being reported to enhance the performance of the laser [21]. In these type of architectures, the length of the MMF is the most crucial parameter which is needed to be optimized. When the self-imaging length of the high peak power pulse matches with the length of the MMF, the pulse gets transmitted and the lower intensity part gets suppressed. The transmission curve of a MMI-based laser is sinusoidal in nature having a potential to generate various pulse dynamics. Exploiting this technique, several Q-switched and mode-locked laser at different wavelength region have been developed [22-24].

A list of different specialty FSA and their working wavelength is shown in table 2.1.

Table: 2.1: Literature related to FSA based Q-switched fiber laser

Gain medium	Dopant of SA	Pulse duration (μs)	Pulse energy (μJ)	Ref.
	Samarium	0.200	27	25
	Samarium	0.041	70	26
Ytterbium	Titanium	2.55	0.191	27
	Thulium	2.87	0.080.7	28
	Thulium	0.42	9	29
	Thulium	0.1	350	30
	Thulium	7.4	22.8	31
Erbium	Thulium	3.28	0.134	32
	Thulium	6.94	0.157	33
	Thulium/Holmium	8.2		34
	Thulium/Holmium	7.8		35
	Thulium/Holmium	10.46	0.496	36
	Samarium	0.45		37
	Chromium	3.85	0.230	38
	Erbium	5.32		39
Thulium	Holmium	1.1		40

2.3. MCVD process of preform fabrication: MCVD is one of the most used technique of optical fibers preform fabrication beside vapor phase axial deposition (VPD), plasma chemical vapor deposition etc [41-43]. It has a precise control over the refractive index of the core by controlling concentration of different constituent materials. A schematic of the whole MCVD set up is shown in figure 2.1. To start the preform making process, a hollow silica rod of suitable inner and outer diameter is inserted in a mechanical lathe. Fluorine gas at suitable flowing rate is used to clean the tube. To maintain the uniformity, all the process is done under constant rotation of the tube placed in a rotor as shown in figure 2.2(a). Following that, a soot layer of constituent materials is deposited inside the tube by flowing halide gases through the tube. To make the cladding, layer of SiO_2 is deposited only. The porous soot layer of SiO2, GeO_2 and P_2O_5 are deposited to increase the refractive index at the core. The source of SiO_2, GeO_2 and P_2O_5 are gases of $SiCl_4$, $GeCl_3$ and $POCl_3$. These gases are produced by bubbling suitable flow of high purity O_2 gas into respective liquid solution inside a bubbler as shown in figure 2.1. After the deposition of the porous soot layer inside the silica tube, such

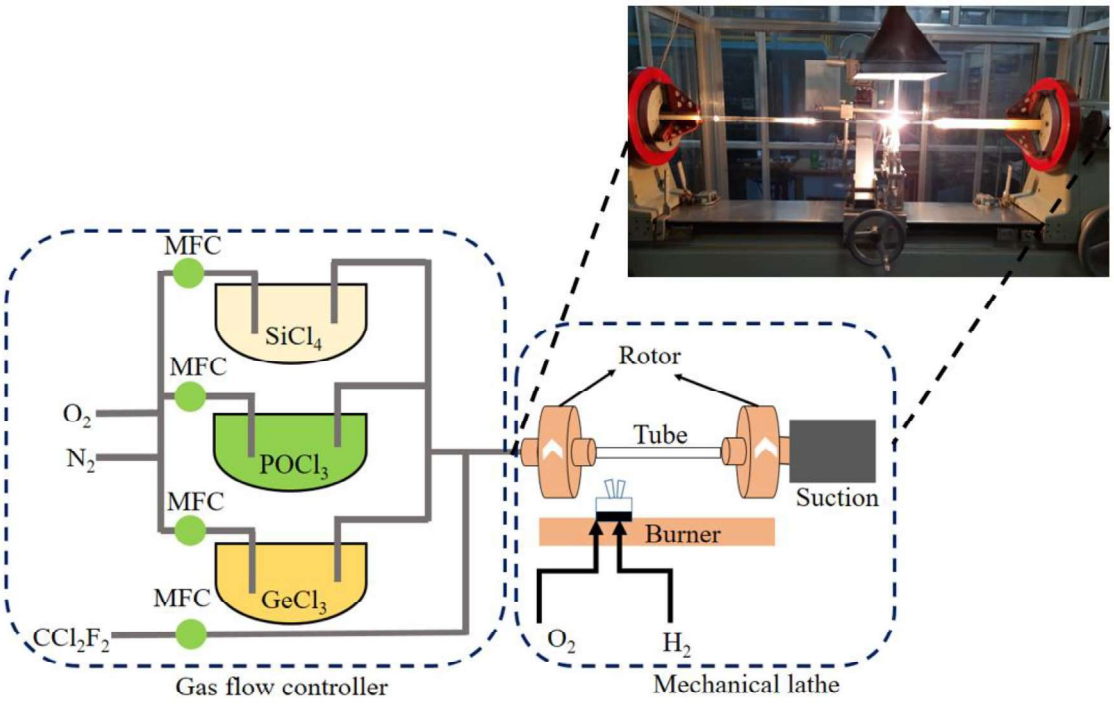

Figure 2.1: Schematic of a MCVD setup indicating direction of gas flow

porous soot layer is ready for solution doping. Figure 2.2(b) is taken during the soot layer deposition. In the solution doping process the active ions are incorporated inside the core region of the preform. The silica tube with deposited soot layer is soaked in an aqueous solution of required dopants for a 1 hour. With time the solution will be adsorbed in the soot

layer. The tube is again placed in the lathe and heated up at around 800^0 c. In this process the halide salts are converted into respective oxides. After the oxidation process a gradual heating from 1000-1900^0 c is done to make a transparent layer from the soaked soot layer. At last, the collapsing is done at 2000^0 c. Functions of different dopants (in oxide form) are listed in Table 2.2 [44-46].

Table: 2.2: Function of passive dopants during fiber fabrication

Dopants name	**Nature**	**Role**	**Linear refractive index**	**Non-linear refractive index (esu)**
GeO_2	Passive	Network modifiers; Increases refractive index, Increases rare earth solubility	1.65	45×10^{-14}
Al_2O_3	Passive	Network modifiers; Increases refractive index, Increases rare earth solubility	1.76	16.9×10^{-14}

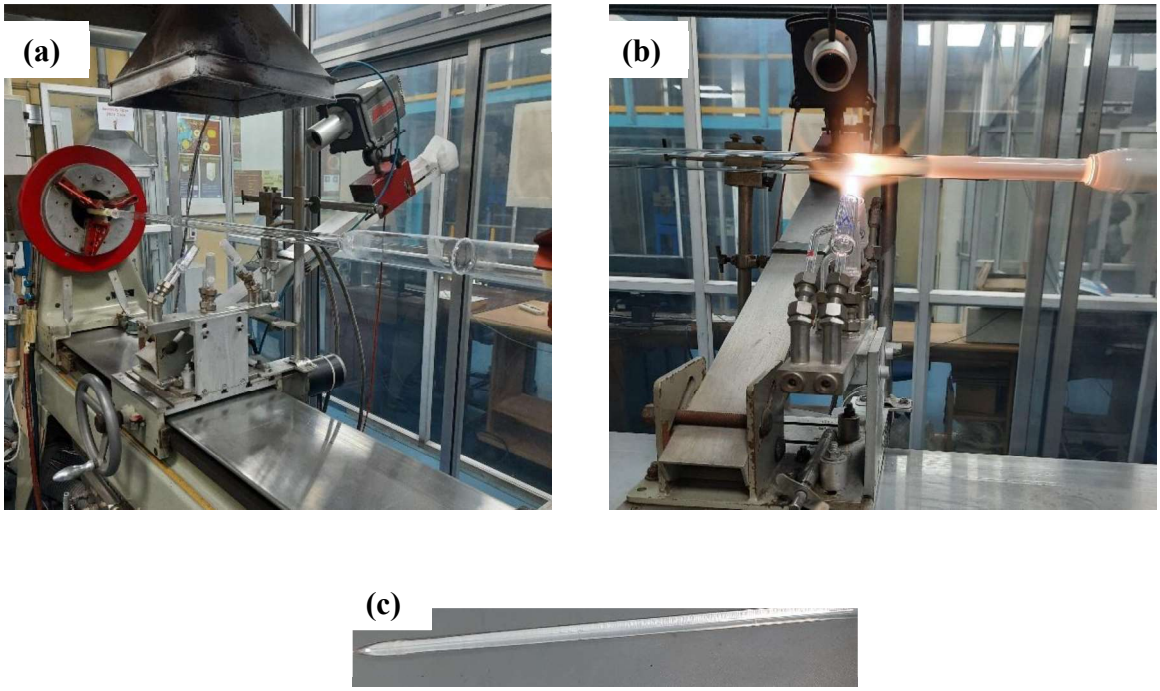

Figure 2.2: (a) Clean silica tube connected on the lathe (b) Developed soot layer inside the silica rod (c) A collapsed preform

Once the preform is ready, the fiber would be drawn from a fiber drawing tower. To control the parameters like dispersion, cut off wavelength etc., sometimes the dimension of the core needs to be lowered than the determined value. In that case Rod-in-tube method is followed to decrease the core: cladding aspect ratio. The fabricated lower dimensional preform rod is inserted in a hollow large thickness silica tube of matching inner diameter and then drawn fiber from the composite preform rod surrounded by another hollow tube of greater inner diameter. Figure 2.2(c) is an end most version from which the fiber will be drawn.

2.4. Erbium doped fiber fabrication: The EFSA is fabricated in the laboratory by the MCVD technique. At first, the porous layer of germanium and silica is deposited at 1350 ± 10^0C temperature inside a hollow glass tube of inner diameter 17.0 mm and outer diameter 20.0 mm. An aqueous solution of a mixture of suitable molar concentration of $Al(NO_3)_3.9H_2O$ and $ErCl_3$, xH_2O is prepared and the tube with porous layer is soaked in the solution for one hour. Thus Al_2O_3 and Er_2O_3 are incorporated inside the preform. After draining out the solution from the tube, the porous layer is air-dried by flowing Nitrogen gas at room temperature. By the flow of Oxygen gas at 800-900^0 C, the salts are then converted to their own oxides. After that, sintering of the layer is done by slowly increasing the temperature

from 1300 to 1900^0 C. Lastly the tube is converted to a solid preform at the collapsing stage. To reduce the fiber core diameter, the preform is then over-cladded by inserting the preform inside another hollow tube of inner diameter 12.0 mm and outer diameter 20.0mm. The outer diameter of the final preform is 18.75mm. Finally, the EFSA is drawn from a fiber drawing tower from the over-cladded preform at 2000^0.

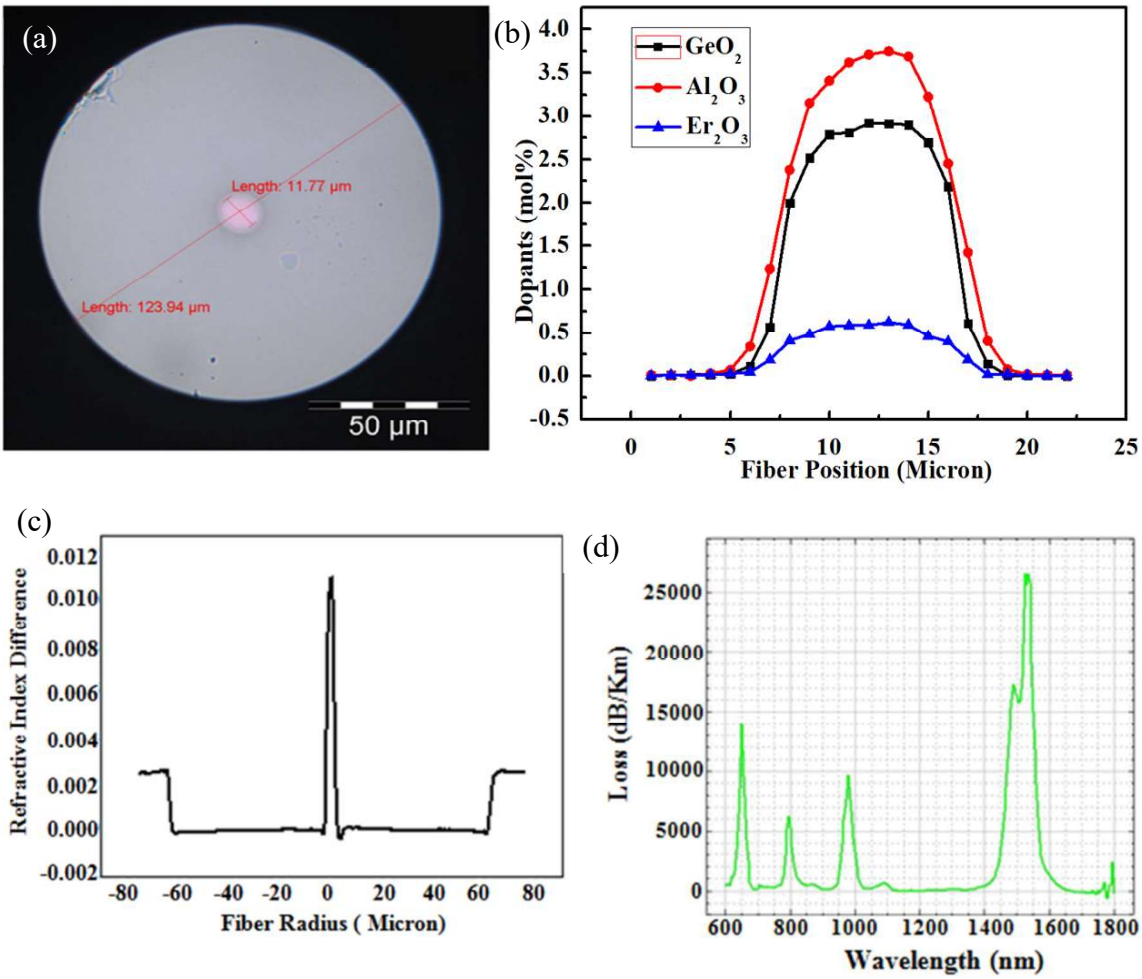

Figure 2.3: (a) Cross-section of EFSA (b) Electron probe microscopy analysis of the EFSA to check the distribution of different dopant levels along the fiber diameter (c) Refractive Index profile of the EFSA (d) Linear absorption curve of the EFSA

2.4.1. Fiber characterization: The microscopic image and the refractive index profile has been measured to get an insight about the fiber dimension and numerical aperture. Figure 2.3(a) shows the cross-sectional view of the EFSA, the core and cladding diameter are 11.7 µm and 123.9 µm respectively. To check the doping concentration of the material inside the core EPMA of the EFSA is performed. Concentration of different materials along the core diameter are shown in figure 2.3(b) which shows EFSA contains 3.75 mol% Al_2O_3, 0.57 mol% Er_2O_3, and 2.6 mol% GeO_2 inside its core. The RI profile is shown in figure 2.3(c) and the NA

is found to be 0.13. Figure 2.3(d) depicts the linear absorption curve which shows the absorption at 976 nm is around 10dB/m and 15 dB/m at 1550nm equivalent to the presence of 5700 ppm of Er_2O_3.

The non-linear transmission of the EFSA at 1556 nm is measured by twin-detector method [47]. A lab made femtosecond laser at 1556 nm is utilized to perform this test. The laser delivers 760 fs pulses at a repetition rate of 25 MHz. The schematic setup to perform this experiment is shown in figure 2.4(a). To record data, the optical power is varied by a variable optical attenuator (VOA) and output power from two ends are enlisted. As our aim is to use the fiber as a SA, the transmissivity of the fiber is expected to increase with the intensity following equation-1.21. Figure 2.4(b) depicts the non-linear transmission curve of 30 cm of EFSA. We have fitted the obtained data with equation-1.21. From the fitted curve we find

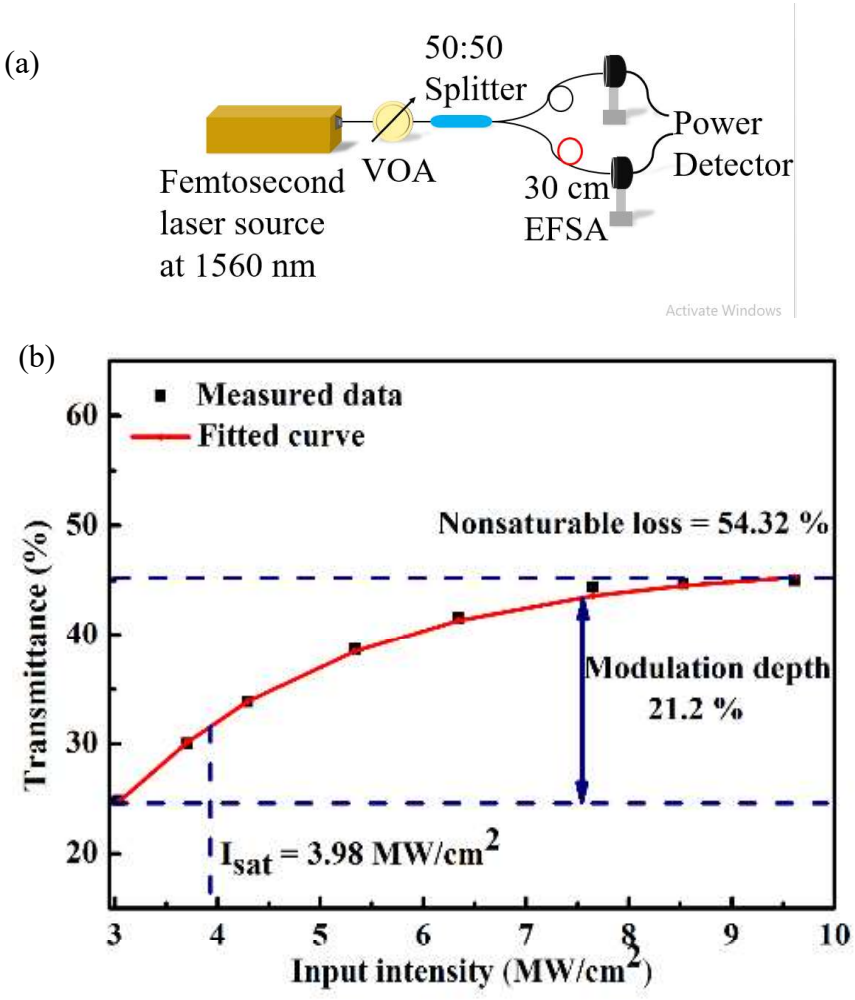

Figure 2.4: (a) Schematic of Twin detector setup to measure nonlinear transmission (b) non-linear transmission curve of 30 cm of EFSA

that the modulation depth is 21 %. The saturation intensity and non-saturable loss are found to be 3.98 MW/cm2 and 54.32 % respectively.

2.5. Design and performance of Q-switched fiber laser using an erbium doped fiber saturable absorber:

2.5.1. Experimental setup: Figure 2.5 represents the schematic of the Q-switched laser designed by using the erbium doped fiber as a SA. To make the laser, an Er/Yb co-doped double clad fiber of length 2 meter is used as the gain medium in cladding pumping scheme. The gain fiber is pumped by a multimode laser diode of 976 nm wavelength through a pump combiner. After the gain fiber a cladding mode stripper (CMS) is utilized to extract the excess pump. A polarization-insensitive isolator (PI) is connected after the CMS to ensure the unidirectional circulation of light. A 90:10 fiber coupler is used after the PI and the 90% port served as the feedback to the signal port of the pump combiner. Different length of EFSA is spliced between the coupler and the signal port of the combiner to check the Q-switching ability. The cavity length is about 6.5 meters without considering the length of EFSA. Measurements at spectral domain are performed by an optical spectrum analyzer (YOKOGAWA A6319). Temporal measurements are done by the combination of a 2.5 GHz Oscilloscope (Tektronix-DPO7254C) along with a fast photodiode (5 GHz, Thorlabs).

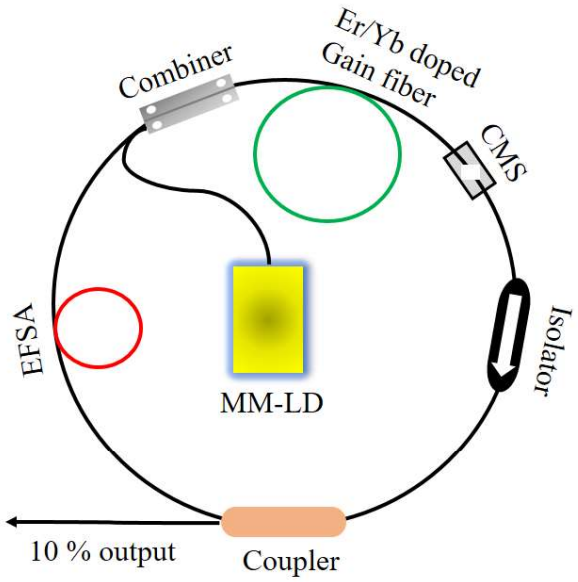

Figure 2.5: A schematic of the experimental setup; EFSA: Erbium fiber saturable absorber; CMS: Cladding mode stripper; MM-LD: Multimode laser diode

2.5.2. Results: The cavity is first checked in simple ring configuration without incorporating the FSA. As the laser crosses the CW threshold of pump power, 600 mW, a spectrum with multiple peaks are seen in OSA. The emission wavelength is not fixed but always in a range between 1595-1615 nm. With time position of the peaks are shifting as there is no wavelength selective components like a band-pass filter. Emission at higher wavelength indicates a minimal presence of loss in the cavity. A spectrum at 900 mW of pump power is presented in figure 2.6(a). As the spectrum is broad in nature, several number of longitudinal modes are excited and the mode-hopping among those modes because of the gain competition causes a random pulsing. By looking into the oscilloscope, pulses of very low intensity are detected. A snapshot of oscilloscope is presented showing the presence of low intensity pulses in figure 2.6(b).

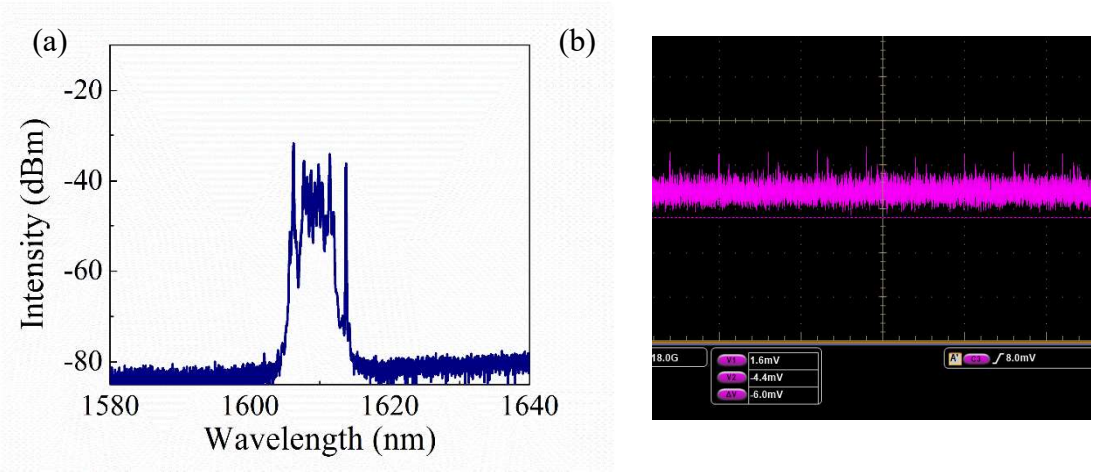

Figure 2.6: (a) Spectrum of the laser in CW condition (b) Oscilloscope snapshot shows the presence of low intensity pulses

To check the Q-switching ability, 30 cm EFSA is connected in the cavity as shown in figure 2.5. The performance of the laser is also checked by varying the length of the EFSA in the range of 20 cm to 60 cm. In the next two sub-sections all the obtained outcomes are presented.

2.5.2.A: Performance of the EFSA with pump power at a fixed length: After connecting the EFSA, at lower pump power the output pulses are not stable because of insufficient gain in the cavity. Low intensity pulses with random time interval are spotted in the oscilloscope. As the pump power is increased to 1.2 W the pulse train stabilizes. Being aware of the optical damage threshold of other components (mainly isolator), the maximum pump power is kept

at 2.4 W. The output pulse train below 1.2 W (unstable) and above 1.2 W (stable) are shown in figure 2.7.

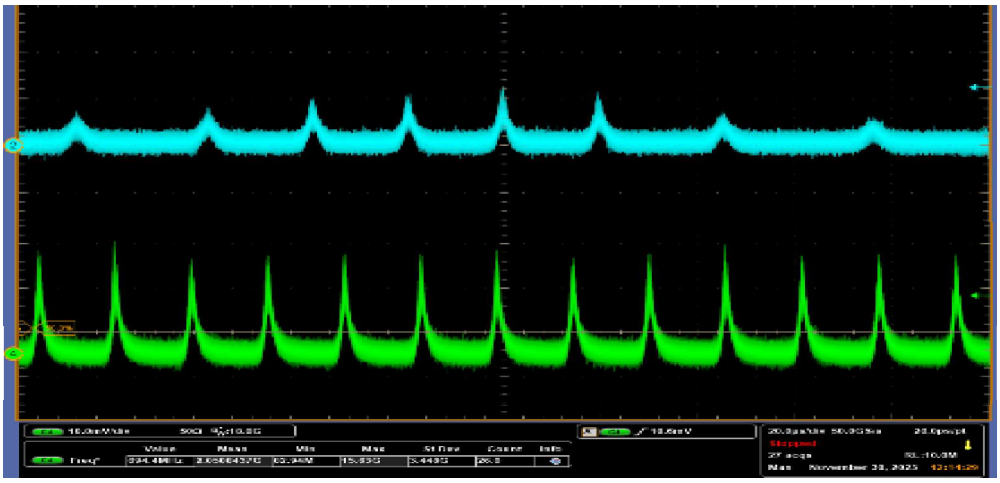

Figure 2.7: Unstable (above) and stable (below) Q-switched pulse train

Figure 2.8(a) depicts the output spectrum of the laser with central wavelength at 1565.9 nm. With the increment of the pump power, the spectral bandwidth broadens slightly from 1.36 nm to 1.52 nm. During the pump power increment, no spectral or temporal instability has been observed. At the stable region, the pulse width decreases with the pump power whereas the repetition rate has been noticed to be increasing as shown in figure 2.8(b), which is a key property of any passively Q-switched laser [48]. At the starting of the stable pulsing, the pulse duration is 2.25 μs with a repetition rate of 23.64 kHz. Next by increasing the pump power to the highest value, 2.4 W, the laser delivered pulses of minimum pulse width and a maximum repetition rate which are 1.87 μs and 38.27 kHz respectively. In figure 2.8(c), four pulse train recorded at different pump power have been presented in equal time span to show the change in repetition rate. Figure 2.8(d) depicts the change of pulse width with the variation of pump power. RF spectrum of the laser at 2.4 W pump power has been shown in figure 2.8e. The signal-to-noise ratio at the fundamental frequency is approximately 58 dB (Inset of figure 2.8(e)). Variation of the output power and pulse energy with pump power has been presented in figure 2.8f. It is found that the average power and pulse energy increases linearly with the pump power. The maximum average power and maximum pulse energy obtained from the laser are 74.6 mW and 1.95 μJ respectively at 2.4 W pump power. As shown in figure 2.8c, the gap between consecutive pulses are noticed to be 26.1 μs at 2.4 W of pump power. The standard deviation from the mean peak intensity (0.97) has been measured to check the pulse to pulse intensity fluctuation which is found to be 1.9 %.

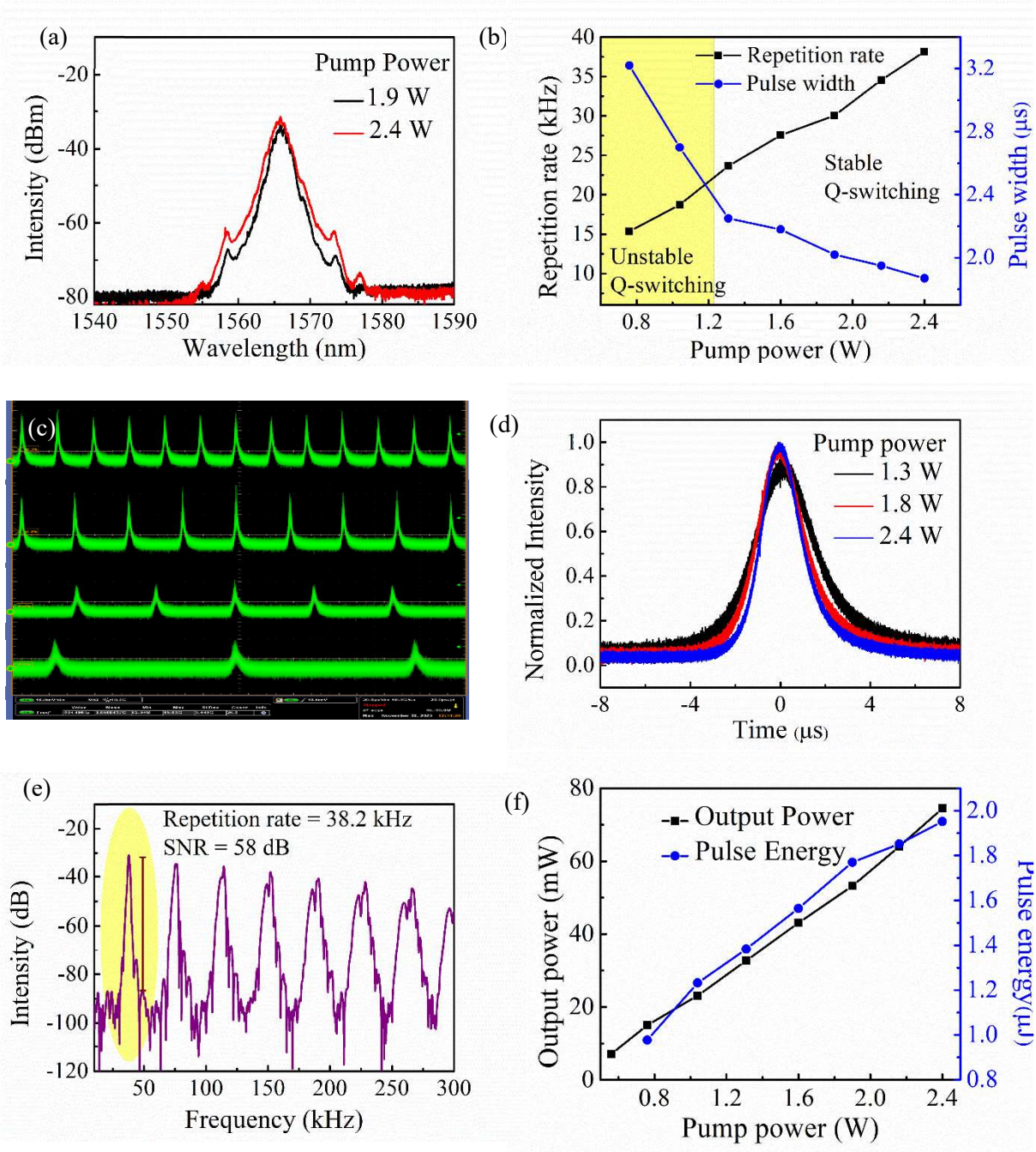

Figure 2.8: (a) Output spectra at different pump power (b) Variation of repetition rate and pulse duration with pump power (c) pulse train showing the variation of repetition rate (d) Intensity profile of single pulse to indicate pulse width variation (e) RF spectrum at maximum pump power of 2.4 Watt. (f) Variation of output power and pulse energy with pump power

2.5.2.B: Performance of different length of EFSA at maximum pump power: The performance of the laser has been checked by varying the length of the EFSA at the maximum pump power of 2.4 W. Five different lengths varying from 20 cm to 60 cm has been connected

in the cavity. Stable Q-switched pulse train has been appeared almost at pump power of 1.2 W at each cases. It has been observed that as the length of EFSA is increased the pulse width and repetition rate at maximum pump power decreases. Figure 2.9(a) represents the variation of pulse width and repetition rate with the length of the EFSA. Although the average power decreases with the increment of the length, it is worth observing that the single pulse energy tends to increase. As the length varied from 20 cm to 60 cm, the single pulse energy increases from 1.6 μJ to 2.81 μJ. Variation of average output power and pulse energy has been shown in figure 2.9(b).

Table 2.3: Variation of Pulse width, repetition rate and pulse energy at different length of EFSA

Length of EFSA (cm)	Pulse width (μS)	Repetition rate (kHz)	Pulse energy (μJ)
20	1.91	47.0	1.60
30	1.87	38.1	1.95
40	1.56	33.0	2.21
50	1.44	28.3	2.50
60	1.36	24.8	2.81

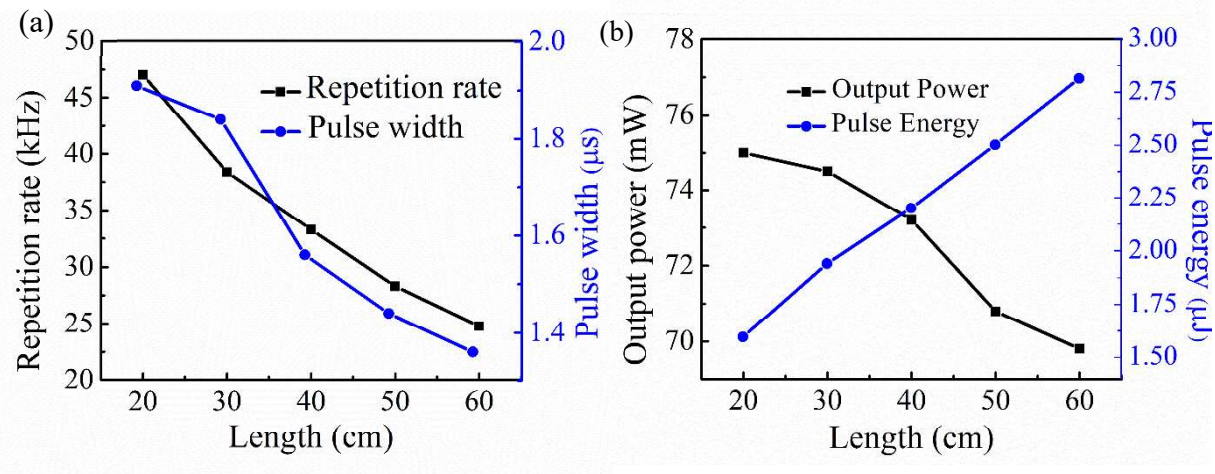

Figure 2.9: (a) Variation of repetition rate and pulse width with the length of EFSA (b) Variation of output power and pulse energy with the length of EFSA

2.6: Conclusions: To put the work briefly, an erbium doped fiber has been fabricated by MCVD process in combination with solution doping technique and important characterizations have been done. It is found that the fiber has a non-linear transmission

property which is appropriate to serve as a saturable absorber. Then the fiber is utilized in an Er/Yb co-doped gain fiber based cavity as a saturable absorber. The cavity delivers stable Q-switched pulses at different length of SA. Maximum energy per pulse extracted from the cavity is 2 uJ. The study also confirms that FSA may not be a good choice to generate mode-locked pulse as the life-time of the rare-earth atoms are sufficiently large.

{Bibliography}

1. Alvarez-Chavez, Jose ALFREDO, Herman L. Offerhaus, Johan Nilsson, P. W. Turner, W. A. Clarkson, and D. J. Richardson. "High-energy, high-power ytterbium-doped Q-switched fiber laser." *Optics letters* 25, no. 1 (2000): 37-39.

2. Singh, Neetesh, Jan Lorenzen, Milan Sinobad, Kai Wang, Andreas C. Liapis, Henry C. Frankis, Stefanie Haugg et al. "Silicon photonics-based high-energy passively Q-switched laser." *Nature Photonics* (2024): 1-7.

3. Huang, Haizhou, Nan Li, Hongchun Wu, Huagang Liu, Jing Deng, Wen Weng, Jinhui Li, and Wenxiong Lin. "Obtaining constant sub-25 ns pulse in a Q-switched Tm laser with around 100 kHz repetition frequency." *Optics & Laser Technology* 172 (2024): 110478.

4. Ajmal, Rizwan, Shakeela Bibi, Rizwan Ahmed, M. Sohail, H. Asghar, Z. A. Umar, N. Shahzad, and M. A. Baig. "The role of saturable absorbers thickness in the Q-switching of the erbium-doped fiber laser." *Laser Physics Letters* 20, no. 3 (2023): 035101.

5. Muhammad, Nur Ainnaa Mardhiah, Noor Azura Awang, and Hatijah Basri. "Recent advancements review in zinc oxide and titanium dioxide saturable absorber for ultrafast pulsed fiber laser." *Optik* (2023): 170855.

6. Peng, Xi, and Yixin Yan. "Graphene saturable absorbers applications in fiber lasers." *Journal of the European Optical Society-Rapid Publications* 17, no. 1 (2021): 16.

7. Shang, Ce, Yongbiao Zhang, Haoye Qin, Boqu He, Chenghong Zhang, Jingxuan Sun, Jing Li et al. "Review on wavelength-tunable pulsed fiber lasers based on 2D materials." *Optics & Laser Technology* 131 (2020): 106375.

8. Mohanraj, J., V. Velmurugan, and S. Sivabalan. "Transition metal dichalcogenides based saturable absorbers for pulsed laser technology." *Optical Materials* 60 (2016): 601-617.

9. Chen, Yu, Chujun Zhao, Shuqing Chen, Juan Du, Pinghua Tang, Guobao Jiang, Han Zhang, Shuangchun Wen, and Dingyuan Tang. "Large energy, wavelength widely tunable, topological insulator Q-switched erbium-doped fiber laser." *IEEE Journal of Selected Topics in Quantum Electronics* 20, no. 5 (2013): 315-322.

10. Zhang, Meng, Qing Wu, Feng Zhang, Lingling Chen, Xinxin Jin, Yuwei Hu, Zheng Zheng, and Han Zhang. "2D black phosphorus saturable absorbers for ultrafast photonics." *Advanced Optical Materials* 7, no. 1 (2019): 1800224.

11. Lü, Yanjia, Chen Wei, Han Zhang, Zhe Kang, Guanshi Qin, and Yong Liu. "Wideband tunable passively Q-switched fiber laser at 2.8 μm using a broadband carbon nanotube saturable absorber." *Photonics Research* 7, no. 1 (2019): 14-18.

12. Wang, Mengxia, Ying Wang, Yi Wu, Hao Ma, Hang Jiang, Yuanan Zhao, Yujie Peng et al. "Tunable and Robust Mid-Infrared Saturable Absorber Employing Tungsten Doping Cadmium Oxide." *Advanced Functional Materials* 34, no. 1 (2024): 2307234.

13. Tordella, Laurent, Hocin Djellout, Bernard Dussardier, André Saïssy, and Gérard Monnom. "High repetition rate passively Q-switched Nd3+: Cr4+ all-fibre laser." *Electronics Letters* 39, no. 18 (2003): 1307-1308.

14. Kurkov, Andrei S., Evgenii Mikhailovich Sholokhov, Andrei Viktorovich Marakulin, and L. A. Minashina. "Effect of the active-ion concentration on the lasing dynamics of holmium fibre lasers." *Quantum Electronics* 40, no. 10 (2010): 858.

15. Tsai, Tzong-Yow, Yen-Cheng Fang, and Shih-Hao Hung. "Passively Q-switched erbium all-fiber lasers by use of thulium-doped saturable-absorber fibers." *Optics express* 18, no. 10 (2010): 10049-10054.

16. Dvoyrin, Vladislav V., V. M. Mashinsky, and E. M. Dianov. "Yb-Bi pulsed fiber lasers." *Optics letters* 32, no. 5 (2007): 451-453.

17. Kurkov, A. S., E. M. Sholokhov, and O. I. Medvedkov. "All fiber Yb-Ho pulsed laser." *Laser Physics Letters* 6, no. 2 (2008): 135.

18. Kurkov, A. S. "Q-switched all-fiber lasers with saturable absorbers." *Laser Physics Letters* 8, no. 5 (2011): 335-342.

19. Grukh, Dmitrii A., Andrei S. Kurkov, Igor'M. Razdobreev, and Andrei Aleksandrovich Fotiadi. "Self-Q-switched ytterbium-doped cladding-pumped fibre laser." *Quantum electronics* 32, no. 11 (2002): 1017.

20. Qi, Yaoyao, Jingjing Wang, Zhenxu Bai, Song Yang, Jie Ding, Bingzheng Yan, Yulei Wang, and Zhiwei Lu. "Tunable all fiber multi-wavelength mode-locked laser with a large dynamic range using polarization controller coiled SMF-GIMF-SMF structure as both saturable absorber and comb filter." *Optical Fiber Technology* 74 (2022): 103055.

21. Fu, Bo, Ce Shang, Hengyu Liu, Shuzheng Fan, Kangjun Zhao, Yule Zhang, Swelm Wageh et al. "Recent advances and future outlook in mode-locked lasers with multimode fibers." *Applied Physics Reviews* 10, no. 4 (2023).

22. Zhao, Kangjun, Yan Li, Xiaosheng Xiao, and Changxi Yang. "Nonlinear multimode interference-based dual-color mode-locked fiber laser." *Optics Letters* 45, no. 7 (2020): 1655-1658.

23. Cheng, Peiyun, Mengmeng Han, Qianying Li, and Xuewen Shu. "Generation of different mode-locked states in a Yb-doped fiber laser based on nonlinear multimode interference." *Optics Express* 30, no. 20 (2022): 35911-35922.

24. Latiff, A. A., N. A. Kadir, E. I. Ismail, H. Shamsuddin, H. Ahmad, and S. W. Harun. "All-fiber dual-wavelength Q-switched and mode-locked EDFL by SMF-THDF-SMF structure as a saturable absorber." *Optics Communications* 389 (2017): 29-34.

25. Lu, Yi, and Xijia Gu. "All-fiber passively Q-switched fiber laser with a Sm-doped fiber saturable absorber." *Optics express* 21, no. 2 (2013): 1997-2002.

26. Hu, Man, Bing He, Houkang Liu, Yifeng Yang, Ye Zheng, Xiaolong Chen, Lei Zhang, and Jun Zhou. "High-peak power, all-fiber passively Q-switched laser using a Sm-doped fiber saturable absorber." *Journal of lightwave technology* 32, no. 14 (2014): 2510-2515.

27. Rahman, Mohd Fauzi Ab, Pinninty Harshavardhan Reddy, Mukul Chandra Paul, Shyamal Das, Anirban Dhar, Mohd Faizal Baharom, Anas Abdul Latiff et al. "Titanium dioxide fiber saturable absorber for Q-switched fiber laser generation in the 1-micrometer region." *Applied optics* 58, no. 13 (2019): 3495-3500.

28. Rahman, Mohd FA, Anas A. Latiff, Muhammad FM Rusdi, Kaharudin Dimyati, and Sulaiman W. Harun. "Q-switched ytterbium-doped fiber laser via a thulium-doped fiber saturable absorber." *Applied optics* 57, no. 22 (2018): 6510-6515.

29. Tsai, Tzong-Yow, Yen-Cheng Fang, and Shih-Hao Hung. "Passively Q-switched erbium all-fiber lasers by use of thulium-doped saturable-absorber fibers." *Optics express* 18, no. 10 (2010): 10049-10054.

30. Kurkov, A. S., Ya E. Sadovnikova, A. V. Marakulin, and E. M. Sholokhov. "All fiber Er-Tm Q-switched laser." *Laser Physics Letters* 7, no. 11 (2010): 795.

31. Tiu, Zian Cheak, Arman Zarei, Sin Jin Tan, Harith Ahmad, and Sulaiman Wadi Harun. "Q-Switching pulse generation with thulium-doped fiber saturable absorber." *Chinese Physics Letters* 31, no. 12 (2014): 124203.

32. Rahman, M. F. A., M. F. M. Rusdi, A. A. Latiff, M. B. Hisyam, K. Dimyati, and S. W. Harun. "Passively Q-switched Erbium doped fiber laser by incorporating a segment of Thulium doped fiber saturable absorber." In *Journal of Physics: Conference Series*, vol. 1151, no. 1, p. 012010. IOP Publishing, 2019.

33. Latiff, A. A., N. A. Kadir, E. I. Ismail, H. Shamsuddin, H. Ahmad, and S. W. Harun. "All-fiber dual-wavelength Q-switched and mode-locked EDFL by SMF-THDF-SMF structure as a saturable absorber." *Optics Communications* 389 (2017): 29-34.

34. Tao, Mengmeng, Xisheng Ye, Ping Wang, Ting Yu, Zhenbao Wang, Pengling Yang, and Guobin Feng. "A Tm–Ho codoped fiber based 38 nm wideband wavelength tunable passively Q-switched Er-doped fiber laser." *Laser Physics* 23, no. 10 (2013): 105104.

35. Tao, Mengmeng, Xisheng Ye, Zhenbao Wang, Pengling Yang, and Guobin Feng. "Tm–Ho co-doped fiber-based high repetition rate passive Q-switching of an Er-doped fiber laser." *Laser Physics Letters* 11, no. 1 (2013): 015103.

36. Anzueto-Sánchez, Gilberto, Romeo Emmanuel Nuñez-Gomez, Alejandro Martínez-Rios, Jorge Camas-Anzueto, Jesus Castrellon-Uribe, and Miguel Basurto-Pensado. "Highly Stable, Tapered Fiber Filter-Assisted, Multiwavelength Q-Switched Er-Doped Fiber Laser Based on Tm-Ho Fiber as a Saturable Absorber." *IEEE Photonics Journal* 9, no. 6 (2017): 1-8.

37. Preda, Cristina Elena, Gautier Ravet, and Patrice Mégret. "Experimental demonstration of a passive all-fiber Q-switched erbium-and samarium-doped laser." *Optics letters* 37, no. 4 (2012): 629-631.

38. Dutta, Debjit, Mukul Chandra Paul, Anirban Dhar, Shyamal Das, Muhammad Farid Mohd Rusdi, Anas Abdul Latiff, Harith Ahmad, and Sulaiman Wadi Harun. "Newly developed chromium-doped fiber as a saturable absorber at 1.55-and 2.0-μm regions for Q-switching pulses generation." *Optical Fiber Technology* 48 (2019): 144-150.

39. Wen, Zengrun, Kaile Wang, Shuangcheng Chen, Haowei Chen, Xinyuan Qi, Baole Lu, and Jintao Bai. "Narrow bandwidth Q-switched Erbium-doped fiber laser based on dynamic saturable absorption filtering effect." *Optics & Laser Technology* 140 (2021): 107045.

40. Sánchez, M. Durán, R. I. Álvarez-Tamayo, B. Posada-Ramírez, J. Alaniz-Baylón, E. Bravo-Huerta, H. Santiago-Hernández, M. V. Hernández-Arriaga, Miguel Bello-Jiménez, B. Ibarra-Escamilla, and E. A. Kuzin. "All-fiber passively Q-switched thulium-doped fiber laser by using a holmium-doped fiber as saturable absorber." In *Fiber Lasers XV: Technology and Systems*, vol. 10512, pp. 483-489. SPIE, 2018.

41. Blanc, Wilfried, Valérie Mauroy, Luan Nguyen, B. N. Shivakiran Bhaktha, Patrick Sebbah, Bishnu P. Pal, and Bernard Dussardier. "Fabrication of rare earth-doped transparent glass ceramic optical fibers by modified chemical vapor deposition." *Journal of the American Ceramic Society* 94, no. 8 (2011): 2315-2318.

42. Li, Tingye, ed. *Optical fiber communications: fiber fabrication*. Elsevier, 2012.

43. Wang, Xunsi, Qiuhua Nie, Tiefeng Xu, and Liren Liu. "A review of the fabrication of optic fiber." *ICO20: Optical Design and Fabrication* 6034 (2006): 346-354.

44. Tumminelli, Richard P., Bill C. McCollum, and Elias Snitzer. "Fabrication of high-concentration rare-earth doped optical fibers using chelates." *Journal of Lightwave Technology* 8, no. 11 (1990): 1680-1683.

45. Dimitrov, Vesselin, and Sumio Sakka. "Linear and nonlinear optical properties of simple oxides. II." *Journal of applied physics* 79, no. 3 (1996): 1741-1745.

46. Katsuyama, Toshio, Tsuneo Suganuma, Kōji Ishida, and Gyōzō Toda. "Refractive index behavior of SiO2-P2O5 glass in optical fiber application." *Optics Communications* 21, no. 1 (1977): 182-184.

47. Xu, Xiang, Minmin He, Chenjing Quan, Ruiduo Wang, Changji Liu, Qiyi Zhao, Yixuan Zhou, Jintao Bai, and Xinlong Xu. "Saturable absorption properties of ReS 2 films and mode-locking application based on double-covered ReS 2 micro fiber." *Journal of Lightwave Technology* 36, no. 22 (2018): 5130-5136.

48. Zheng, Jiancheng. "Experimental and Simulation Study of Passively Q-Switched Fiber Laser." *Available at SSRN 3958869*.

Chapter: 03

State transition SESAM-based mode-locked fiber lasers at 1064 nm

---

Abstract

This chapter delves into the performance SESAMs in generating ultrashort pulse out of a fiber laser. As the property of the state of a laser depends on various controlling parameters e.g. gain, linear and nonlinear loss, dispersion, birefringence, Kerr-nonlinearity; the combined effect of all these parameters often leads the laser to a chaotic or quasi-stable state. Often these transitions happen via some extreme events in ultra-short time span which cannot be captured by traditional measuring instruments because of their limited response time. However, novel approaches like dispersive Fourier transform (DFT), time lensing allows us to look into such random and ultra-short events in real time. In this chapter, the presence of chaotic state with extreme pulsation and their attributes has been presented for an all-normal dispersion and a net normal dispersion laser. We have observed that the reason behind the state transition are different in two cases. The spectral instabilities have been diagnosed by performing DFT and temporal amplitude fluctuation has been measured by looking into the RIN spectrum of the laser.

3.1. Introduction: Being a system with complexity, mode-locked lasers shows extreme complex behaviour relying on a combine effects of the controlling parameters. As the interplay among these factors determine the final state of the laser, any change of their values from a certain range often shifts the result from a steady state solution to a certain state that contain rich nonlinear dynamics making it worthy to explore. Net cavity dispersion of the laser plays the important role in pulse shaping and depending upon the amount of dispersion the steady state solutions of a mode-locked laser can appear in form solitons [1], dissipative solitons [2], dispersion managed solitons [3] and similaritons [4]. They all have their individual attributes which are advantageous for any specific application. As stated in the first chapter, the non-linear transmission of a saturable absorber also plays a key role in pulse shaping and stabilization. Apart from the saturable absorber, spectral filtering is also a process which induces energy dependent non-linear loss in a cavity and comes into play in stabilizing pulses at positive dispersion regime. The bandwidth and transmissivity/reflectivity of the spectral filter are the two parameters which affects the laser output. Combine effect of all these factor decides the properties of final state. All most all the laser possesses more than one stable solution which can be a multi-pulse state [5], higher order harmonic state [6] or a state bound pulse state where two pulse are strongly attached [7]. Transition between these state happens through extreme dissipative events like soliton explosion [8], rouge waves [9] or via weak/severe periodic pulsation [10]. Sometimes these intermediate state can be completely chaotic state without holding any nature of periodicity or reconstruction [11]. All these states are found as the solution of extended version of GNLSE known as cubic quintic generalised Landau equation (CQGLE) [12]. Although, a stable single pulse state is highly desirable from a laser for most of the application, researchers have found modern day applications of these extreme events in different field such as secure communication [13], random number generation [14] owing to their broad spectral bandwidth, random behaviour and incoherence.

3.2. Stable states of mode-locked fiber laser: Mode-locked laser systems deliver different kind of pulses which have distinguished spectral and temporal properties. The net cavity dispersion (NCD) is the main parameter that contributes in pulse shaping along with non-linearity. The states are classified into distinct category depending on the NCD. Brief of each category is described in this section.

3.2. A. Conventional solitons: In the realm of optical pulse propagation in anomalous dispersion regime if the dispersion induced chirp get balanced by the nonlinear chirp, the

pulse can propagate unaltered through the medium which are known as 'solitons' [15]. 'Solitons' are the static solution of NLSE in a negative dispersive medium with secant hyperbolic shape [16]. The first development of fiber laser is based on an Erbium doped gain fiber so that both the gain fiber and passive fiber have negative dispersion at 1550 nm range. As the periodic gain and loss come into play in a laser, the solutions of the laser are actually average solitons. The output spectrum contains several peaks around a secant hyperbolic shaped spectrum which arises because of the interaction between solitons and dispersive waves, known as Kelly's sidebands [17] The energy of a single soliton is limited by the soliton area theorem such that a specific medium with certain values of dispersion and nonlinearity can support a soliton of definite energy [18]. Driving the laser to obtain more single pulse energy will end up generating multiple pulse per cavity roundtrip through several instabilities [19-20].

3.2. B. Dispersion managed solitons: Tamura et. al. proposed that by placing a fiber with positive GVD inside a cavity working in anomalous dispersion, the single pulse energy could be enhanced significantly. While circulating with in the cavity, in the normal dispersive fiber the pulse will be broaden significantly which will reduce its the average peak power and as a consequence the pulse will acquire lesser non-linear phase shift compared to a pulse of near transform limited duration [21]. By this process the cavity supports pulses of higher energy and broader duration in contrast to a soliton. However, the pulse is compressible near to its transform limited width outside the main oscillator by using dispersive delay lines. The output pulse attributes depend on the net cavity dispersion such as the pulse takes Sech-hyperbolic shape if the net GVD is highly negative and Gaussian shape if the net GVD is near zero or slightly positive. At 1-micron region, dispersion management is done by employing CFBGs, photonic crystal fibers or free space delay lines inside the cavity, whereas dispersion shifted active and passive fibers are used at 1550 nm and 2 μm region for this purpose [22-24].

3.2. C. Similaritons: It was found theoretically that a parabolic pulse with linear chirp profile can propagate through a normal dispersive fiber without any deformation in the shape (maintain the parabolic shape) and which is verified later in an experiment by Fermann et al. [25-26]. These types of pulses are called 'similaritons'. Few years after it is found that any pulse with arbitrary shape can evolve to a parabolic shape when propagate through a normal dispersive gain fiber and after that the pulse get the property of similaritons, known as 'amplifier similaritons' among researchers [27]. The properties of evolved pulse depend on

the properties of input pulse & optical fiber. Unlike solitons in anomalous dispersion fiber, spectrum of similariton broadens during propagation in normal dispersive fiber. So, some modifications are necessary to stabilize the similariton solution inside a cavity. It is soon realized that a mode-locked cavity with dispersion map also support similariton in specific position within the cavity. A passive fiber segment of negative dispersion fiber is placed after a normal dispersive gain fiber such that the fiber with negative dispersion support soliton and keeps similariton stabilize in the gain fiber in each roundtrip [28]. It is also reported that a laser built with all normal dispersion configuration can also deliver similariton after appropriate spectral filtering [29].

***3.2.* D. Dissipative solitons:** After the development of soliton, stretch pulse and similariton, it was clear that compensation of GVD-induced chirp is required for to stabilize a mode-locked laser. So, at wavelength regime of 1 micron where both active and passive fibers provide positive dispersion, in other words the net cavity dispersion would be sufficiently high, the chirp compensation was imposing a restriction. In the year 2006, Chong et. Al. have showed that by using a spectral filter of appropriate spectral bandwidth, total chirp can be compensated in each roundtrip and high energy stable mode-locked pulses can be produced [30]. While propagating through normal dispersive fiber, temporal and spectral width increases as it gains large SPM-induced nonlinear chirp which accumulates near the wings of the pulse. But as the pulse passes through the spectral filter, it trims the pulse and shapes the temporal profile by shortening the width. In contrast to solitonic regime where GVD induced chirp get compensated by the nonlinear chirp, an additional dissipative pulse shaping procedure (along with gain & loss) is required to stabilize the pulse in normal dispersion regime. Numerical and experimental research conducted on dissipative solitons confirms that nonlinear phase, filter bandwidth and total GVD are three key parameters which play key role in pulse shaping of dissipative solitons. Dissipative solitons exhibit steep-edged rectangular shaped because of its strong nonlinear chirp [31] which also make them highly compressible outside the cavity.

***3.3.* Extreme events in mode-locked fiber laser:** Solitons which are the static solution of NLSE, are also a local wave packets in a conservative system. On the other hand, other stable states are a dynamic fixed point attractor in dissipative systems. Beyond fixed point attractor, mode-locked laser possesses other stationary solutions like multi-pulse state and harmonic mode-locked states. Transition between stationary solutions can happen by influencing the gain, birefringence in experiment. It is found experimentally and also as the

solution of CQGLE that in the route of transition, a dissipative system can go through various nonlinear dynamics such as bifurcations, explosions, chaos and severe extreme events like rouge waves [32-35]. Among these, soliton explosions are probably most reported events where the soliton spectrum experiences sudden collapse and after a few roundtrips it restores owns integrity. During the explosion, a temporal shift of the pulse is also observed which makes them recognizable in combination with spectrum collapse [36]. Soliton explosion can happen in a periodic or successive way, reported as 'successive soliton explosions' [37]. Soliton explosions are observed in all type of saturable absorber based lasers. Although the origin of explosions in still elusive, mostly it is observed during the transitional regime of different stationary states. Soliton collision induced explosions can happen during the creation or annihilation of extra soliton when the cavity starts to support multiple solitons in each roundtrip [38].

Unlike soliton explosions, which are transient events, breather/pulsating solitons are a type of coherent but dynamical solution whose energy oscillates in space or time [39]. Akin to stationary solitons, breather can present as a bound state, where multiple soliton sustains in molecule form. Breathers can appear both in conservative and dissipative system and are related to Fermi-Pasta-Ulam recurrence [40]. Breathers have been identified both in passive mode-locked laser and micro-resonators. The dynamical evolution of breather/breather molecules in short time scale have been presented in several literatures [41-43]. The breather can arise during the transition to CW to mode-locked or between N and (N+1) th state. Extreme breathing is also found in the transitional regime between two stable point in mode-locked laser which are described as 'chaos' or 'chaotic state' [44].

Rouge waves are high amplitude waves which appears suddenly, first named in Oceanology and later, RWs are identified in the field of optics [45]. Presence of RWs are verified by observing their L-shaped histogram pattern [45]. RWs are first identified during supercontinuum generation where the fluctuations are induced by modulation instability [46]. It is found that soliton collision, soliton explosion also can induce RWs in mode-locked laser system. RW induced by interaction of soliton in chaotic multipulse regime are reported in literatures [47]. These sudden fluctuations are also observed during the Raman conversion in long length cavities [48].

3.4. Effect of spectral filtering in state transition: Other than the conventional solitonic regime where the dispersion induced chirp does not get balanced by the SPM-induced chirp, spectral filtering plays a crucial role to stabilize the pulse in each roundtrip.

When propagating in a normal dispersive medium, a pulse experience optical wave-breaking after accumulating a significant amount of nonlinear phase; then a spectral filter of certain bandwidth is required to chop off excess chirp and maintain the pulse stability. So, a spectral filter becomes an important dissipative component while constructing a laser in ANDi regime. In case of a dispersion managed soliton, intra-cavity spectral breathing and subsequent pulse traits induced by periodically placed components of opposite dispersion often gets affected by the filter bandwidth present in the laser. It is also experimentally proven that the transition between similariton and dispersion managed soliton depends on the filter bandwidth [29].

A spectral filter can present in different form inside a cavity like a birefringence filter, interferometric filter, dispersion managed elements like CFBGs and wavelength specific physical spectral filter. But by default, in all laser gain bandwidth of the gain medium also plays the role of a spectral filter and those pulses which are shaped by gain bandwidth are known as gain guided soliton. As the higher energy pulses feature higher spectral bandwidth, these pulses go through higher loss during spectral filtering and as a consequence maximum single pulse energy is often limited by the bandwidth of the spectral filter [49]. Further increment of the gain to obtain higher energy pulses than a certain value leads the laser to multi-pulsing instability. The number of pulse per roundtrip can increase one by one or can increase randomly depending on other factors. The transition from N pulse state to an N+1 pulse state goes through an intermediate chaotic state [50]. Spectral filtering induced RWs have also been observed in mode-locked lasers [51] where a narrow band spectral filter is used to form a dispersion managed cavity.

3.5.A State transition in an all normal dispersion cavity at 1064 nm

A complete chaotic state is found near the transitional regime between stable single pulse state. Then the laser goes to an unequal multi-pulse state followed by an unstable harmonic mode-locked state. Spectral and temporal properties of each state is shown in this section.

Cavity architecture: The cavity is built in a linear configuration by utilizing a SESAM and a CFBG as two end mirrors. The SESAM acts as the mode-locker and the CFBG is used in normal dispersion condition which makes the configuration 'all-normal'. The CFBG has a 3-bandwidth of 9.8 nm with 40 % reflectivity and adds +0.21 ps^2 GVD to the cavity. The fiber coupled SESAM has a modulation depth of 8 % and relaxation time of 500 fs (BATOP, SAM-1064-13-500fs). A lab-fabricated Yb-doped fiber of length 1.1 m is pumped through a WDM by a single mode laser diode of 976 nm wavelength. The core diameter of the rare-earth doped fiber is 6.4 micron and the NA is 0.14. All other fibers are commercially available HI1060 fiber made of corning. Total cavity length is 3.9 m with a net cavity dispersion 0.39 ps^2. The schematic of the cavity is presented in figure 3.1. To perform the DFT, 10 km of G.652 fiber is used which have second order dispersion of -38.41 ps/nm-km at 1064 nm.

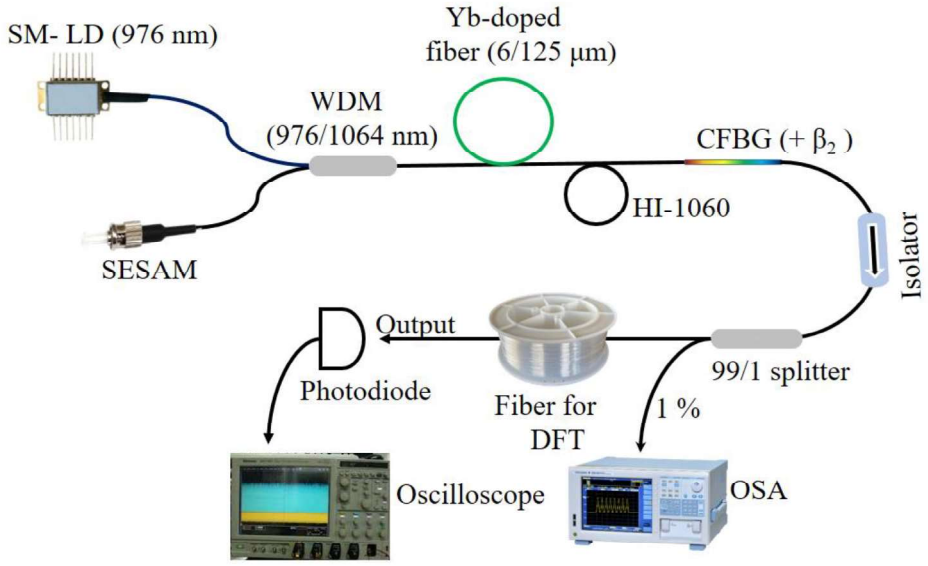

Figure 3.1: Schematic of the fiber laser in all normal dispersion condition

The average output spectrum is recorded via an optical spectrum analyser (YOKOGAWA: AQ6319). The temporal characteristics are measured by the combination of 5 GHz (Thorlabs: DET08C/M) photodiode and 2.5 GHz oscilloscope (Tektronix: DPO7254C). Only the single pulse is captured by a 30 GHz photodiode (Thorlabs: DXM30AF) and 20 GHz oscilloscope (Tektronix: DPO72004C).

Spectral characteristics: The CW lasing with a sharp peak is appeared at a pump power of 42 mW. Figure 3.2(a) represents the CW spectrum. When the pump power is reached 92 mW,

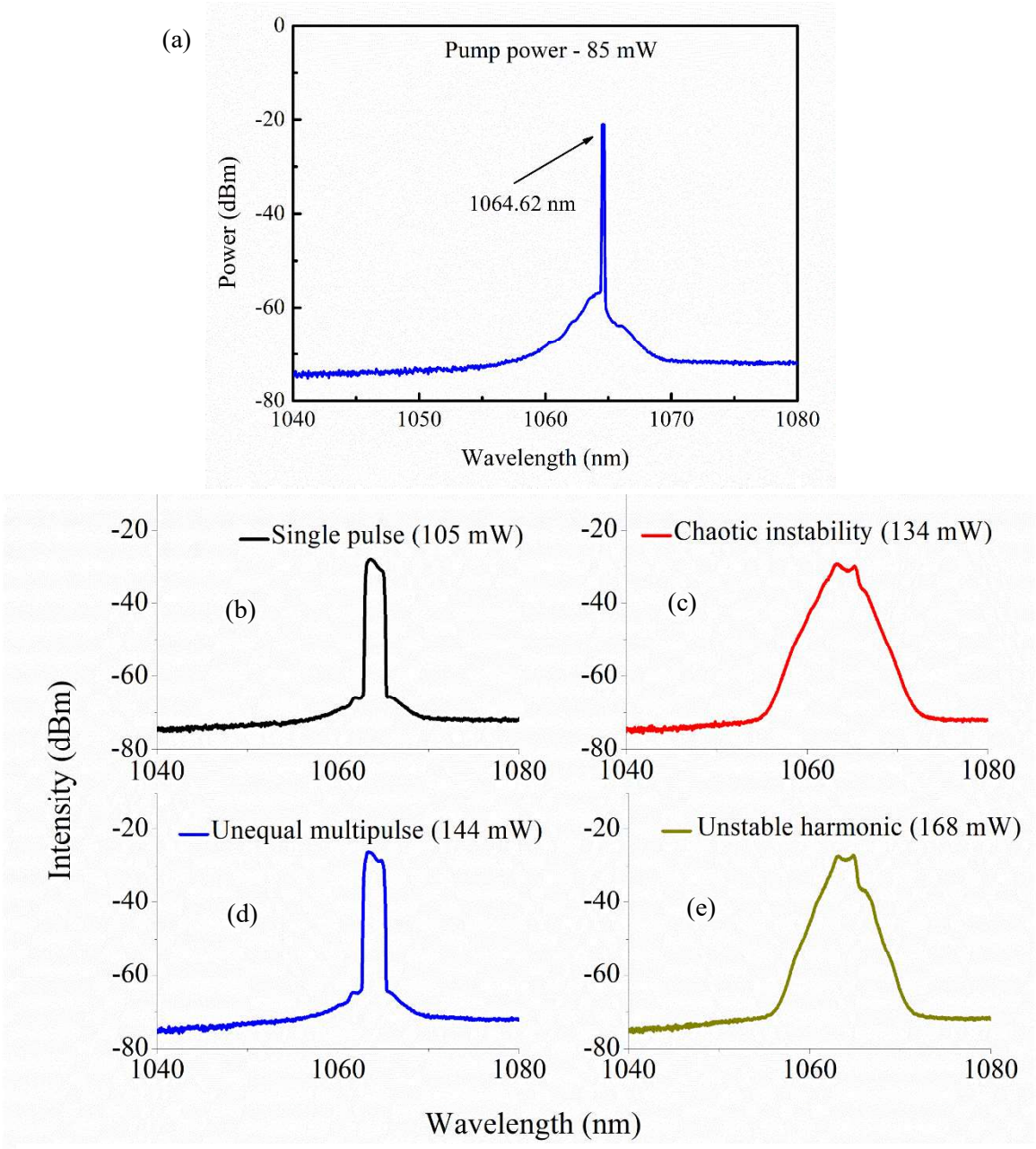

Figure 3.2: Spectrum at different pump powers showing the evolution of spectral shape throughout the experiment. (a) CW (b) stable single pulse state (c) chaotic instability (d) unequal multi-pulse (e) unstable harmonic state

stable mode-locked pulse train is displayed in the oscilloscope. Transition from CW to stable mode-locked occurred via fluctuation in time domain which is discussed in the following section. The stable mode-locked spectrum has a shape of steep-edged rectangular shape with a 3-dB and 10-dB bandwidth of 1.6 nm and 2.1 nm respectively at 92 mW of pump power.

With the increment of the pump power, the 3-dB and 10-dB spectral width increases slightly but as soon as the pump power reached 117 mW, the shape of the spectrum suddenly changes to near trapezoidal shape with significant temporal instabilities in the time domain. Figure 3.2 (b) represents the spectrum of the stable state and 3.2(c) depicts the spectrum of the state with severe temporal instabilities. This state with instabilities sustain almost up to pump power of 140 mW and after that the spectrum recovers its original shape. But at this instant, a pulse of lower amplitude is noticed just beside the main pulse. This state is diagnosed by 'unequal multi-pulsing' state. From this multi-pulsing state an 'unstable harmonic' state is also obtained by increasing pump power only. This state has the repetition rate as double of the stable single pulse state and contains moderate amplitude modulation in the temporal domain. The spectrum takes the trapezoidal state similar to the chaotic state in this regime. Spectrum at 144 mW and 168 mW is presented in figure 3.2(d) and 3.2(e) respectively corresponding to 'unequal multi-pulsing' and 'unstable harmonic' state. The pump power is not increased further because of the maximum limitation of the pump diode. In next section temporal properties of each state is described.

Temporal features: The transition from CW to stable mode-locked state occurs via a large intensity fluctuation in temporal domain as shown in figure 3.3 (a). The transition regime has an oscillating nature similar to a Q-switched mode-locked state for a short time span after that the stable single pulse state is attained. A long pulse train of the stable state is presented in figure 3.3 (b). The time gap between two consecutive pulses is 37.5 ns corresponding to 26.65 MHz repetition rate. The FWHM of a single pulse is 52 ps. As the total dispersion is highly positive, the pulse is expected to be highly chirped. A single pulse is presented in figure 3.4(a) showing a smooth temporal profile. The RF-spectrum has a SNR greater than 54 dB indicating a good stability in time domain. Figure 3.4(b) depicts the RF-spectrum of the stable single pulse state having a fundamental frequency of 26.65 MHz.

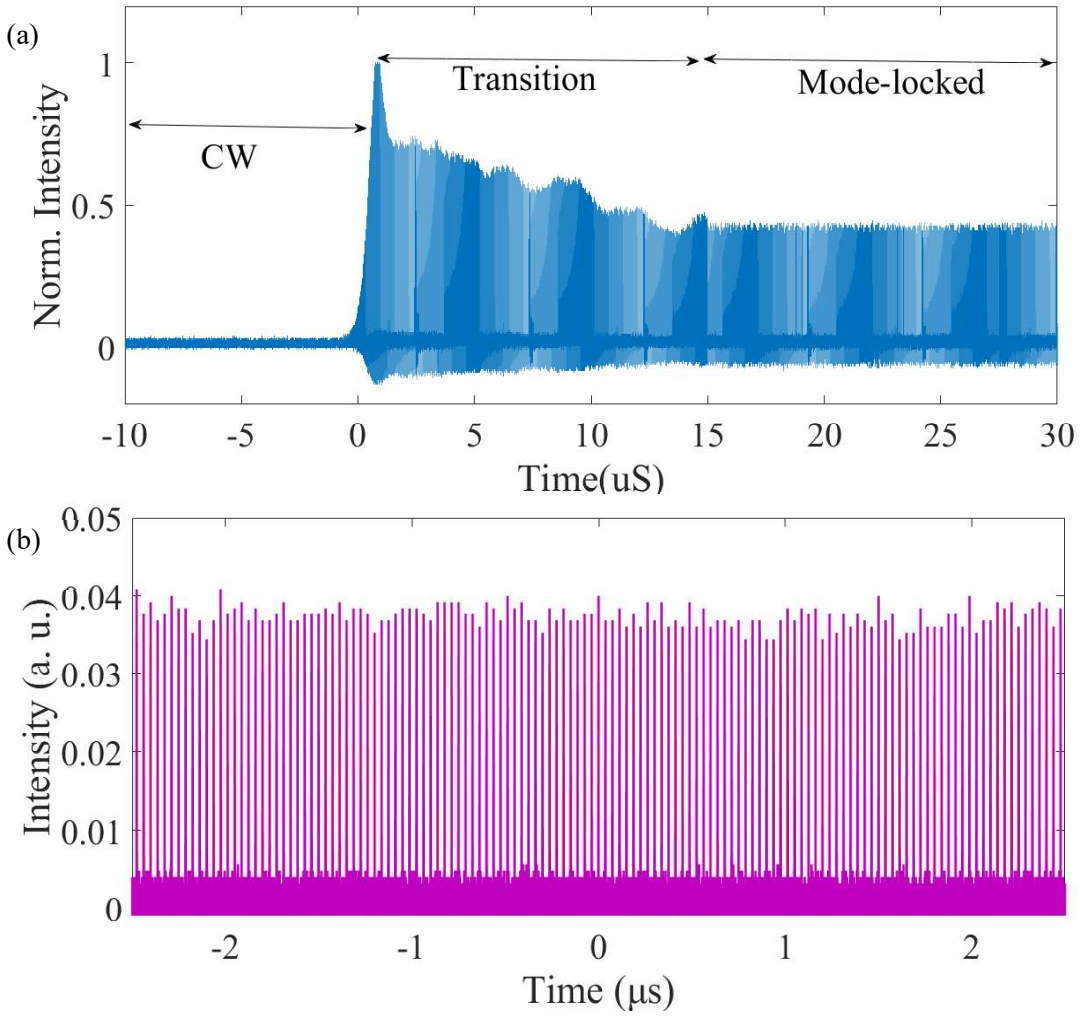

Figure 3.3: (a) Starting of mode-locked state from complete CW (b) Long pulse train showing the stability of stable single pulse state

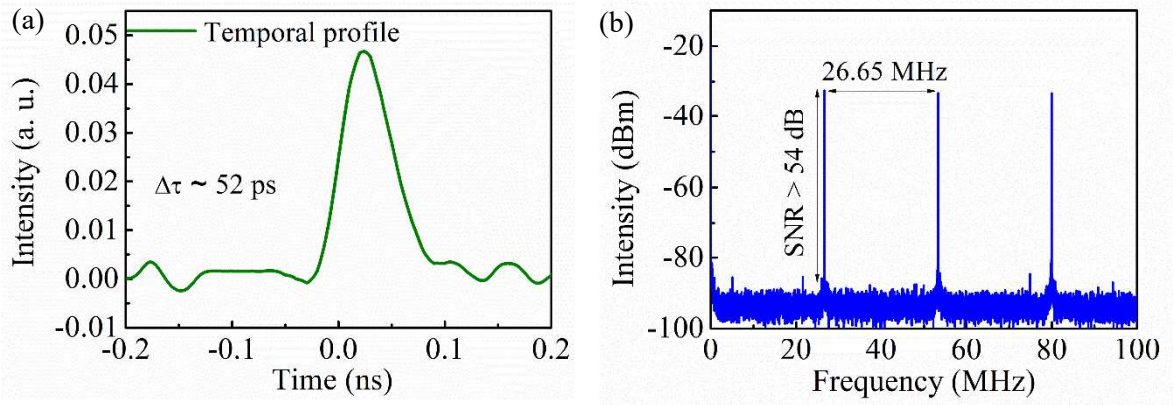

Figure 3.4: (a) Temporal profile of a stable single pulse with pulse duration of 52 ps. (b) RF-spectrum of the stable state with fundamental frequency of 26.65 MHz.

As the pump power reaches 117 mW, the stable state drives to a state that contains random temporal instability. A long pulse train containing 500 consecutive pulses of the chaotic state

is shown in figure 3.5 along with a stable pulse train of same time span for better visualization. Looking into the temporal profile of single pulse we have found that every pulse has a random broken shape and random amplitude. Four consecutive pulse recorded in same condition is shown in figure 3.6(a). Although the repetition rate has not changed, the RF-spectrum contains a sign of presence of this severe amplitude modulation. The RF-spectrum contains few side-lobes around the fundamental frequency which is shown in figure 3.6(b).

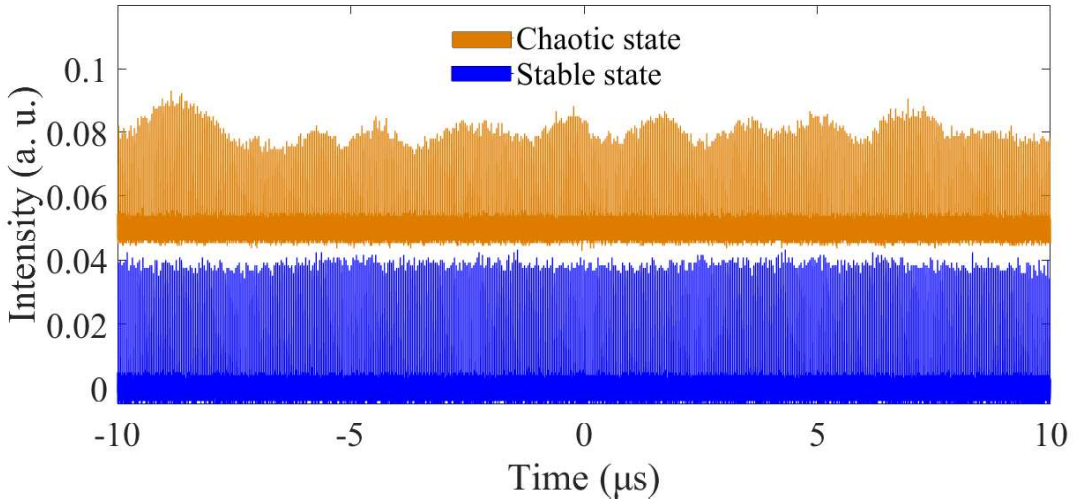

Figure 3.5: Long pulse train containing 550 consecutive pulses of both the chaotic and stable state

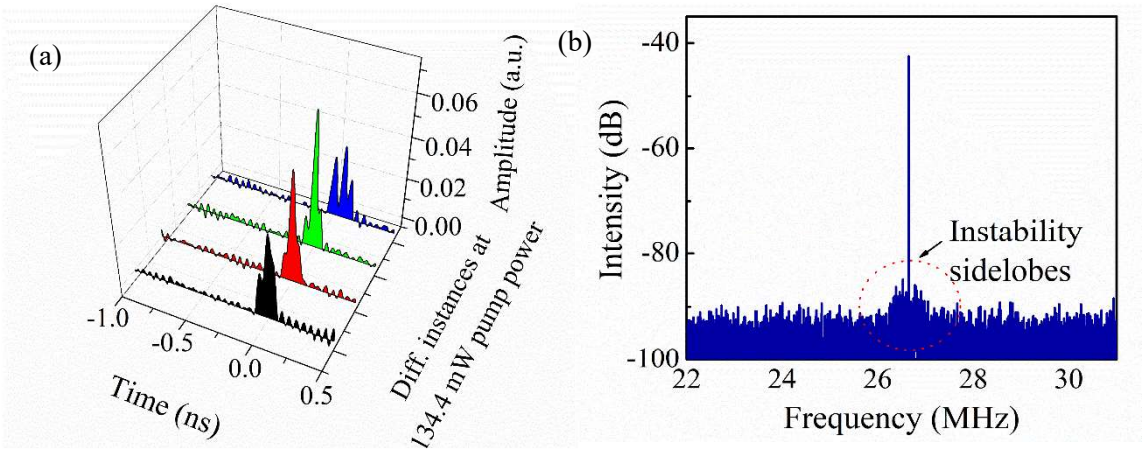

Figure 3.6: (a) Temporal profile of single pulse at fixed pump power in the chaotic state (b) RF-spectrum around the fundamental frequency at the chaotic state showing the presence of instability

This chaotic instability continues to 140 mW of pump power until the 'unequal multi-pulse' state is achieved. The temporal profile of the multi-pulse state is shown in figure 3.7(a). It can be noticed that another pulse of slightly lower amplitude is now present at a time gap of

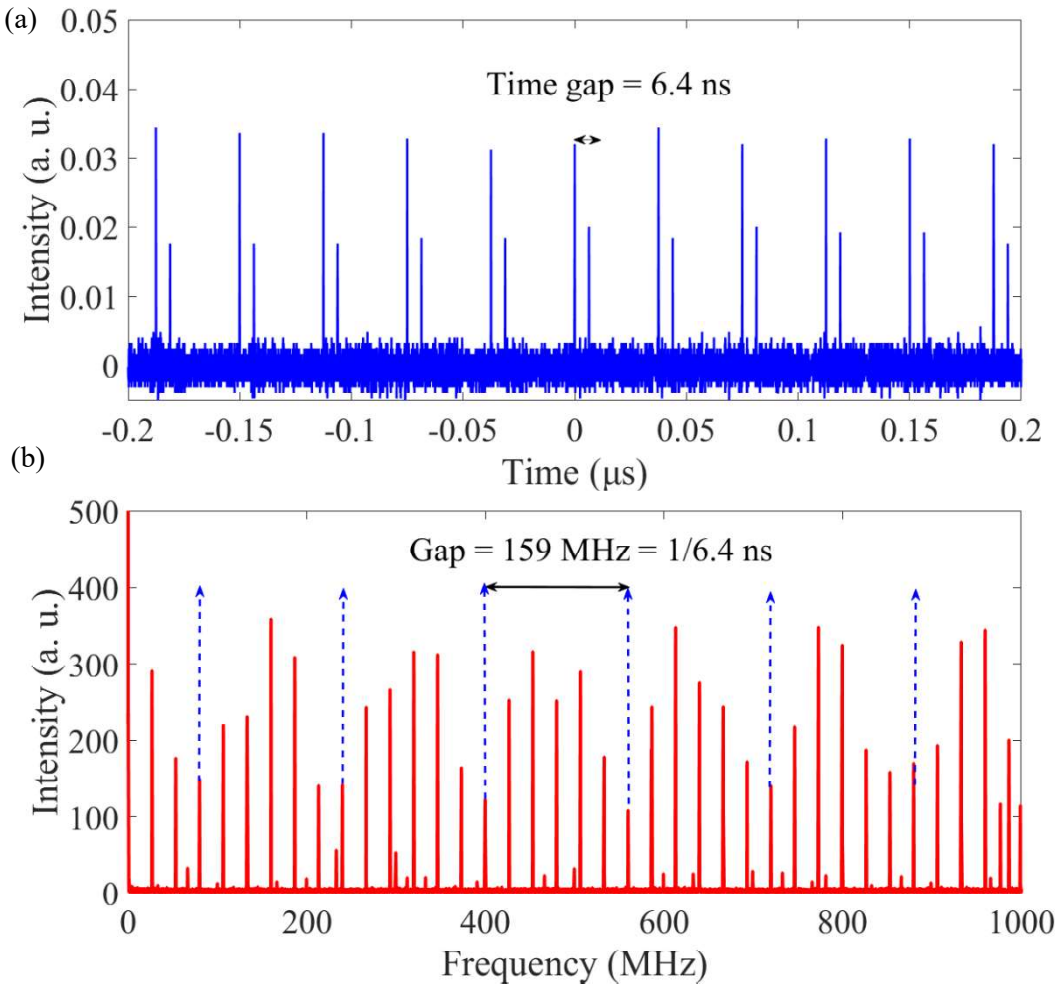

Figure 3.7: (a) Temporal profile & (b) RF-spectrum of the unequal multi-pulsing state

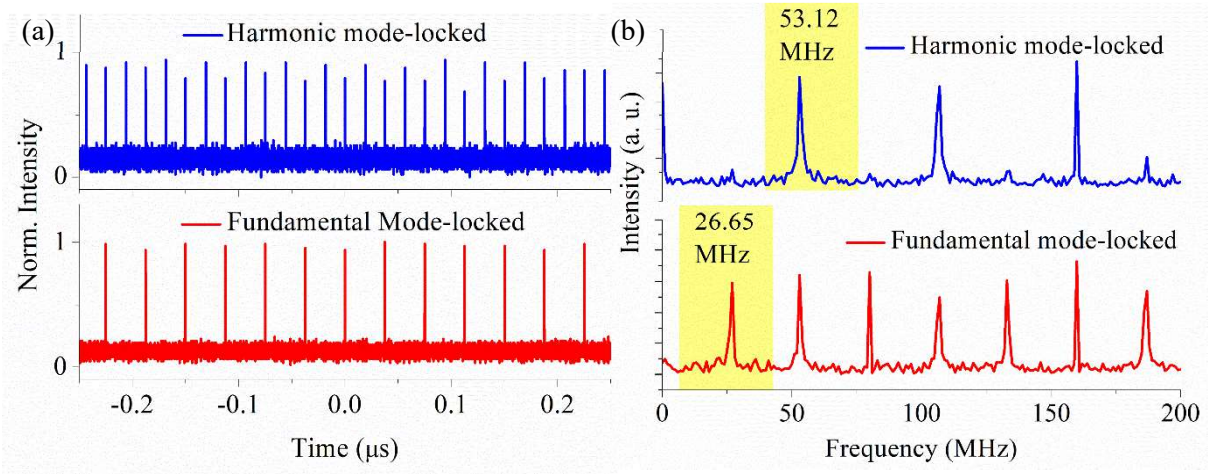

Figure 3.8: (a) Comparison of pulse train between harmonic and fundamental mode-locked state (b) Comparison of RF-spectrum between harmonic and fundamental mode-locked state

6.4 ns around the main pulse. The corresponding RF-spectrum also contain the information

of multi-pulsing as it has a modulation frequency of 159 MHz which is same as the inverse of the time gap between two attached pulses. The RF –spectrum of this state is obtained by performing FFT on a long pulse train because of software issue in the oscilloscope which is shown in figure 3.7(b). However, the multi-pulse state does not sustain for a long pump interval and it soon transits to the 'unstable harmonic' state. The transition pump power is not same at each time we repeat the experiment. A long temporal profile of the harmonic state is presented in figure 3.8(a) along with the fundamental mode-locked state for better visualization. In a similar way the RF-spectrum of both the state is also shown in figure 3.8(b).

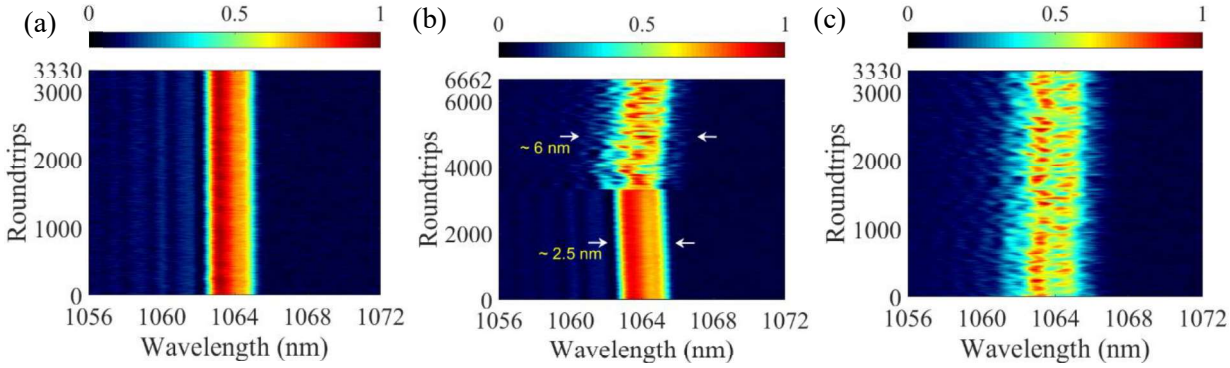

Figure 3.9: Shot-to-shot spectrum evolution of the (a) stable single pulse (b) during transition to chaotic state & (c) complete chaotic state

DFT analysis of the stable and chaotic state: In case of chaotic regime although there is a significant amount of instabilities in the temporal domain, the averaged spectrum is smoothed throughout the experiment (figure 3.2(c)). No other fluctuation or spectral sidebands are also noticed. To look into the spectral evolution in each roundtrip, we have recorded 3330 consecutive pulses recorded from DFT. Figure 3.9(a) depicts 3330 spectrum of consecutive roundtrips when pump power is 110 mW corresponding to stable single pulse state. The intensity bar plot interprets that the amplitude of spectrum is stable over each roundtrip. Transition to the chaotic state is recorded at 116 mW of pump power which is presented in figure 3.9(b). It is clearly visible from the plot that the spectrum contains an intensity fluctuation after 3300 roundtrips approximately. The lower intensity part of the spectrum also gets broaden after the transition because of the shape change. Figure 3.9(c) represents shot-to-shot spectral evolution of the chaotic state. It is seen that akin to the temporal profile of single pulse of each roundtrip, the spectrum also cannot preserve its amplitude. The spectral evolution of the chaotic state is not similar to any kind of breathing soliton which contains periodic nature over roundtrips. There is no clear nature of soliton explosion also. This state can be classified to a purely chaotic state between two stable solutions.

Hysteresis between Chaotic and mode-locked state: Transition between chaotic state to unequal multi-pulse state and unequal multi-pulse to unstable harmonic state does not occur at any particular pump power. It is found by performing the experiments multiple times that chaotic-to-multipulse state occurs within broad range of pump power between 138 mW to 150 mW and multipulse-to-harmonic state occurs between 155-163 mW. But an interesting phenomenon observed near the transition of stable mode-locked and chaotic state. When

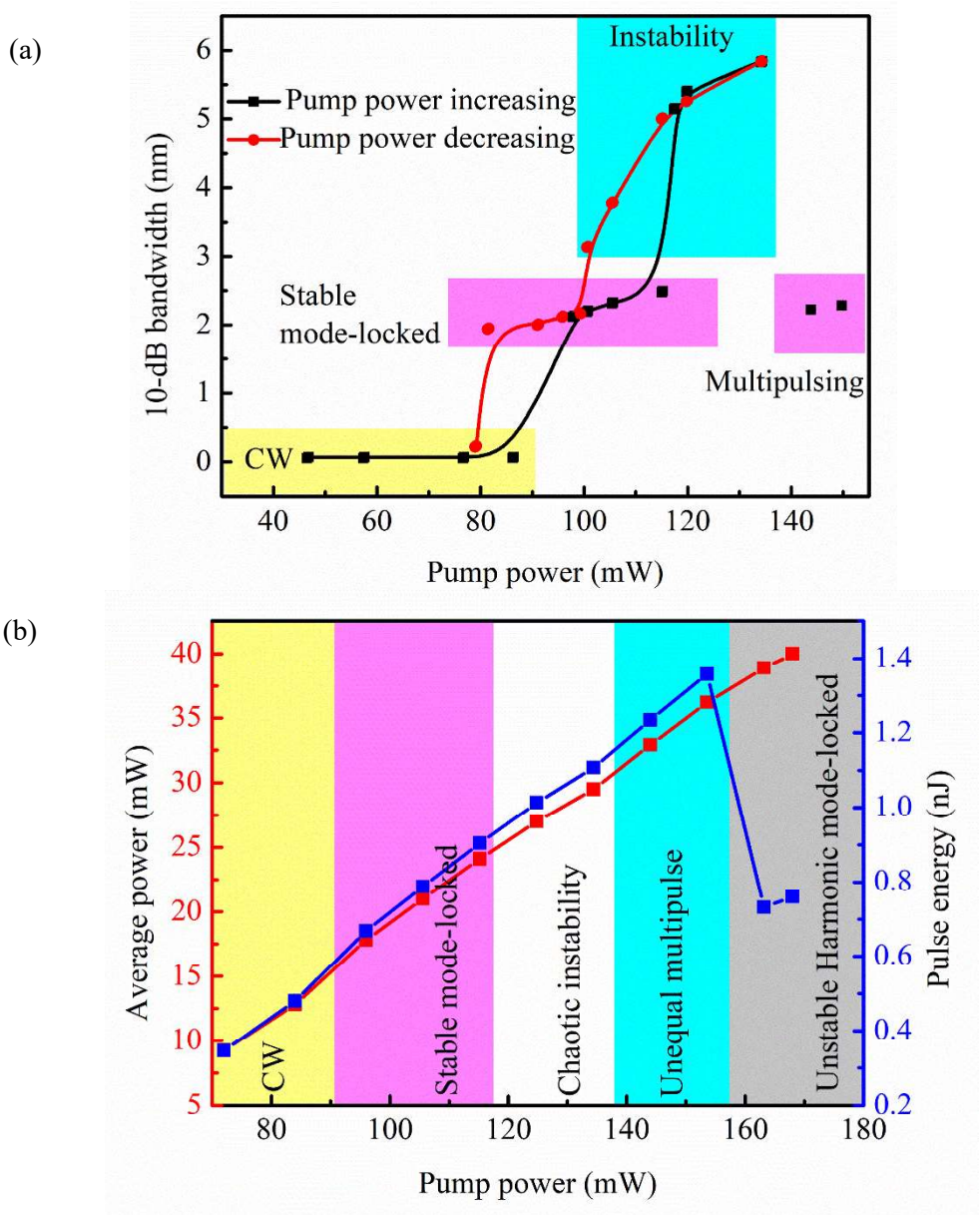

Figure 3.10: (a) Variation of 10-dB spectral width with the pump power showing the presence of hysteresis between stable single pulse and chaotic state (b) variation of average power and pulse energy with pump power

increasing the pump power, transition to mode-locked state from the CW state occurs at 95 ± 2 mW and the transition from mode-locked state to chaotic state happens at pump power

of 116 ± 3 mW. But while reducing the pump power, transition from chaotic state to mode-locked state continues almost to 98 ± 4 mW. Then the same thing happens near the transition of mode-locked to CW state. The stable mode-locked state continues to almost 80 mW. This phenomenon is known as hysteresis of pump power. Hysteresis in mode-locked lasers between to multi-pulse (N and N+1) are reported in several literatures [52-53]. Figure 3.10(a) depicts the variation of 10-dB spectral width and pump power both during increment and decrement of pump power to show the presence of hysteresis. The sudden increment of 10-dB spectral width depicts the transition to chaotic state. As the state transits to multi-pulse state the 10-dB width decreases again by recovering the rectangular spectral shape. Figure 3.10(b) shows the variation of average output power and pulse energy with pump power showing different operational regime. The pulse energy of the multi-pulse state is the energy associated with two attached pulse. As the state goes to harmonic state the pulse energy decreases again to stable pulse state value.

Discussion: In this whole study, the transition among different state in the ANDi-laser is happened by influencing the pump power or energy supply to the cavity. Similar to conventional solitons whose energy is quantified by soliton area theorem, a stable dissipative soliton can also carry a certain amount of energy as presented in literature [54]. The dissipative soliton also tries to in stable form by shedding extra energy in form of dispersive wave. The chaotic state arises due to the interaction between stable soliton and the dispersive wave [55]. This state is like a non-stationary solution which is only observable between to stable solution. This type of intermediate chaotic state is found experimentally and predicted theoretically in dissipative systems [56-57]. Further increment of energy leads the laser to the multi-pulse state, when the intra-cavity energy becomes sufficient to support another pulse of lower energy in each roundtrip. The multi-pulse state tries to go another stable pulsing state to recover single pulse energy when additional energy is supplied.

3.5.B. State transition in dispersion managed cavity at 1064 nm

A dispersion managed oscillator is constructed by utilizing a CFBG in negative dispersion configuration. The cavity architecture is similar to figure 4.1. But in the cavity, the CFBG is replaced by another CFBG which has a 3-dB bandwidth of 18 nm around 1064 nm with reflectivity of 25 %. The SESAM is from BATOP with a modulation depth of 25 % (SAM-1064-40-9ps). Total cavity length is nearly 5.9 m with gain fiber length of 90 cm and net cavity dispersion is approximately 0.048 ps^2. For the characterization same instruments as previous experiment are used. For the intensity noise measurement, a photodiode of 15 MHz bandwidth and a radio frequency analyser (RSA5300B, Tektronix) is used in experiment. A variable optical attenuator is used to keep the average power same at all state during noise characterization.

The CW lasing threshold of the laser is 75 mW which is slight higher than the previous case mainly because of lower reflectivity of the CFBG. As the pump power reaches 102 mW, a stable mode-locked state with broadband rectangular spectrum is obtained. At this instant the 3-dB and 10-dB spectral widths are 10.2 nm and 11.8 nm respectively. With the increment of the pump power both 3-dB and 10-dB width increases but as soon as the pump power reaches 115 mW, some unstable sidebands around the spectrum is noticed and with further increment of pump energy the spectrum changes its shape near to a trapezoid. From 115 mW of pump power, a significant amount of fluctuation is noticed in the temporal domain. The variation of spectral shape at different pump power is shown in figure 3.11(a). The variation of 3-dB and 10-dB spectral width is presented in figure 3.11(b). It is seen that after the transition the 3-dB width reduces slightly and the 10-dB width increases because of the shape change of the averaged spectrum.

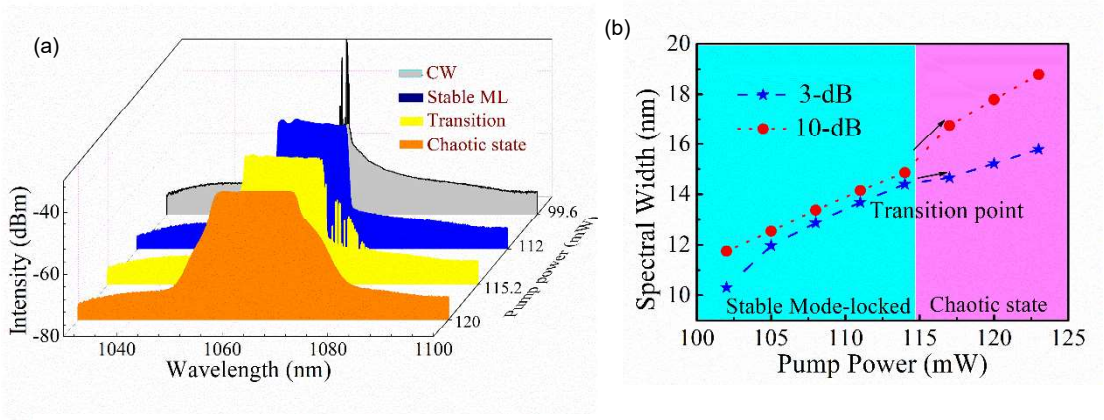

Figure 3.11: (a) Variation of shape of the spectrum at different regime (b) Variation of spectral width with pump power

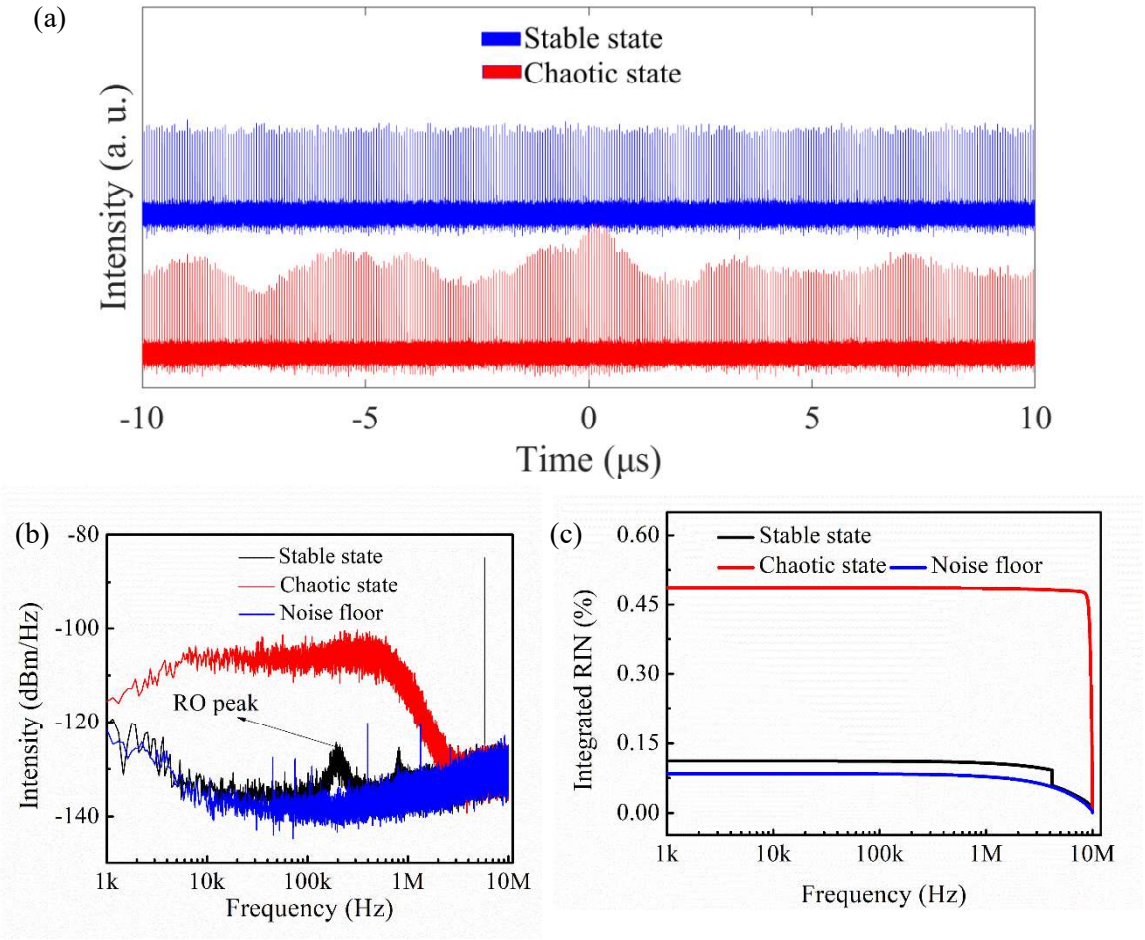

Figure 3.12: (a) Long pulse train of the stable and chaotic state. (b) RIN & (c) integrated RIN at different regime

Figure 3.12(a) shows the long length of consecutive pulses of both the stable and chaotic state. It is evident from the figure that the temporal domain contains significant amount of intensity fluctuation in the chaotic state. Alongside that we have measured RIN at both state which is shown in figure 3.12(b). In the stable mode-locked state the RIN is in the level of -132 dBm around 100 kHz. A peak is noticed 110 kHz which is because of the relaxation oscillation of Yb-ions. But as the state goes to the chaotic state, the noise level increases almost to -105 dBm due to random amplitude fluctuation in each roundtrip. To look into the shot-to-shot spectral evolution DFT is performed. Figure 3.13(a) shows the spectral evolution of the stable mode-locked evolving steadily with no amplitude or shape fluctuation. Figure 3.13(b) depicts the spectral evolution of the chaotic state almost over 2000 roundtrips. Figure 3.13(c) shows

the variation between 800-1000 roundtrips. A weak nature of spectral collapsing is present which can be due to soliton explosion.

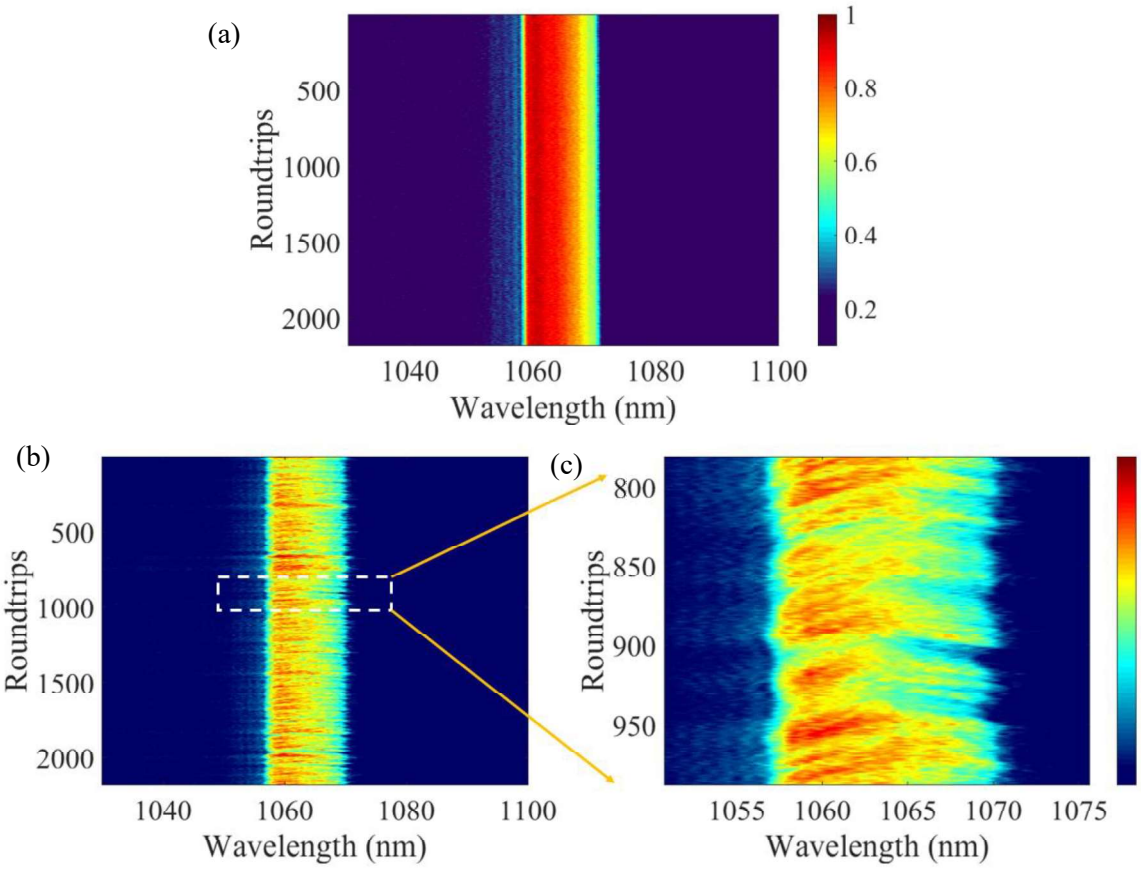

Figure 3.13: (a) DFT spectrum of the stable state. (b) DFT spectrum of the chaotic state (c) 750-1000 roundtrips of figure 3.13(b)

Discussion: The reason behind this state transition is not similar to the previous case of ANDi laser. This state transition is mainly influenced by the strong narrow band spectral filtering. As shown in figure 3.11(b), we can see that when the FWHM of the spectrum becomes comparable to the filter bandwidth, the instability occurs. In few literatures, based on numerical simulation, it is reported that, strong spectral filtering can stimulate soliton explosion in the laser [50] before transiting to the multi-pulse state. In our experiment, we have not increased the pump power further to avoid damage of the SESAM.

***3.6.* Conclusion:** To conclude, this chapter contains the performance of two SESAM-based lasers in two dispersion configuration; one ANDi and one dispersion managed. Both the lasers contain a single pulse state and deliver pulses with picosecond duration in stable condition. Depending on the pump power, the ANDi laser show four different state namely stable single pulse, chaotic, unequal multi-pulse and harmonic mode-locked state. The dispersion managed

oscillator also shows another transient state which contain significant amplitude modulation. The DFT spectrum shows inconsistency in spectrum evolution in each roundtrip and also have a sign of soliton explosion. Although, SESAM provides a good stability in the single pulse state, they are sensitive to the intra-cavity power and the performance degrades in time due to exposure to the heat. The sudden intensity fluctuation of extreme events also can be detrimental for SESAMs performance. Alongside that, as commercial SESAMs do not come with a tunability in controlling parameters, choice of appropriate component and cavity engineering becomes necessary to obtain a stable state.

{Bibliography}

1. Gao, Bo, Ruo-Han Zhang, Jia-Yu Huo, Chun-Yang Ma, Ying Han, Qi-Rong Hou, Fan Deng, Ge Wu, and Yan-Qi Ge. "Generation and categories of solitons in various mode-locked fiber lasers." *Optik* 220 (2020): 165168.

2. Chong, Chin Yu. "Femtosecond fiber lasers and amplifiers based on the pulse propagation at normal dispersion." (2008).

3. Luo, Yiyang, Yang Xiang, Bowen Liu, Yingxiong Qin, Qizhen Sun, Xiahui Tang, and Perry Ping Shum. "Dispersion-managed soliton molecules in a near zero-dispersion fiber laser." *IEEE Photonics Journal* 10, no. 6 (2018): 1-10.

4. Bélanger, Pierre-André. "Stable operation of mode-locked fiber lasers: similariton regime." *Optics Express* 15, no. 17 (2007): 11033-11041.

5. Huang, Jiapeng, Meng Pang, Xin Jiang, Wenbin He, and P. StJ Russell. "Route from single-pulse to multi-pulse states in a mid-infrared soliton fiber laser." *Optics Express* 27, no. 19 (2019): 26392-26404.

6. Li, Xing, Weiwen Zou, and Jianping Chen. "Passive harmonic hybrid mode-locked fiber laser with extremely broad spectrum." *Optics Express* 23, no. 16 (2015): 21424-21433.

7. Wang, Z. Q., K. Nithyanandan, A. Coillet, P. Tchofo-Dinda, and Ph Grelu. "Optical soliton molecular complexes in a passively mode-locked fibre laser." *Nature communications* 10, no. 1 (2019): 830.

8. Runge, Antoine FJ, Neil GR Broderick, and Miro Erkintalo. "Observation of soliton explosions in a passively mode-locked fiber laser." *Optica* 2, no. 1 (2015): 36-39.

9. Zaviyalov, Alexandr, Oleg Egorov, Rumen Iliew, and Falk Lederer. "Rogue waves in mode-locked fiber lasers." *Physical Review A* 85, no. 1 (2012): 013828.

10. Peng, Junsong, Sonia Boscolo, Zihan Zhao, and Heping Zeng. "Breathing dissipative solitons in mode-locked fiber lasers." *Science advances* 5, no. 11 (2019): eaax1110.

11. Zhao, L. M., D. Y. Tang, and A. Q. Liu. "Chaotic dynamics of a passively mode-locked soliton fiber ring laser." *Chaos: An Interdisciplinary Journal of Nonlinear Science* 16, no. 1 (2006).

12. Turaev, Dmitry, Andrei G. Vladimirov, and Sergey Zelik. "Chaotic bound state of localized structures in the complex Ginzburg-Landau equation." *Physical Review E* 75, no. 4 (2007): 045601.

13. Zhang, Feifan, Yuncai Wang, Yuehui Sun, Junpei Xu, Pu Li, Anbang Wang, and Yuwen Qin. "Key Space Enhancement in Chaotic Secure Communication Utilizing Monolithically Integrated Multi-Section Semiconductor Lasers." In *Photonics*, vol. 10, no. 2, p. 213. MDPI, 2023.

14. Li, Jian-Cheng, Jin-Long Xiao, Yue-De Yang, You-Ling Chen, and Yong-Zhen Huang. "Random bit generation based on a self-chaotic microlaser with enhanced chaotic bandwidth." *Nanophotonics* 12, no. 21 (2023): 4109-4116.

15. Liu, X. M., T. Wang, C. Shu, L. R. Wang, A. Lin, K. Q. Lu, T. Y. Zhang, and W. Zhao. "Passively harmonic mode-locked erbium-doped fiber soliton laser with a nonlinear polarization rotation." *Laser physics* 18 (2008): 1357-1361.

16. Arshad, M., Aly R. Seadawy, and Dianchen Lu. "Optical soliton solutions of the generalized higher-order nonlinear Schrödinger equations and their applications." *Optical and Quantum Electronics* 50 (2018): 1-16.

17. G. P. Agrawal, Nonlinear Fiber Optics (Elsevier, 2013).

18. Du, Yueqing, Xuewen Shu, Haoran Cao, and Peiyun Cheng. "Dynamics of dispersive wave and regimes of different kinds of sideband generation in mode-locked soliton fiber lasers." *IEEE Journal of Selected Topics in Quantum Electronics* 24, no. 3 (2017): 1-8.

19. Du, Yueqing, Mengmeng Han, and Xuewen Shu. "A Chaotic State in the Transition From Single Toward Multiple Pulse for Soliton Fiber Lasers." *IEEE Photonics Journal* 12, no. 2 (2019): 1-12.

20. Chen, Hong-Jie, Yan-Jie Tan, Jin-Gan Long, Wei-Cheng Chen, Wei-Yi Hong, Hu Cui, Ai-Ping Luo, Zhi-Chao Luo, and Wen-Cheng Xu. "Dynamical diversity of pulsating solitons in a fiber laser." *Optics express* 27, no. 20 (2019): 28507-28522.

21. Bale, Brandon G., Sonia Boscolo, and Sergei K. Turitsyn. "Dispersion and nonlinearity-management in mode-locked fibre lasers." In *CLEO/Europe-EQEC 2009-European Conference on Lasers and Electro-Optics and the European Quantum Electronics Conference*, pp. 1-1. IEEE, 2009.

22. Liu, Bowen, Yiyang Luo, Yang Xiang, Wei Zhou, Perry Ping Shum, Zhijun Yan, Xiahui Tang, Deming Liu, and Qizhen Sun. "CFBG-based bidirectional mode-locked fiber laser emitting conventional and dissipative solitons." *IEEE Photonics Technology Letters* 31, no. 21 (2019): 1737-1740.

23. Gumenyuk, Regina, Christoph Thur, Samuli Kivisto, and Oleg G. Okhotnikov. "Tapered fiber Bragg gratings for dispersion compensation in mode-locked Yb-doped fiber laser." *IEEE journal of quantum electronics* 46, no. 5 (2010): 769-773.

24. Ma, Wanzhuo, Desheng Zhao, Runmin Liu, Tianshu Wang, Quan Yuan, Hao Xiong, Haiying Ji, and Huilin Jiang. "Observation and optimization of 2 μm mode-locked pulses in all-fiber net anomalous dispersion laser cavity." *Opto-Electronic Advances* 3, no. 11 (2020): 200001-1.

25. Anderson, Dan, M. Desaix, Magnus Karlsson, M. Lisak, and M. L. Quiroga-Teixeiro. "Wave-breaking-free pulses in nonlinear-optical fibers." *JOSA B* 10, no. 7 (1993): 1185-1190.

26. Fermann, Martin E., V. I. Kruglov, B. C. Thomsen, John M. Dudley, and John D. Harvey. "Self-similar propagation and amplification of parabolic pulses in optical fibers." *Physical review letters* 84, no. 26 (2000): 6010.

27. Boscolo, Sonia, Sergei K. Turitsyn, and Christophe Finot. "Amplifier similariton fiber laser with nonlinear spectral compression." *Optics letters* 37, no. 21 (2012): 4531-4533.

28. Oktem, Bulent, Coşkun Ülgüdür, and F. Ömer Ilday. "Soliton–similariton fibre laser." *Nature Photonics* 4, no. 5 (2010): 307-311.

29. Wang, Zhiqiang, Li Zhan, Xiao Fang, and Hao Luo. "Spectral filtering effect on mode-locking regimes transition: similariton-dissipative soliton fiber laser." *JOSA B* 34, no. 11 (2017): 2325-2333.

30. Chong, Andy, William H. Renninger, and Frank W. Wise. "Properties of normal-dispersion femtosecond fiber lasers." *JOSA B* 25, no. 2 (2008): 140-148.

31. Wise, Frank W., Andy Chong, and William H. Renninger. "High-energy femtosecond fiber lasers based on pulse propagation at normal dispersion." *Laser & Photonics Reviews* 2, no. 1-2 (2008): 58-73.

32. Han, Ying, Bo Gao, Yabin Hao, Joice Sophia Ponraj, Chunyang Ma, Jiayu Huo, Ge Wu et al. "Paths from stationary to chaos in passively mode-locked fiber lasers: research progress of soliton pulsations and soliton explosions." *Journal of Physics B: Atomic, Molecular and Optical Physics* 55, no. 22 (2022): 222001.

33. Liu, Meng, Ti-Jian Li, Ai-Ping Luo, Wen-Cheng Xu, and Zhi-Chao Luo. ""Periodic" soliton explosions in a dual-wavelength mode-locked Yb-doped fiber laser." *Photonics Research* 8, no. 3 (2020): 246-251.

34. Huang, Qianqian, Zinan Huang, and Chengbo Mou. "Transient soliton dynamics in a mode-locked fiber laser: from stationary to pulsation." *Optics Letters* 46, no. 22 (2021): 5683-5686.

35. Zaviyalov, Alexandr, Oleg Egorov, Rumen Iliew, and Falk Lederer. "Rogue waves in mode-locked fiber lasers." *Physical Review A* 85, no. 1 (2012): 013828.

36. Runge, Antoine FJ, Neil GR Broderick, and Miro Erkintalo. "Observation of soliton explosions in a passively mode-locked fiber laser." *Optica* 2, no. 1 (2015): 36-39.

37. Liu, Meng, Ai-Ping Luo, Yu-Rong Yan, Song Hu, Yi-Chen Liu, Hu Cui, Zhi-Chao Luo, and Wen-Cheng Xu. "Successive soliton explosions in an ultrafast fiber laser." *Optics letters* 41, no. 6 (2016): 1181-1184.

38. Peng, Junsong, and Heping Zeng. "Soliton collision induced explosions in a mode-locked fibre laser." *Communications Physics* 2, no. 1 (2019): 34.

39. Peng, Junsong, Sonia Boscolo, Zihan Zhao, and Heping Zeng. "Breathing dissipative solitons in mode-locked fiber lasers." *Science advances* 5, no. 11 (2019): eaax1110.

40. Bao, Chengying, Jose A. Jaramillo-Villegas, Yi Xuan, Daniel E. Leaird, Minghao Qi, and Andrew M. Weiner. "Observation of Fermi-Pasta-Ulam recurrence induced by breather solitons in an optical microresonator." *Physical review letters* 117, no. 16 (2016): 163901.

41. Li, Yifang, Ran Xia, Jia Liu, Yutai Zhao, Changqing Li, Maolin Wang, Ruikai Zhang, Xiahui Tang, and Gang Xu. "Real-time measurements of breathing dissipative soliton pairs in mode-locked fiber lasers." Optics & Laser Technology 175 (2024): 110900.

42. Chen, Jie, Xin Zhao, Ting Li, Jianjun Yang, Jiansheng Liu, and Zheng Zheng. "Generation and observation of ultrafast spectro-temporal dynamics of different pulsating solitons from a fiber laser." *Optics Express* 28, no. 9 (2020): 14127-14133.

43. Luo, Yiyang, Yang Xiang, Ran Xia, Wenjun Ni, Bowen Liu, Perry Ping Shum, Xiahui Tang, Deming Liu, and Qizhen Sun. "Breathing Dynamics in a Gain-Guided Dissipative Soliton-Similariton Fiber Laser." *IEEE Photonics Technology Letters* 32, no. 8 (2020): 481-484.

44. Akosman, Ahmet E., and Michelle Y. Sander. "Route towards extreme optical pulsation in linear cavity ultrafast fibre lasers." *Scientific reports* 8, no. 1 (2018): 13385.

45. Solli, Daniel R., Claus Ropers, Prakash Koonath, and Bahram Jalali. "Optical rogue waves." *nature* 450, no. 7172 (2007): 1054-1057.

46. Teğin, Uğur, Peng Wang, and Lihong V. Wang. "Real-time observation of optical rogue waves in spatiotemporally mode-locked fiber lasers." *Communications Physics* 6, no. 1 (2023): 60.

47. Chowdhury, Sourav Das, Bhaswar Dutta Gupta, Sayan Chatterjee, Ranjan Sen, and Mrinmay Pal. "Rogue waves in a linear cavity Yb-fiber laser through spectral filtering induced pulse instability." *Optics Letters* 44, no. 9 (2019): 2161-2164.

48. Runge, Antoine FJ, Claude Aguergaray, Neil GR Broderick, and Miro Erkintalo. "Raman rogue waves in a partially mode-locked fiber laser." Optics letters 39, no. 2 (2014): 319-322.

49. Zhang, Xianting, Feng Li, Kaliyaperumal Nakkeeran, Jinhui Yuan, Zhe Kang, J. Nathan Kutz, and Ping Kong Alexander Wai. "Impact of spectral filtering on multipulsing instability in mode-locked fiber lasers." IEEE Journal of Selected Topics in Quantum Electronics 24, no. 3 (2017): 1-9.

50. Gupta, Bhaswar Dutta, Sourav Das Chowdhury, Devnath Dhirhe, and Mrinmay Pal. "Intermittent events due to spectral filtering induced multi-pulsing instability in a mode-locked fiber laser." JOSA B 37, no. 8 (2020): 2278-2286.

51. Chowdhury, Sourav Das, Bhaswar Dutta Gupta, Sayan Chatterjee, Ranjan Sen, and Mrinmay Pal. "Rogue waves in a linear cavity Yb-fiber laser through spectral filtering induced pulse instability." Optics Letters 44, no. 9 (2019): 2161-2164.

52. Liu, Xueming. "Hysteresis phenomena and multipulse formation of a dissipative system in a passively mode-locked fiber laser." Physical Review A 81, no. 2 (2010): 023811.

53. Komarov, Andrey, Herve Leblond, and François Sanchez. "Multistability and hysteresis phenomena in passively mode-locked fiber lasers." Physical review A 71, no. 5 (2005): 053809.

54. Renninger, William H., Andy Chong, and Frank W. Wise. "Area theorem and energy quantization for dissipative optical solitons." JOSA B 27, no. 10 (2010): 1978-1982.

55. Zhao, L. M., D. Y. Tang, J. Wu, X. Q. Fu, and S. C. Wen. "Noise-like pulse in a gain-guided soliton fiber laser." Optics Express 15, no. 5 (2007): 2145-2150.

56. Zhao, L. M., D. Y. Tang, and A. Q. Liu. "Chaotic dynamics of a passively mode-locked soliton fiber ring laser." Chaos: An Interdisciplinary Journal of Nonlinear Science 16, no. 1 (2006).

57. Zhou, Jiaqi, Weiwei Pan, and Yan Feng. "Period multiplication in mode-locked figure-of-9 fiber lasers." Optics Express 28, no. 12 (2020): 17424-17433.

Chapter: 04

Rectangular pulses in dual gain segment based figure-9 laser

Abstract

This chapter delves into the pulse dynamics observed in a figure-9 laser. As a special design this cavity contains two gain segments which are pumped by two independently controllable current controllers. In contrast to dual gain segment based figure-8 architecture, figure-9 laser provides tunability both in pulse duration and peak power. The stable state is diagnosed as the rectangular noise-like pulse state from its characteristic auto-correlation trace. The repetition rate is 1.96 MHz and pulse duration is few nanoseconds. Pulse dynamics have been studied by varying the gain of both the amplifiers. It is found that the obtained NLPs behaves oppositely compared to conventional NLPs obtained from other cavities. This study has the potential to open up new research direction in studying pulse dynamics in any analogous figure-9 cavity.

4.1. Introduction: In the last two chapters, the performance of two physical saturable absorbers such as FSA, SESAM have presented which have absorption at the working wavelengths. In these material based saturable absorbers, there are atoms/molecules which absorb light at the lasing wavelength. In contrast, working principle of artificial saturable absorbers like NPR, NALM, NPE etc. relies on the fundamental properties of light (interference, birefringence etc.) because of which the response time of these SAs are considered instantaneous. In this chapter, performance of a figure-9 laser is presented where the mode-locking is done by NALM. As a special feature, this cavity contains two amplifiers, one is in the amplifying LOOP and other one is placed in the ARM. The solution of the cavity is identified as the noise-like pulse with rectangular temporal profile. The working principle of NLMs are briefly described below. Following that properties of different rectangular mode-locked pulse state are also described.

4.2. Working principle of non-linear loop mirrors: The working principle of nonlinear loop mirrors relies on the overlap of two electric field having a certain amount of phase shift. The phase difference arises during the propagation in a nonlinear medium because of difference in amplitude of two electric fields. Schematic of a NOLM is shown in figure 4.1(a) whereas 4.1(b) depicts schematic of NALM. An input electric field (E_{in}) splits into two counter-propagating waves (E_{CW} and E_{CCW}) after the splitter according to the splitting ratio (α: 1 - α). After travelling the same length of fiber (L = Fiber length of the loop) these two counter-propagating waves again combine at the splitter. However, during propagation, they acquire certain non-linear phase shift because of the non-linearity of the medium. If E is the electric field and n_2 is the nonlinear coefficient, the acquired phase-shift is given by

$$\varphi = \frac{2\pi n_2 |E|^2 L}{\lambda * Aeff}$$

$Aeff$ is the mode-field area and λ is the working wavelength [1-2]. If the splitter splits the input electric filed in an asymmetrical ratio ($\alpha \neq 0.5$), the amount of phase shift will be different for two counter-propagating waves. As the overlap between these two waves is phase sensitive, the output field will also respond according to the phase difference between two waves in the loop. The output field will also divide into two ports but let us consider a virtual optical isolator at ***port 1*** which will allow the output field in ***port 2*** only.

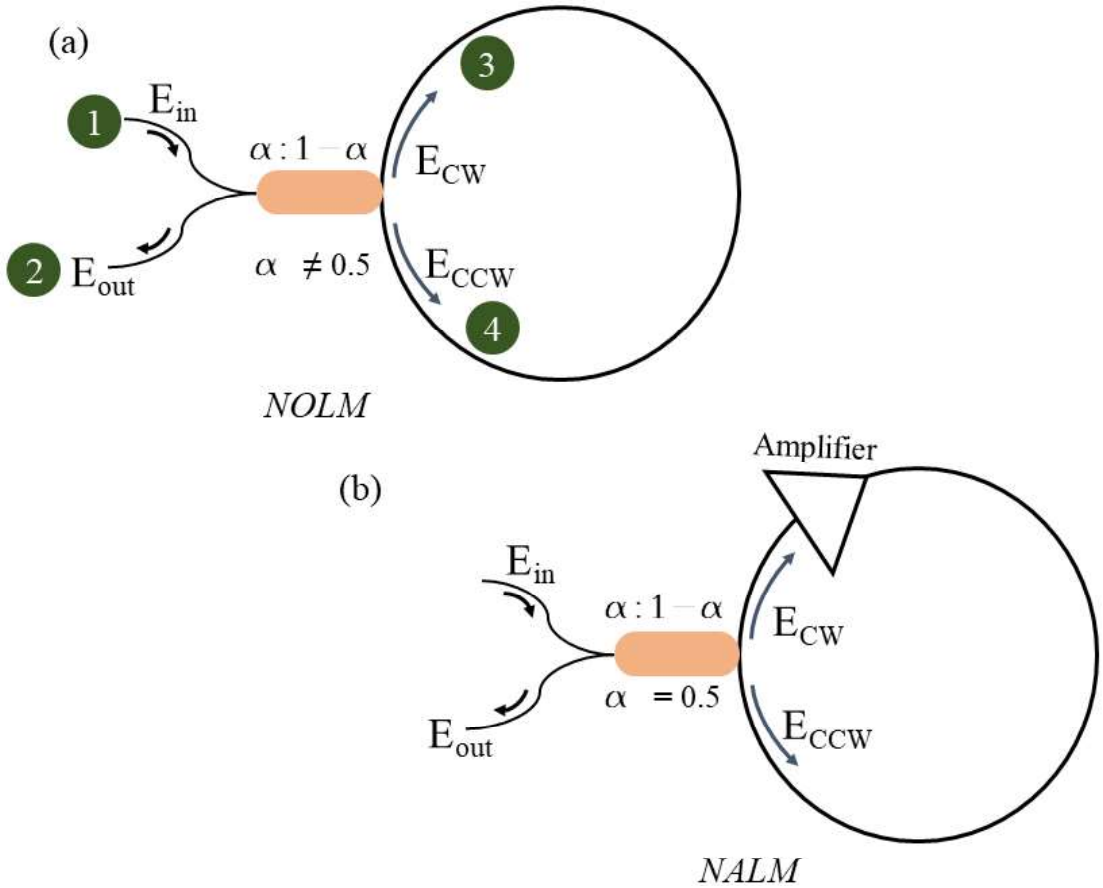

Figure 4.1: Schematic of (a) NOLM and (b) NALM, CW: Clockwise, CCW; Counter clockwise

Let E_{in} is the input electric field entering the splitter from ***port 1*** and splits into two part E_{CW} and E_{CCW} in ***port 3 and 4*** respectively with a splitting ratio α: 1- α.

$$E_{CW} = sqrt(\alpha) * E_{in} \quad \text{and} \quad E_{CCW} = i * sqrt(1-\alpha) * E_{in}$$

After propagating the whole loop when these two waves meet, then the output at ***port 2*** becomes

$$|E_{out}|^2 = |E_{in}|^2 \left(1 - 2\alpha(1-\alpha)\left\{1 + \cos\left[(1-2\alpha)|E_{in}|^2 * \frac{2\pi n_2 L}{\lambda * Aeff}\right]\right\}\right) \_\_\_\_\_ eqn(4.1)$$

From the above equation it is clear that the switching behaviour in other word the transmissivity varies periodically with the input power and in a specific wavelength region the periodicity depends on the coupling ration and the length of the loop. The transmissivity is given by the ratio of $|E_{out}|^2$ with $|E_{in}|^2$. Figure 4.2(a) corresponds to the normalized transmission spectrum at different coupling ratio (20 % and 40 %) keeping the loop length fixed at 5 m. For this plotting, value of n_2 is considered to be 3.16 x 10^-20, and Aeff is 30 μm^2. It is clear from the figure that a higher coupling ration provides higher modulation depth

but also possesses higher saturation power. Figure 4.2(b) corresponds to the normalized transmission spectrum at different loop length (5 m, 2m) keeping the coupling ratio fixed at 40 %. As the length of the fiber increases there is a greater non-linear phase shift between two counter-propagating waves which lowers the saturation power. For this reason, in an experiment longer length of fiber is required to easily start the oscillator.

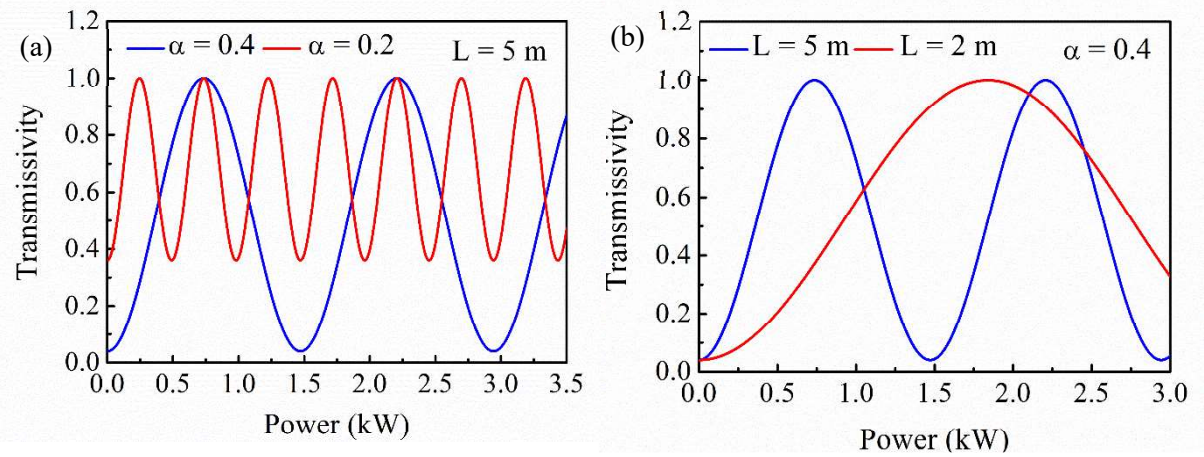

Figure 4.2: Transmission function of an NOLM for (a) different loop length keeping the splitting ratio same (b) different splitting ratio keeping the loop length same

When $\alpha = 0.5$, two counter propagating waves acquire same amount of non-linear phase,

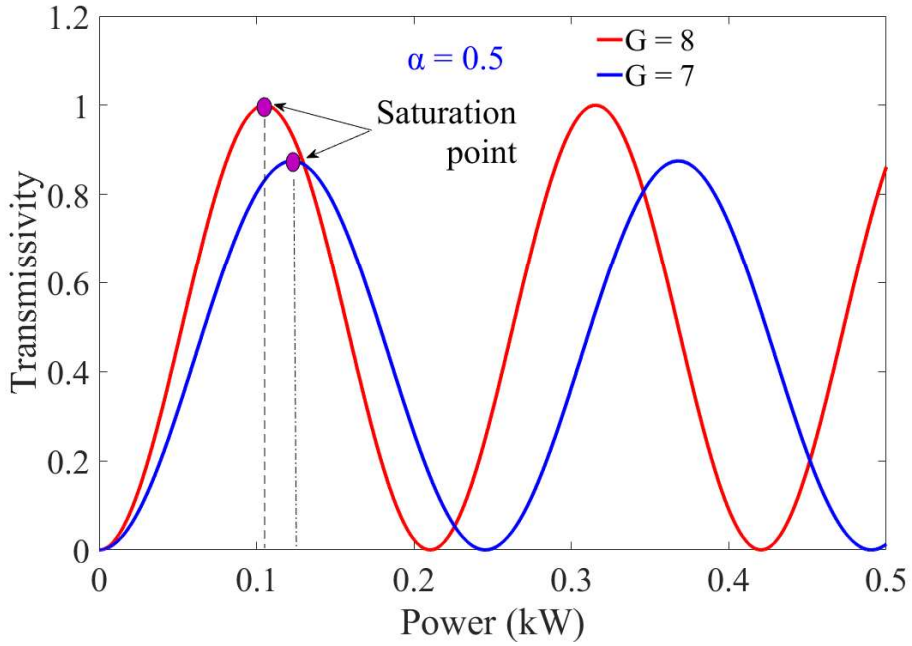

Figure 4.3: Transmission function of a NALM for different amplification factor

then no such switching occurs. However, placing an amplifier asymmetrically in the loop such that any of these two waves gets the gain early compared to other and propagates a longer length with higher power. In contrast, the other waves get the gain much later and as a

consequence a phase difference arises between two waves. Then it also acts as a switching device and known as NALM. In this case the transmissivity depends also on the gain of the amplifier. The function is given by the following equation.

$$T = G * [1 - 0.5\{1 + \cos\left(0.5 * (1 - G) * \frac{2\pi n_2 L}{\lambda * Aeff}\right] \quad \text{\_\_\_\_\_} eqn\ (4.2)$$

Where G is the amplification factor [3]. Increment of G is analogous as increasing the pump power in an experiment. Figure 4.3 shows the transmission curve of a NALM for different value of amplification factor. For higher value of G, the saturation power of the NALM reduces as the sufficient phase shift occurs between two counter-propagating waves.

4.3. Rectangular mode-locked pulse: As discussed on earlier chapters, single pulse energy of a stable single pulse state is limited by mainly energy quantization [4-5]. In 2008, it is theoretically predicted that, the pulse energy of a single pulse can be increased indefinitely without optical wave breaking in certain configuration. Later, these pulses are found in experiment and gained popularity as dissipative soliton resonances (DSRs) widely [6-7]. While increasing the pump power, the amplitude/peak power of these pulses remain constant but the pulse energy increases. As a result, the pulse duration increases. The temporal profile of these type of pulses is rectangular-shaped and often arises as a result of peak power clamping effect in saturable absorption curve. In artificial saturable absorbers, where the transmission function varies periodically such condition arises when intra-cavity reaches the crest of the transmission function [8-9]. Cavity made of physical saturable absorbers also shows this phenomenon as a result of reverse saturable absorption (RSA) [10]. Another type of square-shaped solutions are Noise-like pulses (NLPs), which possesses almost similar artefacts as DSRs including smooth optical spectrum and temporal profile [11-13]. However, many femtosecond incoherent sub-pulses are present within the square envelope of NLPs and in contrast to DSRs, spectrum of NLPs are broad. In experiment, NLPs are easier to obtain and diagnosed from its double-scaled auto-correlation trace [14]. At present, the demand of square wave pulses is increasing, as researchers have found their application in several field such as optical square clock, broadband generation for optical coherence tomography [15].

Both DSRs and NLPs are extensively studied in various SA-based cavities covering NPR, NALM, NOLM, CNTs, TIs etc. Recently, few works are reported where researchers have utilized two distinct gain module to further scale up the pulse energy in figure-8 configuration [16-18]. Surprisingly, they have found that the pulse duration and peak power behaves oppositely with the gain of two amplifiers. In these works, they have considered NALM based

figure-8 structure where the amplifiers are placed both in NALM loop and the unidirectional ring. Few works are also reported where the NALM itself contains two amplifiers [19-20]. It is found that the pulse duration increases with the gain of amplifier placed in the NALM loop keeping the peak power unaltered. However, the peak power depends on the gain of another amplifier that is placed in the unidirectional ring. These work concludes that dual amplifier based cavities provide an extra degree of freedom to achieve the tunability. Exploring in this direction, a figure-9 cavity has been constructed exploiting two independent gain section which eliminates the necessity of a high power optical isolator. Alongside, the pulse dynamics that we have observed is different in contrast to the figure-8 counterpart.

4.4. Dual gain segment based figure-9 cavity: Figure-4.4 shows the schematic of laser architecture which utilizes a NALM as a mode-locker. The laser consists of two part; one NALM LOOP and one ARM, coupled by a 3-dB coupler. In the LOOP, an Yb-doped double clad fiber of 2.5 meters of length is pumped by MM-LD through a pump combiner. A lab-made cladding mode stripper (CMS) is incorporated to extract the unused pump. Following the CMS, a 3-dB coupler is used to couple the NALM to the ARM. In one of the port, 90 meter HI1060 fiber is connected to elongate the cavity length. The cavity length is increased to introduce greater amount of non-linearity. A polarization controller (PC) is connected to easily start the oscillator. The ARM also comprises another Yb-doped fiber of 2.5 meter which is pumped by another MM-LD. After the gain fiber, another CMS is used to fulfil its usual purpose. Following the CMS, a chirped fiber Bragg grating (CFBG) is used to reflect (40 % reflectivity) a part of electromagnetic field back to the LOOP. The CFBG is employed in positive dispersion mode ($\beta 2 = +0.21$ ps^2) and also serves as an output coupler. The FWHM is 9.2 nm centered at 1064 nm. The net cavity dispersion is near to 2.58 ps^2. The cavity consists of two gain modules which are pumped by two independent current controllers. The pump power of two gain modules is named as $pump_{LOOP}$ and $pump_{ARM}$. In the same way the output terminals are named as $output_{LOOP}$ and $output_{ARM}$. An optical spectrum analyzer (YOKOGAWA, AQ6319) is used to record optical spectrum. The temporal characteristics are captured by an oscilloscope (DPO72004C, Tektronix, 20 GHz) and photodiode (DET08C/M, Thorlabs, 5 GHz). The consecutive pulses are captured in FastFrame setup of the oscilloscope in a fixed temporal window. The RF spectrum is recorded via FFT based software SignalVu of the oscilloscope. The autocorrelation trace is measured via Avesta auto-correlator (AA-10DD-30PS).

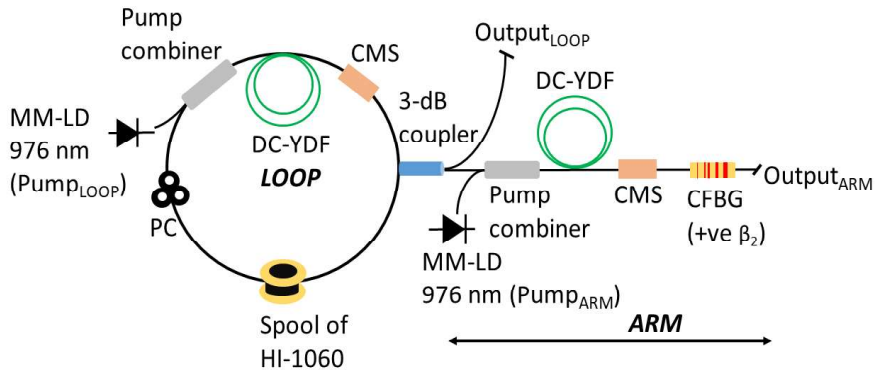

Figure 4.4: Schematic of the dual gain segment based figure-9 cavity, PC: Polarization controller, CMS: Cladding mode stripper, CFBG: Chirped fiber Bragg gratings

4.5. Results: Stable mode-locked pulse train appeared by adjusting the PC when pump$_{LOOP}$

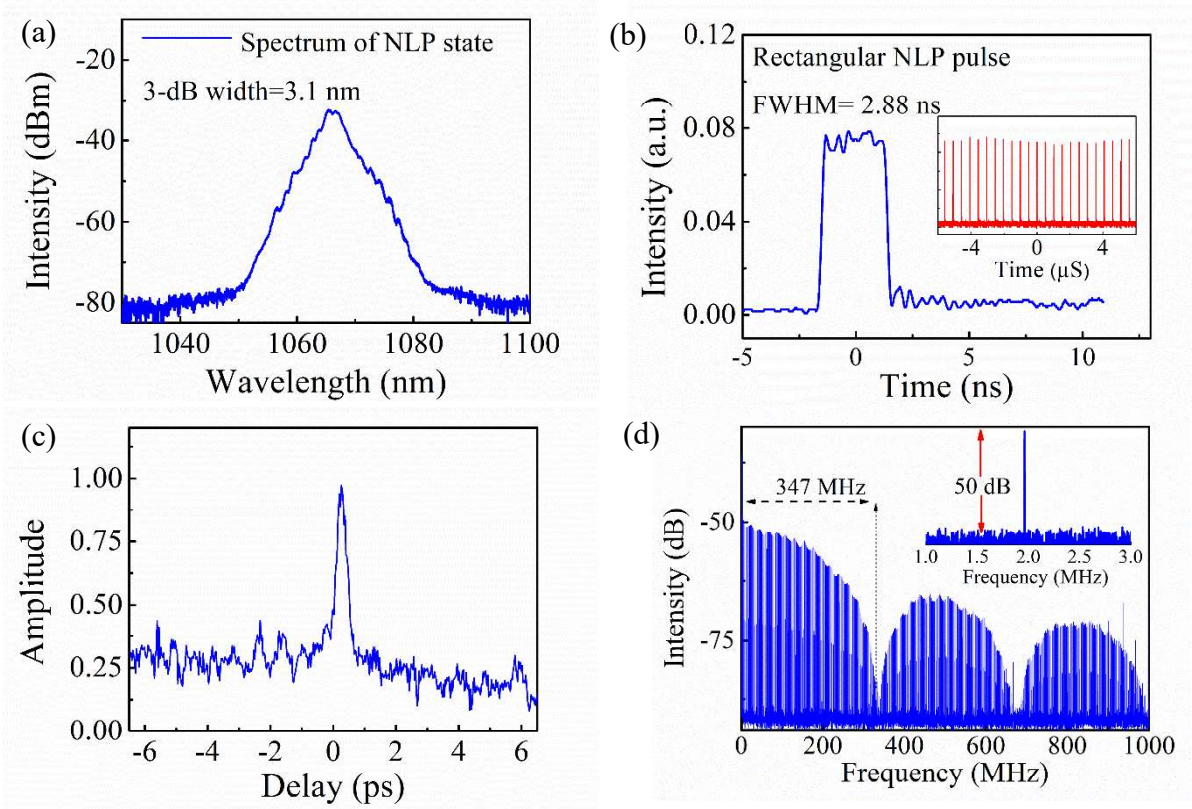

Figure 4.5: Characteristics of the noise-like pulse state, (a) output spectrum with triangular shape (b) Rectangular single pulse temporal profile (c) Autocorrelation trace of the NLP state (d) The RF-spectrum showing the repetition rate of 1.96 MHz with SNR > 50 dB

and pump$_{arm}$ are 2.1 W and 3.9 W respectively. The threshold pump powers are comparatively higher however the stable state persists at lower pump power also, once the stability is achieved. Figure-4.5(a) corresponds to the optical spectrum which possesses a triangular shape with a FWHM of 3.1 nm. The temporal intensity profile in shown in figure-4.5(b) which

is rectangular in shape. In inset, the long pulse train is also presented which confirms the stability. The autocorrelation trace confirms that the obtain state is a noise-like pulse state as it possesses the key signature of NLPs i.e., a femtosecond peak over a pico-second pedestal. Figure-4.5(c) corresponds to the auto-correlation trace. The RF-spectrum clarifies the fundamental frequency of the obtained state is 1.96 MHz and shown in figure-4.5(d). A frequency modulation of 347 MHz is present in the RF-spectrum which is due to the ns pulse duration, the modulation frequency is reciprocal of the pulse duration (2.88 ns). The SNR is above 50 dB. To check the spectral stability, output spectrum is recorded at same condition but after a time interval and shown in figure-4.6(a). No spectral fluctuation is noticed in that time duration. In figure-4.6(b), 1000 consecutive pulses are shown in colormap which shows the temporal stability of the state.

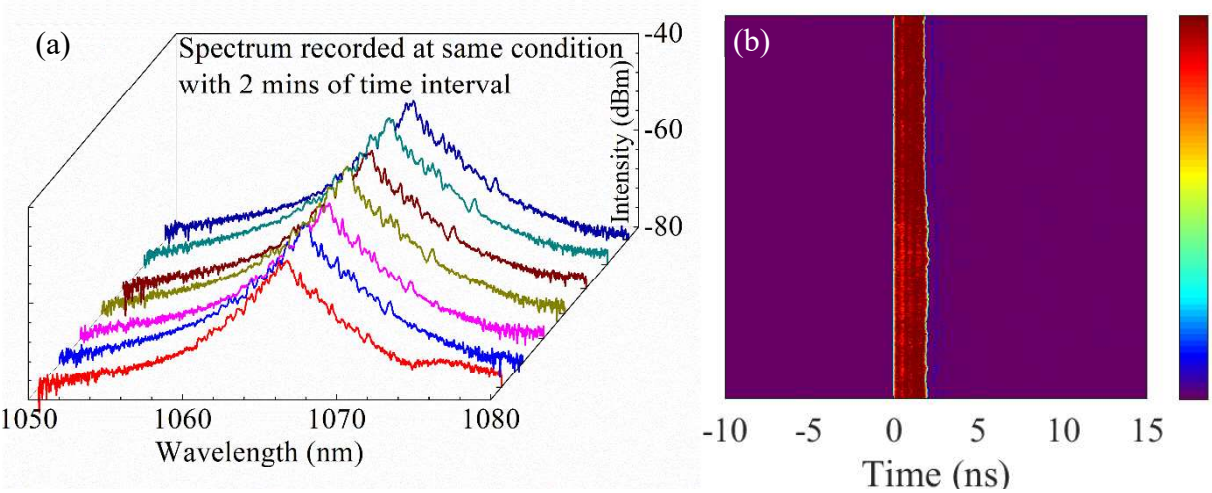

Figure 4.6: (a) Output spectrum recorded at different time but same condition (b) 1000 consecutive pulses recorded via *FastFrame* setup

Laser dynamics by gain variation in LOOP: Both the spectral and temporal dynamics is checked by varying the gain of the amplifier placed in the LOOP (varying the pumpLOOP power). During this characterization, $pump_{ARM}$ is kept fix at 3.9 W. Figure-4.7(a) shows the output spectrum at different $pump_{LOOP}$ power. The figure indicates that with the increment of the $pump_{LOOP}$ power the spectral width reduces. Figure-4.7(b) depicts the single pulse temporal profile at different $pump_{LOOP}$ power. It shows the increment of pulse duration (FWHM) with the increment of the $pump_{LOOP}$ power. Both spectral width and pulse duration corresponding to distinct value of $pump_{LOOP}$ power is plotted in figure-4.7(c). The

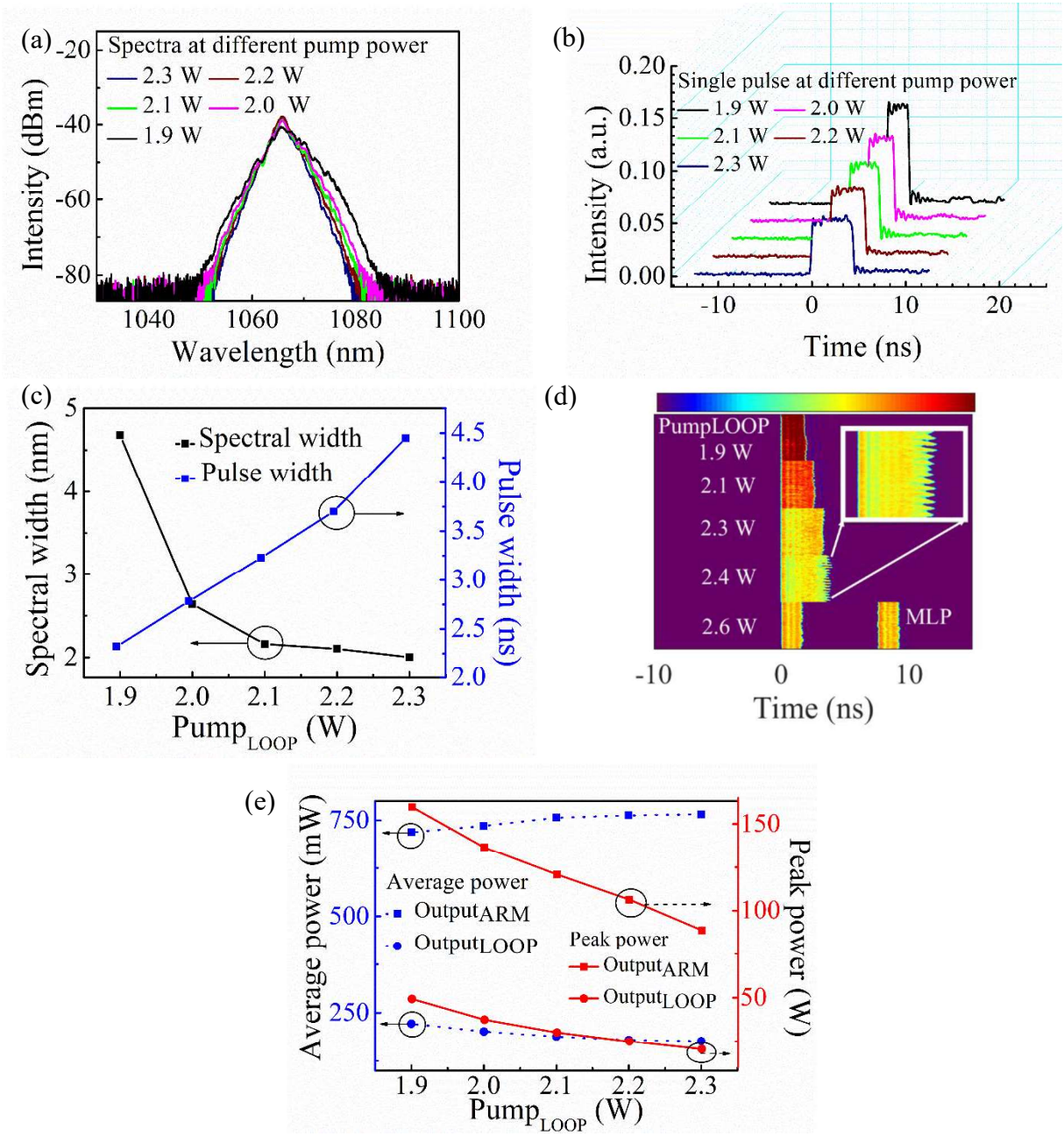

Figure 4.7: Laser dynamics by varying the gain of the LOOP. (a) Output spectrum at different power at the LOOP (b) Single pulse profile at different power. (c) variation of spectral and temporal width with the pump power (d) colormap of the consecutive pulses recorded at different pump power (e) Variation of average power and peak power with the pump power.

pulse duration increases from 2.3 ns to 4.5 ns. As soon as the pumpLOOP power reached 2.6 W, the pulse splits into a double pulse state with reduced pulse duration. In figure-4.7(d), 400 consecutive pulse at distinct $pump_{LOOP}$ is plotted in colormap configuration. The figure interprets that with the increment of pulse duration, the peak power reduces and before entering into the multi-pulse state the pulse duration goes through severe breathing as recorded at 2.4 W of $pump_{LOOP}$ power. The average power and peak power at two output

terminals are plotted in figure-4.7(e) which shows the peak power reduces with the $pump_{LOOP}$ power although the average power stays almost same. The peak power reduction and increment of pulse duration is noticeable in NALM-based lasers [20-22]. It happens when the cavity goes through peak power clamping effect. With the increment of the $pump_{LOOP}$ power, the phase shift between two counter-propagating waves increases which reduces the saturation power of the NALM as a consequence [3]. This behavior is common for conventional NLP and DSR states. Figure 4.8(a) depicts the temporal profile recorded at 2.6 W of $pump_{LOOP}$ power which corresponds to a double pulse state. The FWHM of individual pulse is 1.66 ns and the time interval between them is 7.6 ns. RF-spectrum of the double pulse state is shown in figure-4.8(b). The frequency spectrum contains two modulations at frequency reciprocal to the individual pulse duration (615 MHz = 1/1.66 ns) and time interval (130 MHz = 1/7.6 ns).

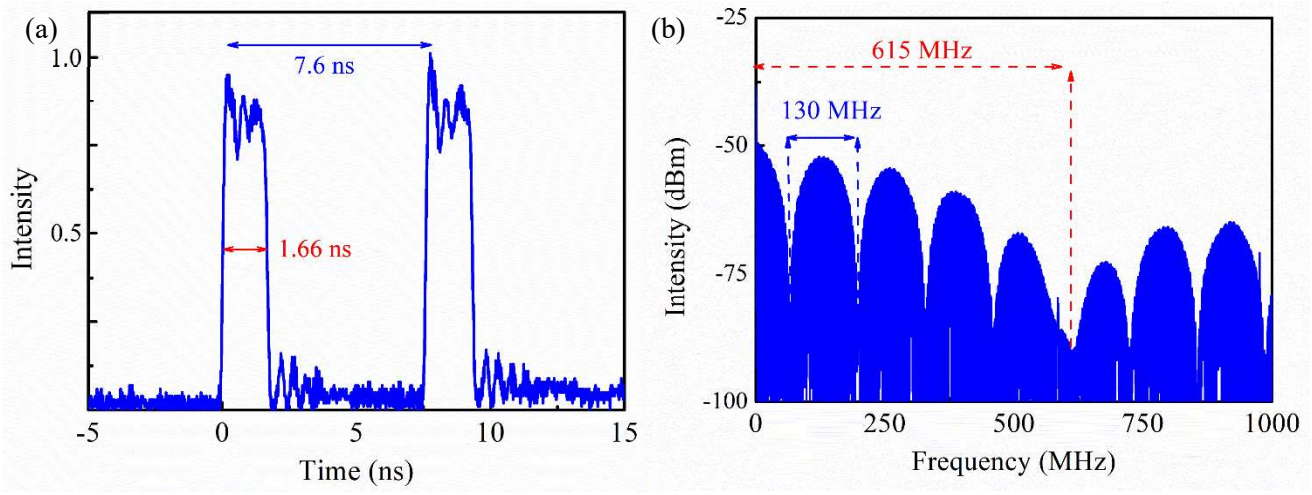

Figure 4.8: (a) Temporal intensity profile of a double pulse state (b) Rf-spectrum of the double pulse state

Laser dynamics by gain variation in ARM: The laser performance is studied by keeping the gain of the LOOP fixed and varying the gain of the ARM. The $pump_{LOOP}$ is fixed at 2 W and the $pump_{ARM}$ is varied from 2.8 W to 3.9 W. The output spectrum at different $pump_{ARM}$ is shown in figure-4.9(a) which shows the spectrum becomes broader with the increment of the $pump_{ARM}$ power. The single pulse profile in corresponding pump power is plotted in figure-4.9(b). It can be noticed that the pulse duration gets narrower with pump power and the peak power is also noticed to be increasing. The spectral width and pulse duration at different $pump_{ARM}$ power is plotted in figure-4.9(c) which possesses an exact opposite nature

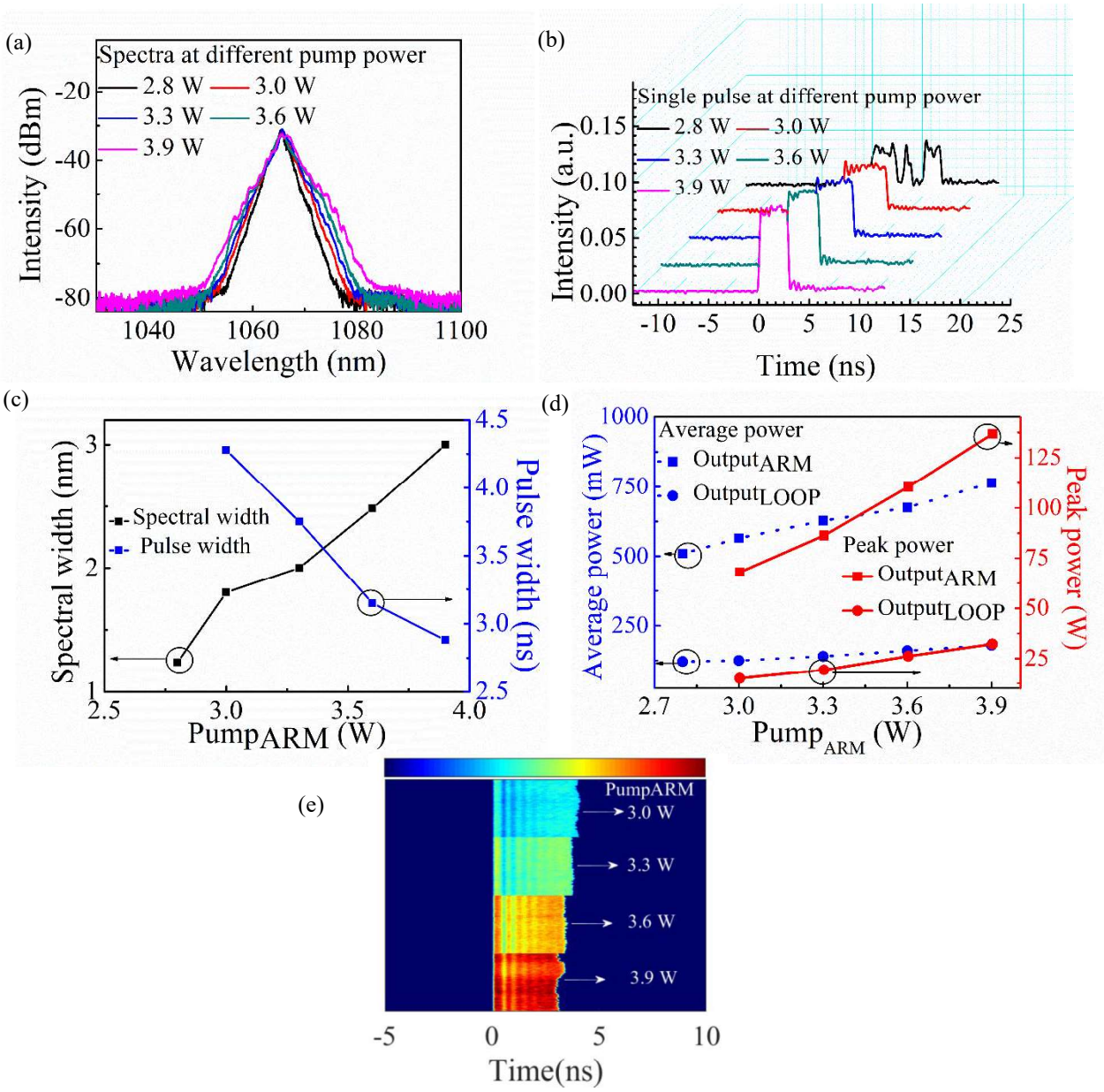

Figure 4.9: Laser dynamics by varying the gain of the ARM. (a) Output spectrum at different pump power (b) Single pulse temporal profile at distinct power (c) Variation of spectral and pulse width with pump power (d) variation of average and peak power (e) colormap of the consecutive pulses recorded at different pump power

of figure 4.7(c). The peak power also shows an opposite variation compared to figure-4.7(e). The average power and peak power at two terminals are plotted in figure-4.9(d). A colormap of 400 consecutive pulses at distinct pumpARM is shown in figure-4.9(e) which shows the pulse duration reduces as well as peak power increases.

4.6. Conclusion: In conclusion, a novel pulse dynamics of NLP state in a figure-9 cavity is revealed in this work. The laser contains two amplifiers which are independently controllable. In the stable condition the laser deliver rectangular pulses of few nano-second durations. The cavity length is sufficiently long to provide enough non-linear phase shift between two counter propagating waves in the NALM. The state is identified as NLP from its double-scaled auto-correlation trace. The peak power and pulse duration is dependent on the gain of both the amplifiers but they behave in an opposite manner. The study explores a possible direction of studying pulse dynamics in dual gain-segment based figure-9 cavities.

{Bibliography}

1. Doran, N. J., and David Wood. "Nonlinear-optical loop mirror." *Optics letters* 13, no. 1 (1988): 56-58.
2. Fermann, Martin E., F. Haberl, Martin Hofer, and H. Hochreiter. "Nonlinear amplifying loop mirror." *Optics Letters* 15, no. 13 (1990): 752-754.
3. Liu, Xuesong, Li Zhan, Shouyu Luo, Zhaochang Gu, Jinmei Liu, Yuxing Wang, and Qishun Shen. "Multiwavelength erbium-doped fiber laser based on a nonlinear amplifying loop mirror assisted by un-pumped EDF." *Optics express* 20, no. 7 (2012): 7088-7094.
4. Grudinin, A. B., D. J. Richardson, and D. N. Payne. "Energy quantisation in figure eight fibre laser." *Electronics Letters* 28 (1992): 67.
5. Bale, Brandon G., Khanh Kieu, J. Nathan Kutz, and Frank Wise. "Transition dynamics for multi-pulsing in mode-locked lasers." *Optics express* 17, no. 25 (2009): 23137-23146.
6. Chang, Wonkeun, Adrian Ankiewicz, J. M. Soto-Crespo, and Nail Akhmediev. "Dissipative soliton resonances." *Physical Review A* 78, no. 2 (2008): 023830.
7. Chang, Wonkeun, J. M. Soto-Crespo, Adrian Ankiewicz, and Nail Akhmediev. "Dissipative soliton resonances in the anomalous dispersion regime." *Physical Review A* 79, no. 3 (2009): 033840.
8. Wu, X., D. Y. Tang, Han Zhang, and L. M. Zhao. "Dissipative soliton resonance in an all-normal-dispersion erbium-doped fiber laser." *Optics express* 17, no. 7 (2009): 5580-5584.
9. Ding, Edwin, Philippe Grelu, and J. Nathan Kutz. "Dissipative soliton resonance in a passively mode-locked fiber laser." *Optics letters* 36, no. 7 (2011): 1146-1148.
10. Cheng, Zhaochen, Huihui Li, Hongxing Shi, Jun Ren, Quan-Hong Yang, and Pu Wang. "Dissipative soliton resonance and reverse saturable absorption in graphene oxide mode-locked all-normal-dispersion Yb-doped fiber laser." *Optics Express* 23, no. 6 (2015): 7000-7006.
11. Cheng, Zhaochen, Huihui Li, and Pu Wang. "Simulation of generation of dissipative soliton, dissipative soliton resonance and noise-like pulse in Yb-doped mode-locked fiber lasers." *Optics express* 23, no. 5 (2015): 5972-5981.
12. Zheng, Xu-Wu, Zhi-Chao Luo, Hao Liu, Nian Zhao, Qiu-Yi Ning, Meng Liu, Xin-Huan Feng, Xiao-Bo Xing, Ai-Ping Luo, and Wen-Cheng Xu. "High-energy noiselike rectangular pulse in a passively mode-locked figure-eight fiber laser." *Applied Physics Express* 7, no. 4 (2014): 042701.
13. Dong, Tianhao, Jiaqiang Lin, Yong Zhou, Chun Gu, Peijun Yao, and Lixin Xu. "Noise-like square pulses in a linear-cavity NPR mode-locked Yb-doped fiber laser." *Optics & Laser Technology* 136 (2021): 106740.
14. Zhao, Kangjun, Pan Wang, Yihang Ding, Shunyu Yao, Lili Gui, Xiaosheng Xiao, and Changxi Yang. "High-energy dissipative soliton resonance and rectangular noise-like pulse in a figure-9 Tm fiber laser." *Applied Physics Express* 12, no. 1 (2018): 012002.

15. Lin, Shih-Shian, Sheng-Kwang Hwang, and Jia-Ming Liu. "Supercontinuum generation in highly nonlinear fibers using amplified noise-like optical pulses." *Optics express* 22, no. 4 (2014): 4152-4160.
16. Mei, Li, Guoliang Chen, Lixin Xu, Xianming Zhang, Chun Gu, Biao Sun, and Anting Wang. "Width and amplitude tunable square-wave pulse in dual-pump passively mode-locked fiber laser." *Optics letters* 39, no. 11 (2014): 3235-3237.
17. Semaan, Georges, Fatma Ben Braham, Jorel Fourmont, Mohamed Salhi, Faouzi Bahloul, and François Sanchez. "10 μJ dissipative soliton resonance square pulse in a dual amplifier figure-of-eight double-clad Er: Yb mode-locked fiber laser." *Optics letters* 41, no. 20 (2016): 4767-4770.
18. Bahloul, Faouzi, Khmaies Guesmi, Mohamed Salhi, François Sanchez, and Rabah Attia. "Control of the square pulse properties in figure-of-eight microstructured fiber laser." *Optical Engineering* 55, no. 2 (2016): 026102-026102.
19. Smirnov, Sergey, Sergey Kobtsev, Alexey Ivanenko, Alexey Kokhanovskiy, Anna Kemmer, and Mikhail Gervaziev. "Layout of NALM fiber laser with adjustable peak power of generated pulses." *Optics letters* 42, no. 9 (2017): 1732-1735.
20. Du, Wenxiong, Heping Li, Yanjia Lyu, Chen Wei, and Yong Liu. "Period doubling of dissipative-soliton-resonance pulses in passively mode-locked fiber lasers." *Frontiers in Physics* 7 (2020): 253.
21. Krzempek, Karol, Jaroslaw Sotor, and Krzysztof Abramski. "Compact all-fiber figure-9 dissipative soliton resonance mode-locked double-clad Er: Yb laser." *Optics letters* 41, no. 21 (2016): 4995-4998.
22. Kharitonov, Svyatoslav, and Camille-Sophie Brès. "All-fiber dissipative soliton resonance mode-locked figure-9 thulium-doped fiber laser." In *The European Conference on Lasers and Electro-Optics*, p.

Chapter: 05

Lyot filter-based Mamyshev Oscillator: Design & Simulation

Abstract

The last three chapters present the pulse dynamics of Q-switched and mode-locked fiber lasers constructed with various saturable absorbers. In this chapter, a novel saturable absorption technique is introduced, elucidating its operational principles. Relying on the theory of Mamyshev regenerator, this approach involves periodic spectral filtering and successive amplification to generate ultra-short pulses. A new Mamyshev oscillator architecture is proposed, incorporating a tunable Lyot filter (LF) as one spectral filter, alongside a Gaussian filter of fixed bandwidth and central wavelength. Generalized nonlinear Schrodinger equation (GNLSE) is solved on the architecture to look into the pulse dynamics. The tunability of the proposed LF is achieved through the introduction of stress-induced birefringence. Distinct pulse dynamics are observed based on the overlap between the two filters. Under optimized conditions, the oscillator produces parabolic pulses with a linear chirp profile. Numerical assessments of pulse compressibility are conducted. The study also explores the evolution of intra-cavity spectrum and pulse dynamics. The numerical study is structured in a way that an experimentalist can reproduce the results from an analogous experimental setup.

5.1. Introduction: The generation ultra-short pulse requires an approach by which the cavity supports high intensity components over the low intensity components. Then, through an iterative process, a high-intensity noise fluctuation transforms into a stable pulse after several roundtrips. This process is known as saturable absorption, which is implemented in the laser through either an artificial or physical method. In their work [1], North et. Al. have proposed an architecture where two optical regenerators are placed in a closed loop form and observed ultra-short pulses of few picosecond durations at the communication wavelength. They have explained that the saturable absorption effect arises in the cavity because of nonlinearity-induced spectral broadening and consecutive spectral filtering that is occurring in each roundtrip due to its component-specific design. The technique was based on the theory of Mamayshev regenerator [2], proposed on 1998 and draws a significant attention from researchers after the work of Relegeskis et. Al. in 2015 where they have built an oscillator capable to deliver 2.6 nJ pulses with 3 ps duration at 1060 nm [3]. Following this work, Samartsev et. Al. [4] and Siderenko et. Al. [5] have reported their work which are relied on the same method and any laser built using this approach is referred to as a '*Mamyshev oscillator*'(MO).

A simplest architecture of MO consists of two arms; each arm contains one amplifier and a band-pass filter as shown in figure 5.1. The key point is that the central wavelength of the two BPFs should have an optimized offset. Any intensity fluctuation form noise will experience SPM-induced spectral broadening while propagating down the amplifier. Then the first spectral filter will allow a part of the spectrum and the same process will happen in second arm. So a fluctuation with sufficient peak power can only persists in the cavity and eventually evolves into a stable pulse after sufficient roundtrips. So, it is evident that performance of a MO depends on the offset between two filters. It is easier to start a MO at lower offset, however better pulse quality and higher pulse energy is achieved at greater offset value [6]. To initiate a MO, researchers use tunable BPFs; initially the offset is kept low and once the pulsing starts, the pulse quality is improved by tuning the BPFs to a greater offset value. However, a several approach have been adopted to start a MO easily. The next section delves into some techniques that researchers have adopted to start a MO.

5.2. Starting dynamics of a MO: As complete suppression of the CW requires higher offset, it automatically hinders the growth of fluctuations from noise. Although a certain

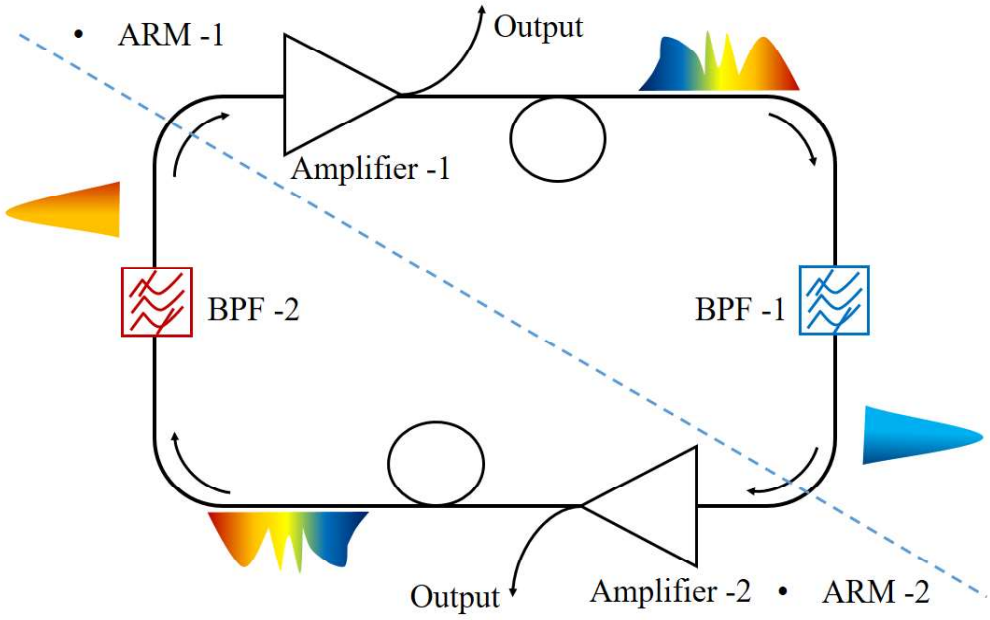

Figure 5.1: A simplest schematic diagram of Mamyshev oscillator showing generation of short pulse by SPM-induced spectral broadening and successive spectral filtering

amount of overlap between filters helps to initiate pulsing, this method limits the pulse energy to a lower value. Keeping the offset at greater value, the fluctuation is initiated by an additional arm which contains a SESAM, by utilizing NPE with offset spectral filtering, pump modulation, and feed backing the rejected components from the filter into the cavity. The most adopted technique is seeding another short duration and low-energy pulse to start the oscillator. Systematic tuning of spectral filtering along with pump modulation is also adopted by the researchers to initiate MO. Several numerical study is also conducted on MO where both the seed pulse and white Gaussian noise (WGN) is used as the initial electric field to start the simulation [6]. It is found that a certain amount of overlap between filters is needed to get a stable solution when WGN is used to initiate the simulation.

MOs have been built by using various types of filters such as FBGs, CFGBs, gratings pair, free space or fiber coupled band pass filter which works in either transmissive or reflective mode. Few works which dealt with filter separation used tunable spectral filter where tunability is achieved by using temperature or stress-controlled FBG or by using commercial thin film based spectral filter. A table is appended below which contains information on the working wavelength, type of spectral filter and the adopted method to start the laser.

Table – 5.1: Mamyshev Oscillator at three main wavelength regime

Type of gain medium	*Type of filters*	*Starting procedure*	*Pulse width/pulse energy*	*Ref.*
Yb^{3+} doped fiber	Commercial fixed Band-pass filter	External seed	73 fs /122 nJ	[7]
	FBG pair	Pump modulation	38 fs/102 nJ	[8]
	Free space filters	Microchip Q-switched laser		[9]
	Commercial tunable Band-pass filter	Pump modulation +filter shifting	40 fs/80 nJ	[10]
	Commercial tunable Band-pass filter	Pump modulation + filter shifting		[11]
	Free space filters	Pump modulation + filter shifting	65 fs/21 nJ	[12]
	Grating pair	NPE + external seed	58 fs/1.2 μJ	[13]
	Commercial fixed Band-pass filter	External seed	56 fs/83.5 nJ	[14]
	grating	External seed	50 fs/1 μJ	[15]
	grating	NPR	1.5 ps	[16]
	grating	NPE		[17]
Er^{3+} doped fiber	grating	NPE	100 fs/31.3 nJ	[18]
	Grating+BPF	External seed	2.9 ps/ __	[19]
	Commercial tunable Band-pass filter	External seed	83 fs/0.1 nJ	[20]
	Commercial fixed Band-pass filter	Self-start	3 ps (HML)	[21]
	cfbg	Additional arm with SAM	103 fs/21.3 nJ	[22]
	Commercial Band-pass filter	External seed	1.61 ps	[23]

Tm^{3+} doped fiber	Grating pair	NPE + external seed	140 fs/15 nJ	[24]
	grating	NPE + seed	208 fs/3.5 nJ	[25]

A Lyot filter is another type of spectral filter which is constructed by using a birefringent crystal (quartz, liquid crystal etc.) placed in a proper orientation to the polarization direction of the input light [26]. In case of optical fiber based LF, a polarization maintaining fiber (PMF) of specific length in spliced between two polarizers [27-28]. The wavelength selectivity of the LF depends on the amount of optical phase acquired by the light and total birefringence of the PMF. So, by modifying the value of total birefringence, the transmission curve can be shifted. In the field of mode-locked fiber laser, LF is adopted to build tunable ultrafast laser or to achieve multi-wavelength operation [29-30].

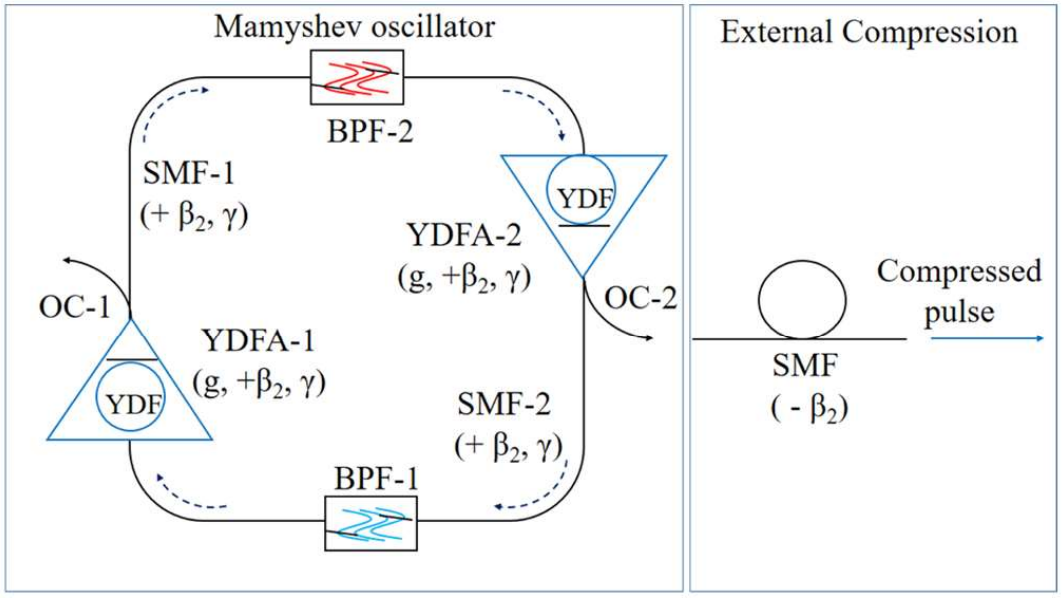

Figure 5.2: Schematic of the proposed LF-based MO at 1064 nm considered for theoretical simulation

5.3. Design of Lyot filter based Mamyshev oscillator & simulation details:

Figure 5.2 depicts a schematic representation of the laser cavity in a MO configuration, which is simulated numerically. The MO comprises two ytterbium-doped fiber amplifiers (YDFA-1 and YDFA-2), each having a gain fiber length of 1 meters and two band-pass filter (BPF-1 and BPF-2). A 90:10 splitter is considered after each amplifier, 10 % of which is used to collect the output field after each roundtrip. The output ends following the two amplifiers are

denoted as OC-1 and OC-2 respectively. After each splitter, 2 meters of single mode passive fiber is considered to get enough spectral broadening. For simplicity, we have assumed identical values for dispersion (β_2) and nonlinear coefficient (γ) for both the fibers set at 22.7 x 10^{-3} ps^2/m and 5.1 /W/km, respectively at the operating wavelength of 1060 nm to align with the characteristics of the commercial fiber HI1060 from Corning. The simulation is done in a unidirectional manner by solving the generalized nonlinear Schrodinger equation (GNLSE). The GNLSE considering second-order dispersion and Kerr-nonlinearity is solved by well-known SSFM method. The mentioned equation is given by

$$\frac{\partial A}{\partial z} - \frac{i\,\beta_2}{2}\frac{\partial^2 A}{\partial T^2} = g(z)\left[\frac{A}{2} + \frac{1}{2\Omega_g^2}\frac{\partial^2 A}{\partial t^2}\right]A - i\,\gamma\,|A|^2 A \qquad \text{_____}eqn.\,5.1$$

A is slowly varying envelope, β_2 is the second order dispersion, γ is the nonlinear coefficient. The additional term is for the gain segment where $g(z)$ is the saturable gain coefficient, can be expressed as a function of small signal gain (g_0) as $g(z) = \frac{g_0}{1+\frac{E}{E_{sat}}}$. E_{sat} is the saturation energy and E is the energy of a single pulse denoted as $\int_{-\infty}^{+\infty}|A|^2 dt$. Manipulation the value of E_{sat} and g_0 is analogous to alter the pump power in a hypothetical experiment. In our work, value of E_{sat} is kept fixed at 10 nJ and only the value of g_0 is varied in a range to study the effect of gain on the oscillator performance. To initiate the simulation, a white Gaussian noise is introduced at the beginning of YDFA-1. Several number of simulations are performed and analyzed by altering the initiation point, but it is observed that the final pulse properties do not depend on the selection of the starting point. The compressibility of output pulse is checked by solving NLSE in a negatively dispersive fiber of 1 meter with suitable GVD.

5.4. Architecture of a Lyot filter & other filter properties:

Working principle of a LF: In figure 5.3(a), a simplest architecture of a LF is shown. A birefringent crystal of a certain length is placed between two polarizers. To obtain maximum modulation depth, the axis of birefringent crystal is aligned to 45^0 with the axis of polarizers. Considering a randomly polarized light at the input, first polarizer allows the light of a particular direction which is divided into two orthogonal components in the birefringent crystal. While propagating through the birefringent crystal, each wavelength component experiences a distinct amount phase shift. Second polarizer serves as an analyzer and transmits each wavelength according to their associated phase (orientation). In this way an amplitude modulated transmission is obtained. In case of single-stage LF, a sinusoidal

transmission is obtained. Wavelength gap between two consecutive peaks is known as free spectral range (FSR). By utilizing multiple birefringent crystals, the value FSR can be controlled. A schematic of a double-stage LF is shown in figure 5.3(b). In this multi-stage cases, length of every second birefringent has to be half of the length of previous crystal to obtain side-band free transmission curve.

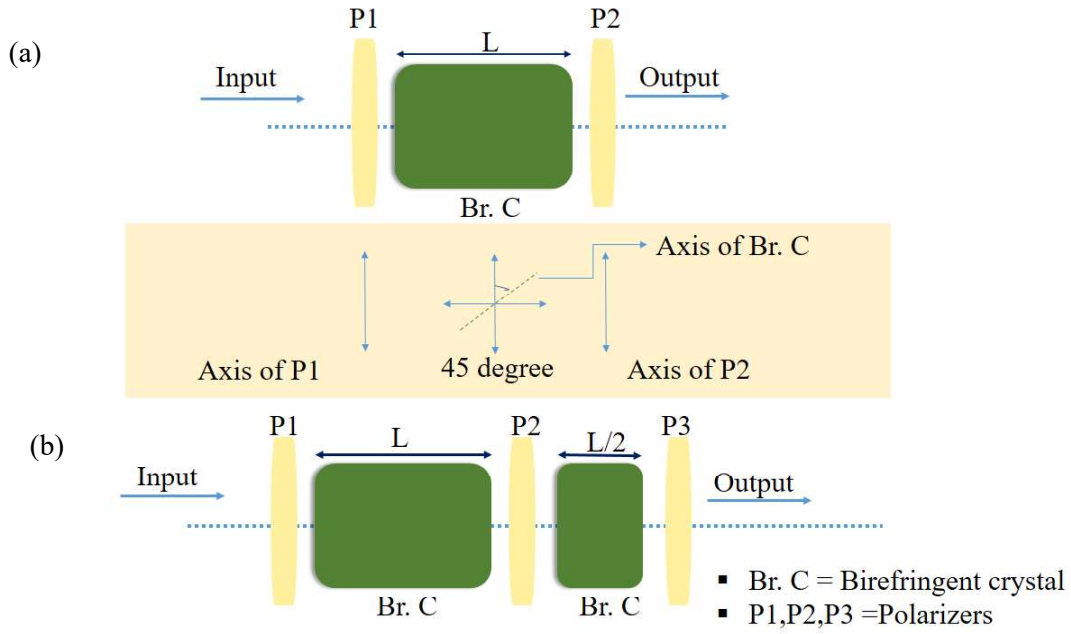

Figure 5.3: Schematic of crystal based (a) single-stage (b) double-stage Lyot filter

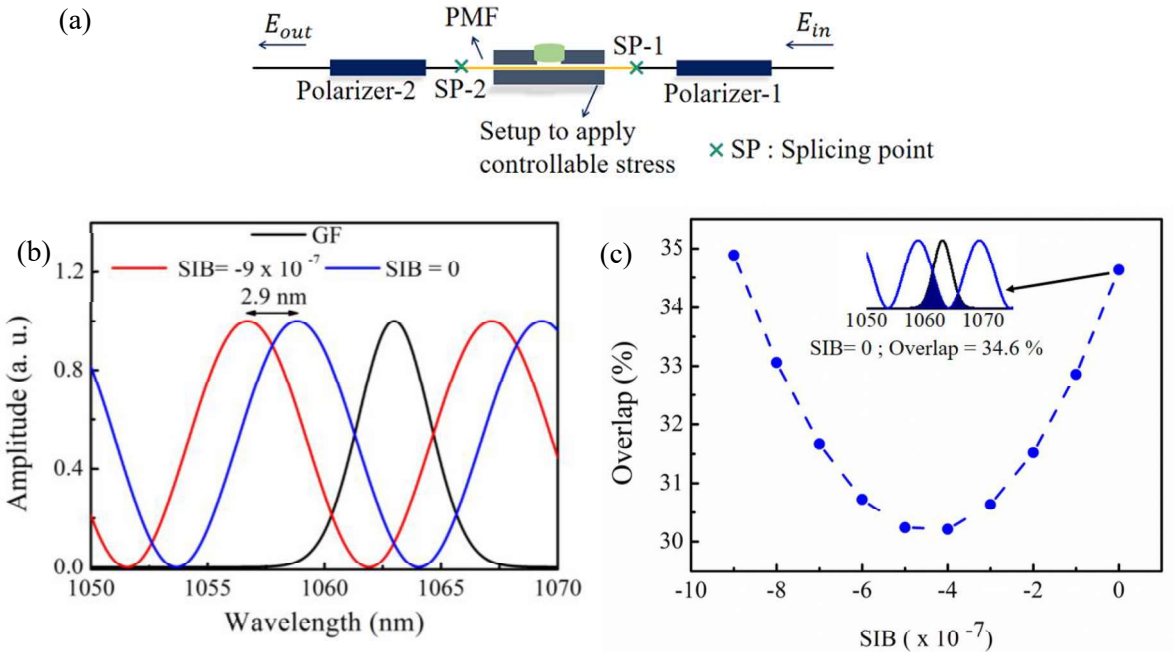

Figure 5.4: (a) Schematic of a Lyot filter (LF) (b) transmission function of LF at different stress-induced birefringence (SIB) value; (c) variation of spectral overlap between LF and GF with SIB of LF

A basic configuration of a LF involves placing a polarization-maintaining fiber (PMF) between two inline fiber polarizers, as depicted in figure 5.4(a). Similar architecture has been adopted in various literature for different application. The purpose of each component is described below.

Polarizer-1: Initially, polarizer-1 transforms a randomly polarized light into linearly polarized light. The light then enters a PMF at a 45-degree angle relative to the input light's polarization direction (SP1 denotes a 45-degree splice).

Birefringent fiber: Inside the PMF, the light is divided along two perpendicular axes. Each spectral component acquires a unique phase shift depending on the birefringent value of the fiber.

Polarizer-2: At end polarizer-2 is placed at a 45-degree angle with the fast axis of the PMF (SP2 represents a 45-degree splice), converts the acquired phase shift into an amplitude-modulated transmission spectrum. To maximize modulation depth, it is important to align polarizer-2 precisely.

Applying stress to the PMF allows the alteration of its total birefringence, leading to a shift in the spectral window. This modification is key to achieve the desired changes in the

transmission spectrum. The mathematical representation of the LF's transmission function can be calculated by transfer matrix method.

The transfer matrix of the different elements has been presented below.

$$E_{in} = \begin{bmatrix} 1 \\ 1 \end{bmatrix} \text{ is the input electric field}$$

P1 is the matrix for first polarizer

$$P1 = \begin{bmatrix} 1 & 0 \\ 0 & 0 \end{bmatrix}$$

PM is the matrix for the PM –fiber

$$PM = \begin{bmatrix} e^{-i\phi} & 0 \\ 0 & e^{i\phi} \end{bmatrix}$$

Where

$$\phi = \frac{\pi * L * \Delta n}{\lambda}$$

L is the length of the polarization-maintaining fiber (PMF). $\Delta n = \Delta n_{PM} + \Delta n_S$, represents the effective birefringence of the PMF, sum of both the inherent birefringence of the PMF (Δn_{PM}) and the stress-induced birefringence (Δn_S). λ is the operating optical wavelength. P2 is the matrix for the last polarizer

$$P2 = \begin{bmatrix} \cos\theta & \sin\theta \\ -\sin\theta & \cos\theta \end{bmatrix}$$

Θ is the angle of the polarizer with the fast axis of PMF. The output electric field E_{out} is given by

$$E_{out} = [P2][PM][P1][E_{in}]$$

Transmissivity is given by

$$T(\theta, \lambda, \Delta n) = \frac{1}{2} * (1 + sin2\theta) * cos^2\left(\frac{\pi * \Delta n}{\lambda} L\right)$$

for the special case $\theta = 45^0$ this equation reduces to

$$T(\theta, \lambda, \Delta n) = \left|\frac{E_{out}}{E_{in}}\right|^2 = cos^2\left(\frac{\pi * \Delta n}{\lambda} L\right) \_\_\_\_\_ eqn.5.2$$

According to Equation-5.2, the transmission function of the LF is directly related to the effective birefringence of the fiber. To change the stress induced birefringence, we can place the PMF is within an in-line fiber polarization controller (PC). By rotating the paddle of the PC, the PMF will experience a certain amount of stress and as a consequence the transmission function will be shifted. Although the stress-induced birefringence is in the order of 10^-7, it is sufficient to generate a measurable shift to the transmission spectrum. In literature, several experimentally proven methods of tuning a LF exist. In the most recent approach, the PMF is placed on a piezoelectric stretcher and a controllable amount of stress is introduced to the fiber electronically [31]. The same research group also demonstrates tunability of the LF by placing the fiber on a heated surface and systematically varying the system temperature [32]. Transmission curve at different values of SIB is plotted in figure 5.4(b). The inherent birefringence is fixed at 4.5×10^{-4} [33]. The FSR which is defined as the gap between two consecutive peaks, is determined from the formula: $FSR = \frac{\lambda^2}{\Delta n * L}$. The bandwidth is calculated from the formula: $BW = \frac{\lambda^2}{2 * \Delta n * L}$. In this work, is chosen to be 24 cm which fixes the BW at 6 nm and FSR at 12 nm. The other filter of the MO is a Gaussian filter centered at 1064 nm with a FWHM of 3 nm which is kept fixed throughout the numerical investigation.

Overlap factor: In figure 5.4(c), the spectral overlap between two filters is plotted against the SIB of PMF. The spectral overlap which is defined as the common area under the transmission function of both the filters, is shown in figure 5.4(c) (inset). The maximum overlap is set at 100 % corresponding when the Gaussian filter entirely falls inside the LF's transmission band. By varying SIB, the position of LF is shifted and the spectral overlap at different position of LF is plotted. As the transmission function of the LF undergoes a blue shift, the overlap initially decreases. However, beyond a certain point, the overlap increases again, taking on a shape of a parabola. This behaviour is attributed to the sinusoidal

transmission spectrum of the LF. The succeeding section delves into the detailed properties of the output from the cavity depending on the amount of spectral overlap.

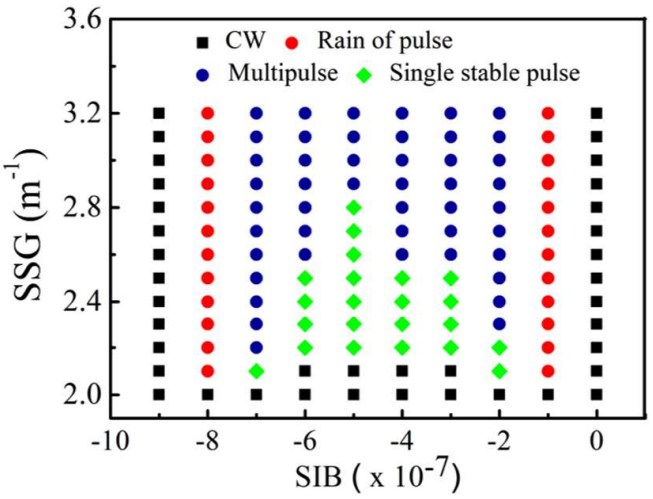

Figure 5.5: Various pulsing regimes obtained as the solution of GNLSE over a two parameter space (SIB & SSG)

5.5. Results & discussions: To look into the performance of a LF-based MO, GNLSE is solved by varying two parameters; one is SIB and another one is SSG. Variation of SIB is akin to tuning of the LF by shifting the transmission peaks and variation of SSG is similar to adjusting the pump power. Over this two parameter space, distinct solutions have been obtained which includes stable single pulse state, multiple pulse state and 'rain of pulse'. Fixing the SSG at 2.4, when the filter is set in a position where the overlap between two filters is high enough, the cavity couldn't suppress the CW part even after a large number of roundtrips, that state is named as 'CW'. By reducing the overlap slightly, a state is found which contain multiple pulses with irregular time gap over CW background. This state can be considered as an intermediate state between pure CW and stable single pulse state. Further reduction of filter overlap leads to a multiple pulse state. From a multiple pulse state, a single pulse is realized by either reducing SSG or by tuning the filter to a lower overlap position. Attributes of each state and probable reasons are discussed in the subsequent section. The obtained pulse states over two parameter space is shown in Figure 5.5.

5.5. A. Rain of pulses: In the position of intermediate spectral overlap, the cavity can't filter out the CW components completely. Due to weak saturable absorption affect, certain number of pulses appear over the CW background with random time interval between them. This type of state was observed in various mode-locked cavities utilizing both physical and artificial

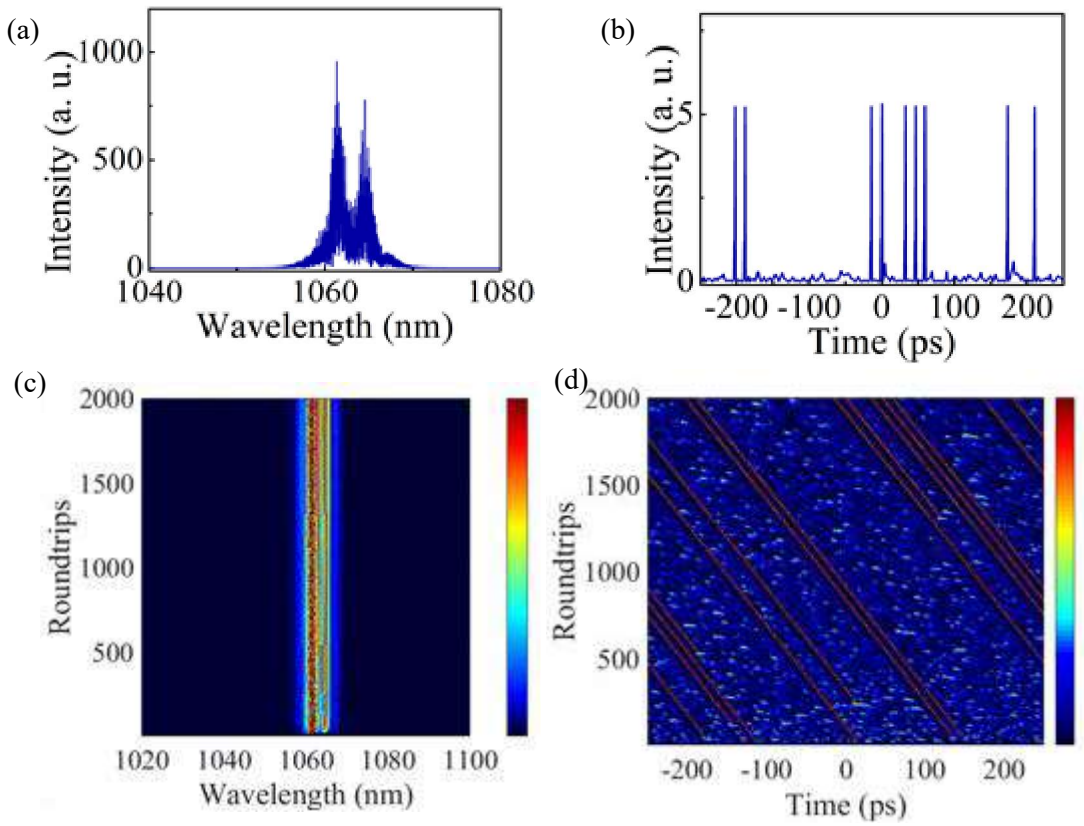

Figure 5.6: Attributes of 'rain of pulse' state. (a) Final obtained spectrum & (b) pulses after completing 2000 roundtrips. Roundtrip-to-roundtrip (c) spectral & (d) temporal variation over 2000 roundtrips

saturable absorbers such as NPR, material-based SA, NOLM, etc [34-35].In reference [36], Chouli et al. have characterized these states as an intermediate stage between a continuous wave and a stable mode-locked state, resulting from weak mode-locking. The output spectrum of the corresponding state is depicted in figure 5.6(a). The output spectrum contains sharp peaks which is a sign of CW breakthrough. The output pulse is presented in figure 5.6(b). 9 pulses are present with in the time interval of 500 ps, the time gap between consecutive pulses are also not consistent. Roundtrip-to-roundtrip spectral and temporal evolution over 2000 consecutive roundtrips are shown in figure 5.6(c) and 5.6(d) respectively. The cavity could not supress the CW part even after 2000th roundtrips.

5.5. B. Stable single pulse state: After attaining the rain of pulse state, the single pulse state is attained by tuning the spectral overlap. The spectral build up at OC-2 over consecutive roundtrips is shown in figure 5.7 (a). The figure indicates that although there was strong CW component initially, over the roundtrips, CW part got suppressed and a smooth steady spectrum is attained. Figure 5.7(b) shows the spectra at 760th roundtrips which contains CW

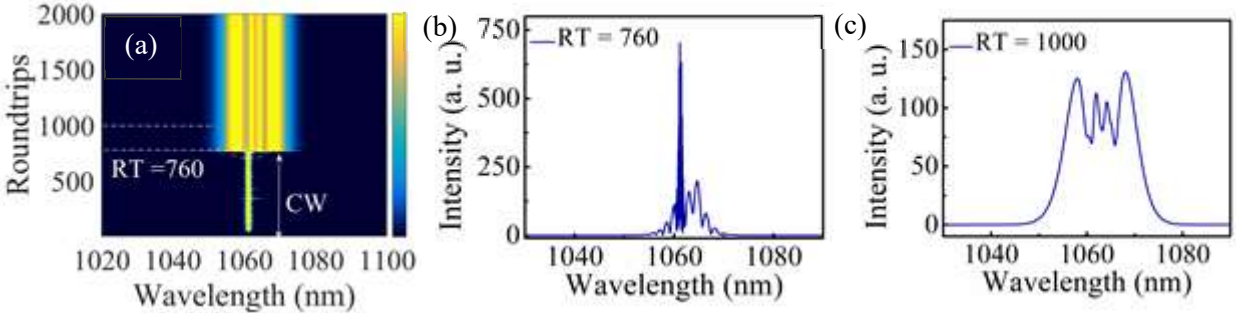

Figure 5.7: Spectral evolution of a single pulse state. (a) Spectral evolution over 2000 roundtrips. (b) Spectrum after 760 roundtrips (c) Spectrum after 1000 roundtrips

spike, whereas figure 5.7(c) represents the spectrum at 1000th roundtrip without any CW spike. The final spectrum is smooth and have a sign of SPM-induced spectral broadening. This spectrum has a FWHM of 15.9 nm corresponding to 105 fs transform-limited pulse.

The roundtrip-to-roundtrip temporal evolution is shown in figure 5.8(a). The intensity profile and its associated chirp is presented in figure 5.8(b). The intensity profile is smooth and chirp is almost linear at the center of the pulse. Both the Gaussian fitting and parabolic fitting is done to investigate the pulse shape. After fitting the misfit parameter is calculated from the following formula

$$M^2 = \frac{\int (I - I_{fit})^2 \, dt}{\int I^2 \, dt}$$

Where I and I_{fit} is the intensity of the actual and fitted curves respectively. For the parabolic fitting the misfit parameter is 0.26 % whereas for Gaussian fitting the misfit parameter is 3.6 %. In figure 5.8(c), actual temporal profile with Gaussian and parabolic fitting is shown. Thus, the state can be diagnosed as '*amplifier similariton*' for its parabolic intensity profile with linear chirp. Amplifier similariton is particularly known for its high compressibility [37-40]. We have checked the compressibility of the stable state numerically and found that the pulse is compressible to 125 fs which is near to its transform-limited duration (105 fs). The intensity profile after compression is presented in figure 5.8(d).

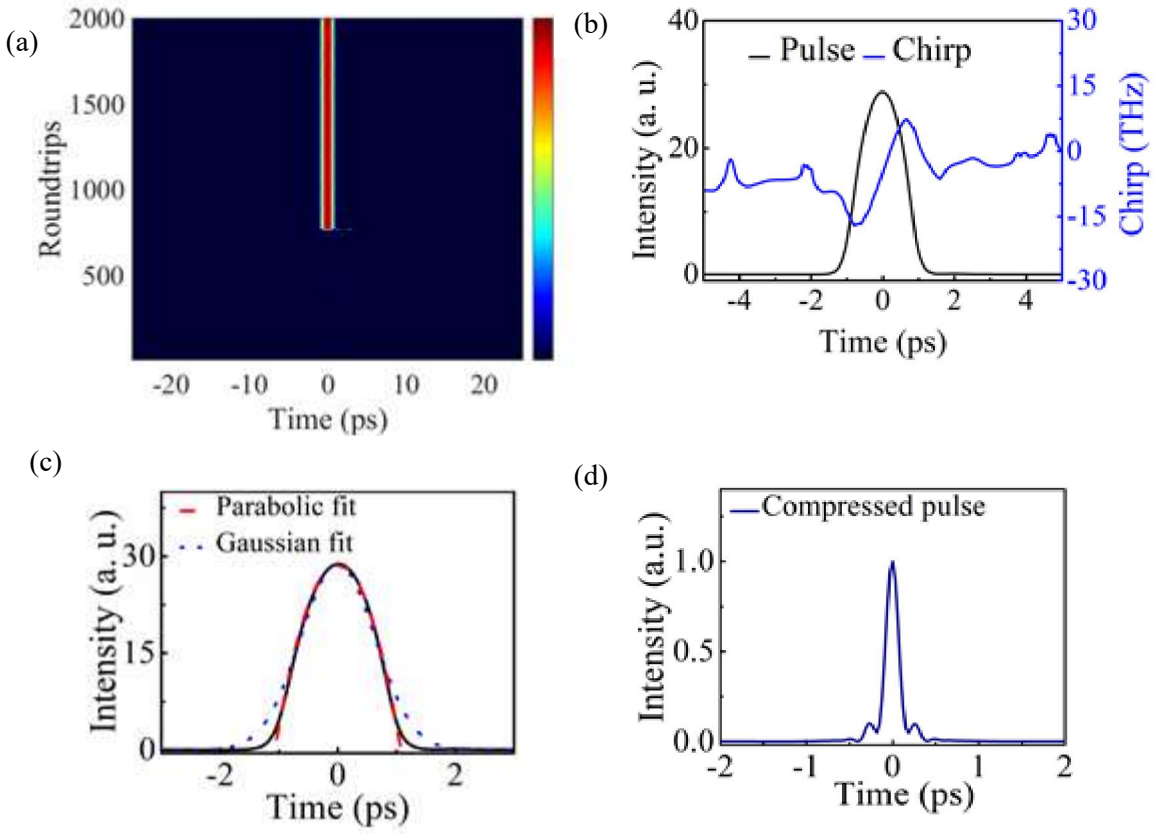

Figure 5.8: Temporal properties of a single pulse state. (a) Temporal evolution over 2000 roundtrips. (b) Intensity profile and associated chirp of a single pulse (c) Actual intensity profile with Gaussian and parabolic fit (d) intensity profile of a compressed pulse

While the intensity profile of both the spectrum and pulse is smooth at OC-2, it exhibits a broken nature at OC-1 termination. The spectrum is presented in figure 5.9(a) and the pulse is shown in figure 5.9(b). The roundtrip-to-roundtrip spectral and temporal evolution is shown in figure 5.9(c) and 5.9(d) respectively. These figures interpret that spectrum and pulse shape and intensity is stable once the steady state is achieved. The broken nature of spectrum and pulse could be explained by looking into the intra-cavity pulse propagation which is presented in figure 5.9(e). The LF possesses multiple spectral windows due to its sinusoidal nature, permitting various spectral components to pass through and after amplification, these components interact irregularly, forming a fringe pattern on the spectrum and, consequently, in the pulse. In contrast, the GF only possesses a single transmission window, enabling a specific part of the spectrum to pass through without any hindrance to maintain an even and consistent broadening.

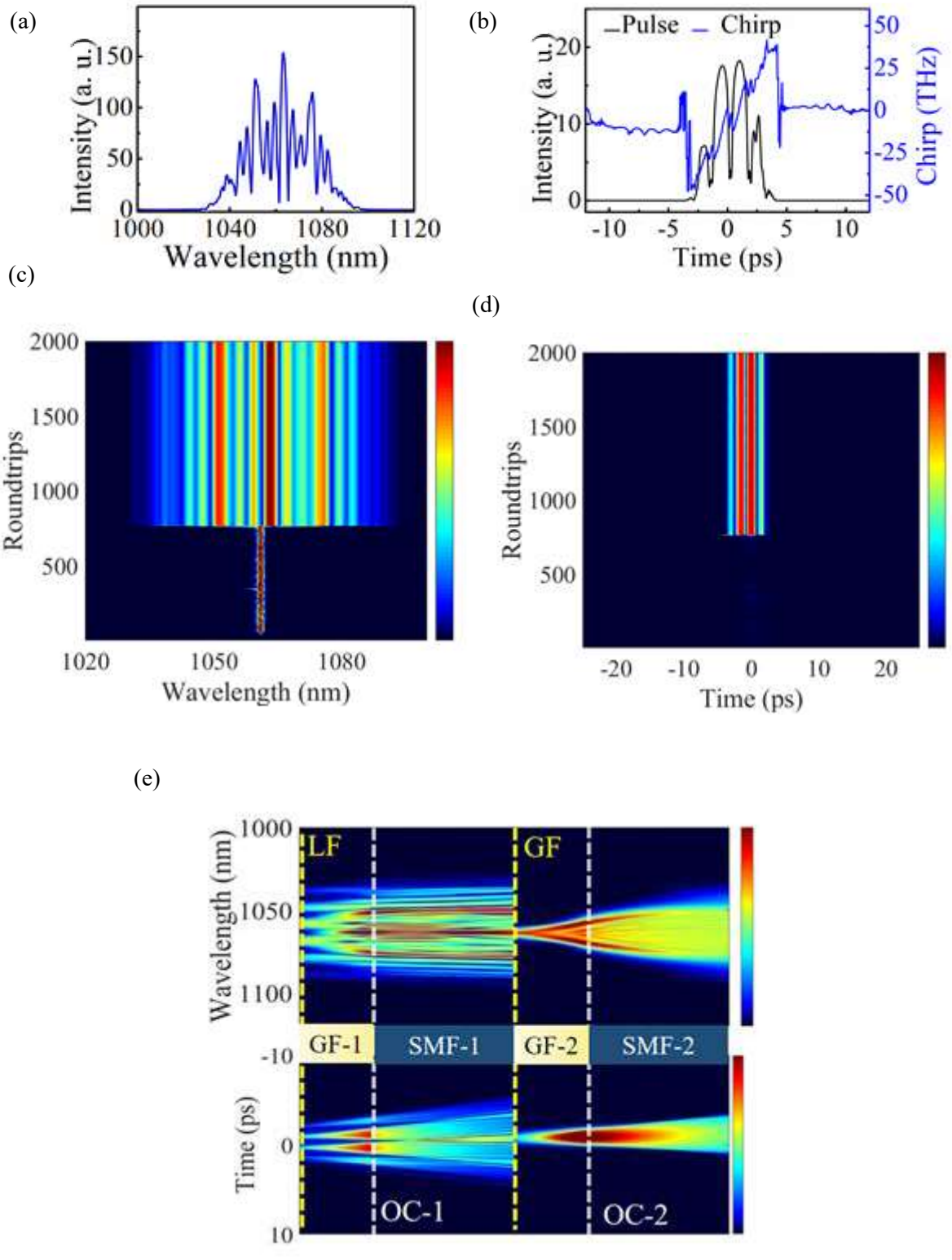

Figure 5.9: Spectral and temporal attributes at OC-2 end. (a) Spectrum after 2000 roundtrips (b) a single pulse after 2000 roundtrips (c) spectral & (d) temporal evolution over 2000 roundtrips. (e) Intra-cavity spectral & temporal evolution

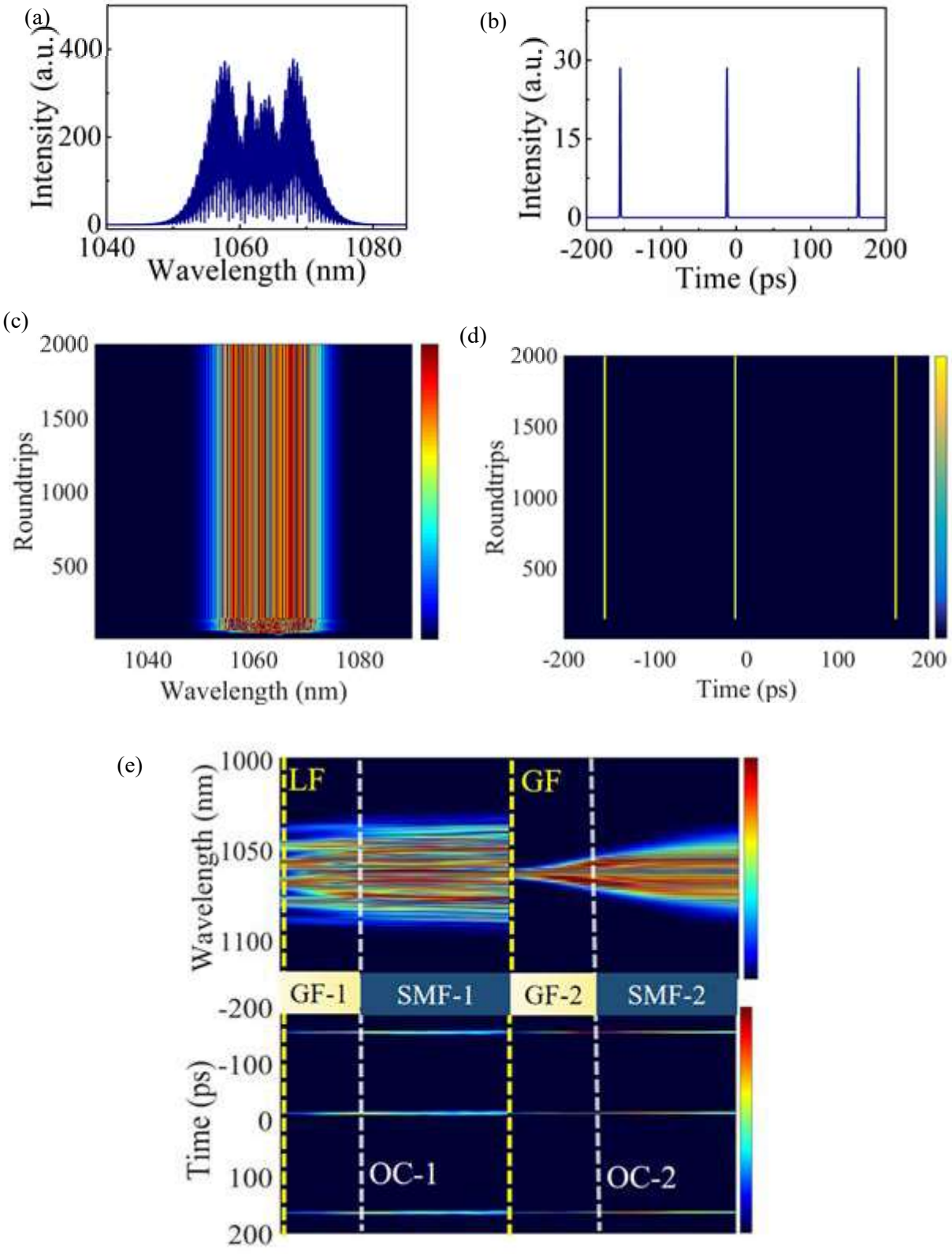

Figure 5.10: Properties of a multi-pulse state observed at OC-1. (a) Final stable spectrum (b) final temporal window contain three pulses. Roundtrip-to-roundtrip (c) spectral & (d) temporal evolution. (e) Intra-cavity spectral & temporal evolution of the multi-pulse state.

***5.5.* C. Multi-pulse state:** Figure 5.5 indicates the possibility of achieving multi-pulse operation through two distinct approaches. The first method involves tuning the filter position while maintaining a fixed Single Sideband Generator (SSG). Alternatively, multi-pulse operation can be realized by keeping the SSG fixed and increasing the overlap to allow more energy into the oscillator through the filters. Attributes of a three pulse state are presented in figure 5.10. Figure 5.10(a) is the evolved spectrum after 2000th roundtrips and the roundtrip-to-roundtrip spectrum variation is shown in figure 5.10(c). The spectrum contains fringes which is a property of a multi-pulse state, unlike the rain of pulse state no CW part is noticed in this state. The obtained temporal state after 2000 roundtrips and corresponding roundtrip-to-roundtrip variation is shown in figure 5.10(b) and (d) respectively. The intra-cavity spectral and temporal variation is shown in figure 5.10(e).

***5.6.* Conclusion**: This study concludes that LF can be an alternate choice of tunable spectral filter maintaining robust all-fiber architecture. Besides, there is a possibility to observe various pulse dynamics relying on the overlap of spectral filters. In the stable state, it can deliver 'Amplifier similariton' which is compressible to its transform-limited duration. A disadvantage of LF-based MO is that it can't deliver a smoothed spectrum from both output terminals because of LF's FSR. However, utilizing a double-stage all-fiber LF will help to maintain the FSR keeping the bandwidth fixed.

{Bibliography}

1. North, Thibault, and Martin Rochette. "Regenerative self-pulsating sources of large bandwidths." *Optics Letters* 39, no. 1 (2014): 174-177.

2. Mamyshev, P. V. "All-optical data regeneration based on self-phase modulation effect." In *24th European Conference on Optical Communication. ECOC'98 (IEEE Cat. No. 98TH8398)*, vol. 1, pp. 475-476. IEEE, 1998.

3. Regelskis, Kęstutis, Julijanas Želudevičius, Karolis Viskontas, and Gediminas Račiukaitis. "Ytterbium-doped fiber ultrashort pulse generator based on self-phase modulation and alternating spectral filtering." *Optics letters* 40, no. 22 (2015): 5255-5258.

4. Samartsev, Igor, Andrey Bordenyuk, and Valentin Gapontsev. "Environmentally stable seed source for high power ultrafast laser." In *Components and Packaging for Laser Systems III*, vol. 10085, pp. 201-209. SPIE, 2017.

5. Sidorenko, Pavel, Walter Fu, Logan G. Wright, Michel Olivier, and Frank W. Wise. "Self-seeded, multi-megawatt, Mamyshev oscillator." *Optics Letters* 43, no. 11 (2018): 2672-2675.

6. Wang, Pan, Shunyu Yao, Philippe Grelu, Xiaosheng Xiao, and Changxi Yang. "Pattern formation in 2-μm Tm Mamyshev oscillators associated with the dissipative Faraday instability." *Photonics Research* 7, no. 11 (2019): 1287-1295.

7. Wang, Tao, Can Li, Bo Ren, Kun Guo, and Pu Zhou. "All-PM Fiber Mamyshev Oscillator Delivers Hundred-Nanojoule and Multi-Watt Sub-100 fs Pulses." *Ultrafast Science* 3 (2023).

8. Boulanger, Vincent, Michel Olivier, François Trépanier, Pascal Deladurantaye, and Michel Piché. "Multi-megawatt pulses at 50 MHz from a single-pump Mamyshev oscillator gain-managed amplifier laser." *Optics Letters* 48, no. 10 (2023): 2700-2703.

9. Pizzurro, Sara, Riccardo Gotti, Luca Carrà, Giuliano Piccinno, Antonio Agnesi, and Federico Pirzio. "Femtosecond Mamyshev fiber oscillator started by a passively Q-switched microchip laser." *Optics Letters* 47, no. 8 (2022): 1960-1963.

10. Haig, Henry, Pavel Sidorenko, Robert Thorne, and Frank Wise. "Megawatt pulses from an all-fiber and self-starting femtosecond oscillator." *Optics Letters* 47, no. 4 (2022): 762-765.

11. Poeydebat, Etienne, Giorgio Santarelli, Alexis Casanova, Florent Scol, Olivier Vanvincq, Géraud Bouwmans, and Emmanuel Hugonnot. "Measurements of the absolute timing jitter and intensity noise of an all-fiber Mamyshev oscillator." *Optics Letters* 46, no. 11 (2021): 2698-2701.

12. Chen, Yi-Hao, Pavel Sidorenko, Robert Thorne, and Frank Wise. "Starting dynamics of a linear-cavity femtosecond Mamyshev oscillator." *JOSA B* 38, no. 3 (2021): 743-748.

13. Lin, Di, Duanyang Xu, Jing He, Yutong Feng, Zhengqi Ren, Raghuraman Sidharthan, Yongmin Jung, Seongwoo Yoo, and David J. Richardson. "The generation of 1.2 μJ pulses from a Mamyshev oscillator based on a high concentration, large-mode-area Yb-doped fiber." *Journal of Lightwave Technology* 40, no. 21 (2022): 7175-7179.

14. Wang, Tao, Bo Ren, Can Li, Jian Wu, Rongtao Su, Pengfei Ma, Zhi-Chao Luo, and Pu Zhou. "Over 80 nJ sub-100 fs all-fiber Mamyshev oscillator." *IEEE Journal of Selected Topics in Quantum Electronics* 27, no. 6 (2021): 1-5.

15. Repgen, Paul, Dieter Wandt, Uwe Morgner, Jörg Neumann, and Dietmar Kracht. "Sub-50 fs, μJ-level pulses from a Mamyshev oscillator–amplifier system." *Optics Letters* 44, no. 24 (2019): 5973-5976.

16. Cao, Bo, Kangjun Zhao, Chenxin Gao, Xiaosheng Xiao, Chengying Bao, and Changxi Yang. "Observation of pulsating dissipative solitons in a Mamyshev oscillator." *Physical Review A* 106, no. 2 (2022): 023519.

17. Yan, Dan, Xingliang Li, Shumin Zhang, and Jingmin Liu. "Pulse dynamic patterns in a self-starting Mamyshev oscillator." *Optics Express* 29, no. 7 (2021): 9805-9815.

18. Olivier, Michel, Vincent Boulanger, Félix Guilbert-Savary, Pavel Sidorenko, Frank W. Wise, and Michel Piché. "Femtosecond fiber Mamyshev oscillator at 1550 nm." *Optics letters* 44, no. 4 (2019): 851-854.

19. Xu, Shi-Sheng, Meng Liu, Zhi-Wei Wei, Ai-Ping Luo, Wen-Cheng Xu, and Zhi-Chao Luo. "Multipulse dynamics in a Mamyshev oscillator." *Optics Letters* 45, no. 9 (2020): 2620-2623.

20. Zheng, Jian-Cheng, Song Yang, Zhi-Wei Zhu, Kuen-Yao Lau, and Li Li. "Low mode-locking threshold and sub-90 fs Er-doped Mamyshev oscillator." *Optics Communications* 508 (2022): 127711.

21. Sui, Yu, Liang Jin, Yikai Liu, He Zhang, and Yingtian Xu. "Harmonic Mode-Locking From Erbium-Doped Fiber Self-Starting Mamyshev Oscillator." *Journal of Lightwave Technology* (2023).

22. Boulanger, Vincent, Michel Olivier, Félix Guilbert-Savary, François Trépanier, Martin Bernier, and Michel Piché. "All-fiber Mamyshev oscillator enabled by chirped fiber Bragg gratings." *Optics Letters* 45, no. 12 (2020): 3317-3320.

23. Zhang, Yusheng, Ke Dai, Bin Zhang, Daru Chen, Zuguang Guan, and Yudong Cui. "Investigations on pulse dynamics and offset spectral filtering in Er-doped Mamyshev fiber oscillator." *Optics Communications* 529 (2023): 129103.

24. Schuhbauer, Benedikt, Veronika Adolfs, Frithjof Haxsen, Andreas Wienke, Uwe Morgner, Jörg Neumann, and Dietmar Kracht. "Generation of 15 nJ pulse energy by a sub-150 fs thulium-doped fiber Mamyshev oscillator." *Optics Letters* 47, no. 21 (2022): 5610-5613.

25. Repgen, Paul, Benedikt Schuhbauer, Moritz Hinkelmann, Dieter Wandt, Andreas Wienke, Uwe Morgner, Jörg Neumann, and Dietmar Kracht. "Mode-locked pulses from a Thulium-doped fiber Mamyshev oscillator." *Optics Express* 28, no. 9 (2020): 13837-13844.

26. Lyot, Bernard. "Un monochromateura grand champ utilisant les interférences en lumiere polarisée." *Compt. Rend. Acad Sci* 197, no. 1593 (1933): 1933.

27. Zhao, Siyang, Zhigang Cao, Hefei Li, Weidong Luo, Jiaming Chen, Yuxuan Fu, Bin Liu, Jiping Lin, and Benli Yu. "A highly sensitive temperature and strain sensor based on fiber lyot filter with vernier effect." *Optical Fiber Technology* 73 (2022): 103062.

28. Huang, Bo, Ying Wang, Changrui Liao, and Yiping Wang. "Highly sensitive temperature sensor based on all-fiber polarization interference filter with Vernier effect." *IEEE Access* 8 (2020): 207397-207403.

29. Zhu, Yuanjun, Zekun Cui, Xiangnan Sun, Takuma Shirahata, Lei Jin, Shinji Yamashita, and Sze Yun Set. "Fiber-based dynamically tunable Lyot filter for dual-wavelength and tunable single-wavelength mode-locking of fiber lasers." *Optics Express* 28, no. 19 (2020): 27250-27257.

30. Ding, Jianyi, Zengrun Wen, Baole Lu, Kaile Wang, Haowei Chen, and Jintao Bai. "Wavelength switchable dissipative soliton mode-locked fiber laser based on Lyot filter." *Optics & Laser Technology* 144 (2021): 107460.

31. Sun, Xiangnan, Shinji Yamashita, and SzeYun Set. "Fast wavelength-swept polarization maintaining all-fiber mode-locked laser based on a piezo-stretched fiber Lyot filter." *Optics Express* 31, no. 8 (2023): 12837-12846.

32. Sun, Xiangnan, Yuanjun Zhu, Lei Jin, Shinji Yamashita, and Sze Yun Set. "Polarization-maintaining all-fiber tunable mode-locked laser based on a thermally controlled Lyot filter." *Optics Letters* 47, no. 19 (2022): 4913-4916.

33. Szczepanek, Jan, Tomasz M. Kardaś, Czesław Radzewicz, and Yuriy Stepanenko. "Ultrafast laser mode-locked using nonlinear polarization evolution in polarization maintaining fibers." *Optics Letters* 42, no. 3 (2017): 575-578.

34. Huang, S. S., Y. G. Wang, P. G. Yan, G. L. Zhang, J. Q. Zhao, H. Q. Li, and R. Y. Lin. "Soliton rains in a graphene-oxide passively mode-locked ytterbium-doped fiber laser with all-normal dispersion." *Laser Physics Letters* 11, no. 2 (2013): 025102.

35. Niang, Alioune, Foued Amrani, Mohamed Salhi, Philippe Grelu, and François Sanchez. "Rains of solitons in a figure-of-eight passively mode-locked fiber laser." *Applied Physics B* 116 (2014): 771-775.

36. Chouli, Souad, and Philippe Grelu. "Soliton rains in a fiber laser: An experimental study." *Physical Review A* 81, no. 6 (2010): 063829.

37. Liu, Zhanwei, Zachary M. Ziegler, Logan G. Wright, and Frank W. Wise. "Megawatt peak power from a Mamyshev oscillator." *Optica* 4, no. 6 (2017): 649-654.

38. Olivier, Michel, Mathieu Gagnon, Simon Duval, Martin Bernier, and Michel Piché. "All-fiber amplifier similariton laser based on a fiber Bragg grating filter." *Optics Letters* 40, no. 23 (2015): 5650-5653.

39. Fermann, Martin E., V. I. Kruglov, B. C. Thomsen, John M. Dudley, and John D. Harvey. "Self-similar propagation and amplification of parabolic pulses in optical fibers." *Physical review letters* 84, no. 26 (2000): 6010.

40. Kruglov, V. I., A. C. Peacock, J. M. Dudley, and J. D. Harvey. "Self-similar propagation of high-power parabolic pulses in optical fiber amplifiers." *Optics letters* 25, no. 24 (2000): 1753-1755.

Chapter: 06

Ultra-short pulse amplification via Chirped Pulse Amplification technique

Abstract

The dispersion managed oscillator in the stable single pulse state discussed in chapter 03 is considered for further amplification. Multiple amplifier stages are implemented in all-fiber configuration and at every stage the performance is optimized. Two different architectures are made; one provides high peak power around 540 kW, which comprises single booster stage followed by the compression stage. The final compressed duration is approximately 295 fs. For final compression a pair of diffraction gratings in are exploited in Littrow position. The second setup provides higher pulse energy which is approximately 2 μJ. A pulse picking system is exploited to reduce the repetition rate to a desired value. At the final amplifying stage LMA fiber is utilized. The final beam maintains a good beam quality with a M^2 value around 1.25.

6.1. Introduction: As of now, mode-locking remains the most effective technique for generating pulses of ultra-short duration. However, its drawback lies in producing pulses with very low average power, typically in the milliwatt (mW) range. Consequently, the peak power and pulse energy generated are often insufficient to meet the requirements of many applications. So, amplification of the seed pulses is necessary to comply with the demands. However, there are several non-linear affects that comes into play during the amplification which becomes detrimental to maintain the pulse quality. To address these issues CPA is the most adopted technique among researchers. In this method, the pulse is broadened before amplification via some dispersive delay lines. Then, the amplified pulse is compresses down to ultrashort time scale. Multiple amplification stage can be employed according to the power/energy requirement. In the compression stage grating pairs is preferable because of its low non-linearity. Based on the grating pair-based configuration, complete CPA system is reported at three main wavelength regimes (1064 nm, 1550 nm, 2000 nm) which are capable to deliver pulses of energy nJ-μJ level [1-3]. To maintain the all fiber architecture, researchers are now adopting hollow core PCFs as an alternative of grating pairs because of their special light guiding property [4-5]. As the core of these fibers are air filled, the total dispersion is mainly dominated by the waveguide dispersion which provides as large range of design flexibility according to the needs. Recently, researchers are adopting multiple rod-types fiber as amplifiers and then combining them via coherent beam combination (CBC) technique to achieve 10.4 kW average power in femtosecond duration [6-8]. However, these procedures require multiple bulk optics and meticulous adjustments to maintain the coherence, making the system complex and constraining its robustness. A table is included showing achieved output parameters from Yb-doped CPA system.

Table: 6.1: Review of Yb-doped CPA system

Central wavelength	Average power	Pulse duration	Repetition rate	Ref.
1064 nm	28 W	350 fs	15.4 MHz	9
1040 nm		349 fs	35 kHz	10
1030 nm	20 W	764 fs	200 kHz	11
1040 nm	32 W	153 fs	40.3 MHz	12
1040 nm	131 W	220 fs	73 MHz	13
1030 nm	100 W	270 fs	1 MHz	14

1030 nm	100 W	330 fs	500 kHz	15
1060 nm	17.5 W	172 fs	500 kHz	1
1034 nm	11 W	340 fs	21.35 MHz	16

6.2. Architecture -1: 160 nJ pulse energy, sub-300 fs duration, 17.65 MHz system

The SESAM-based dispersion managed seed, discussed in chapter-03 in the stable single pulse state, is considered for further amplification via CPA technique. After this low power oscillator, a pre-amplifier stage is included to scale up the average power. The gain fiber is a single clad Ytterbium doped fiber with core diameter of 6.2 micron and NA = 0.14. Single mode-optical having normal dispersion at 1064 nm is used as the stretcher. This fiber is a commercial fiber (HI1060-xp) from Corning with dispersion -38 ps/nm/km. After the stretcher, the main booster

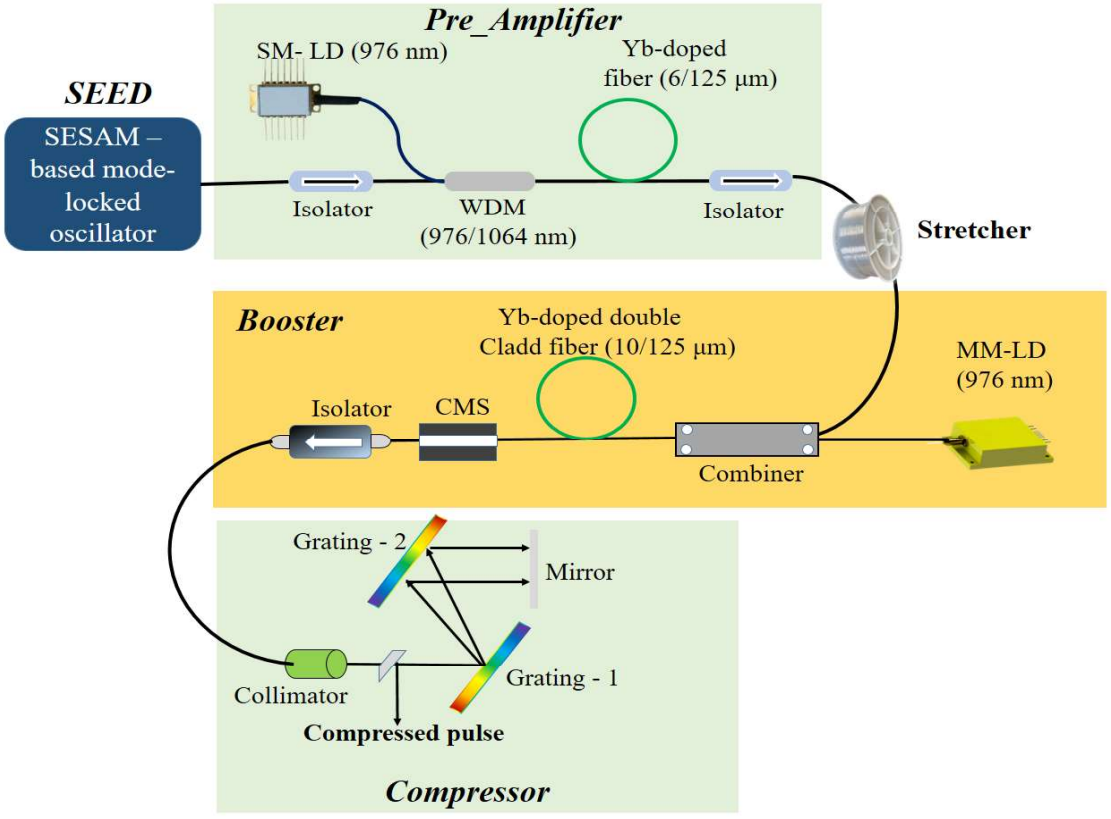

Figure 6.1: Schematic of the whole CPA system which delivers 160 nJ pulses of duration 295 fs.

stage is implemented. Here the gain fiber is a double clad Ytterbium doped fiber

(Core/Cladding dia = 10/125 micron; NA = 0.08) which is pumped via a multimode laser diode of 976 nm in cladding pump configuration. A lab-made cladding mode stripper (CMS) is used to extract the extra pump energy. Appropriate isolation is made in the junction between any two stages via ln-line fiber coupled isolator. For compression, two diffraction gratings are used in Treacy configuration to obtain maximum efficiency. The whole set up is shown in figure 6.1 in schematic form.

6.2.1: Construction of seed oscillator: The seed oscillator here is the dispersion managed mode-locked fiber laser in stable single pulse state. The laser delivers pulses of below 58 ps durations at a repetition rate of 17.65 MHz. The output spectrum is sufficiently broad with a 3-dB bandwidth of 14.2 nm and rectangular in nature as the net cavity dispersion is positive. The

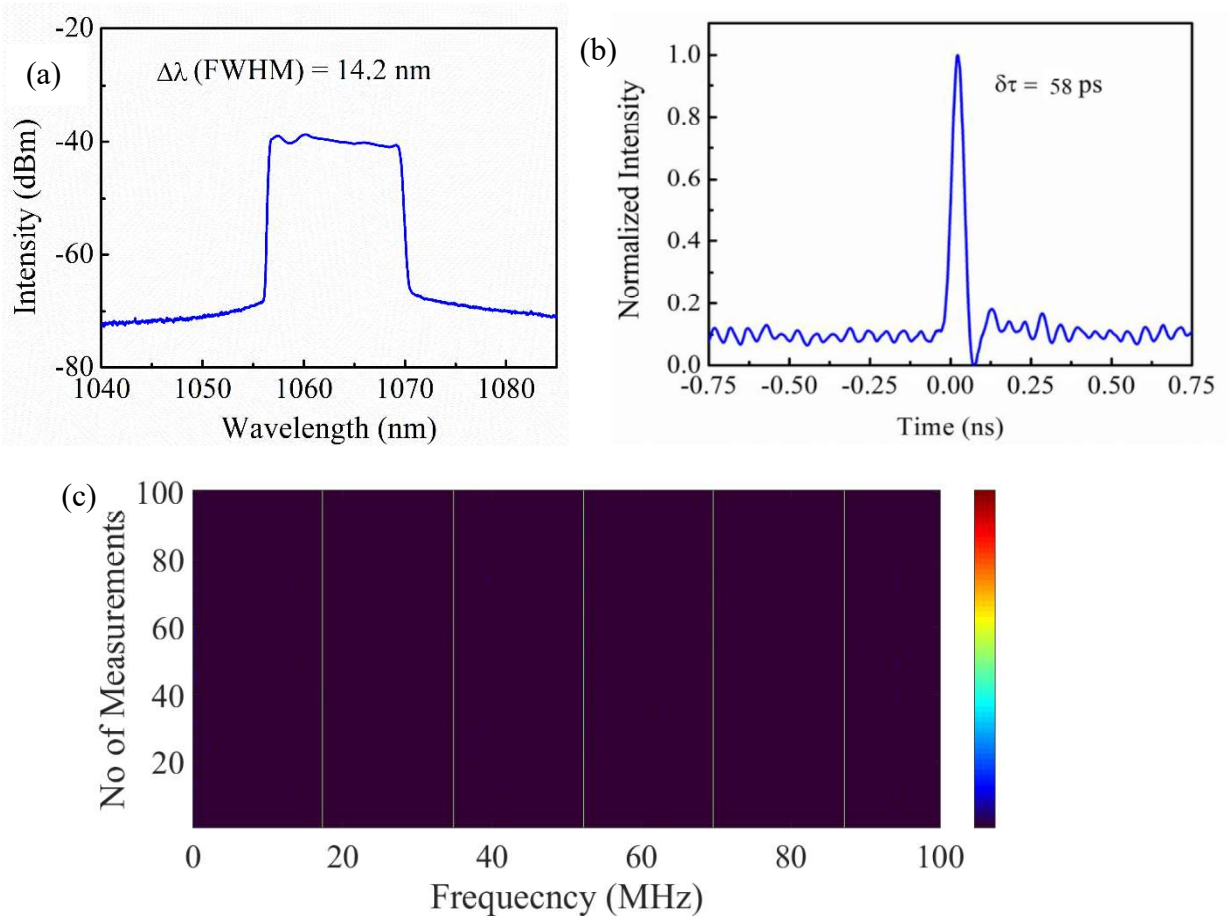

Figure 6.2: SEED properties. (a) Output spectrum (b) Temporal profile of the single pulse (c) 100 RF-spectrum recorded after 5 second time gap

output spectrum is shown in figure 6.2 (a). Figure 6.2(b) depicts the intensity profile of a single pulse having pulse duration of 58 ps. In figure 6.2 (c) the RF-spectrum is plotted with time in 100 MHz frequency interval to show no significant frequency drift at a particular

pump power. The fundamental frequency is 17.65 MHz. The average output power is 14 mW. In the next stage, the average power is scaled up via a pre-amplifier state.

6.2.2: Pre-Amplifier: Before amplifying the signal in the main booster stage, the average power of seed is scaled up to 100 mW at the expense of 312 mW pump power. With the increment of pump power, the spectral width also increases almost linearly. The maximum spectral width obtained is 15.2 nm. The spectrum after the pre-amplifier is shown in figure 6.3(a) at different

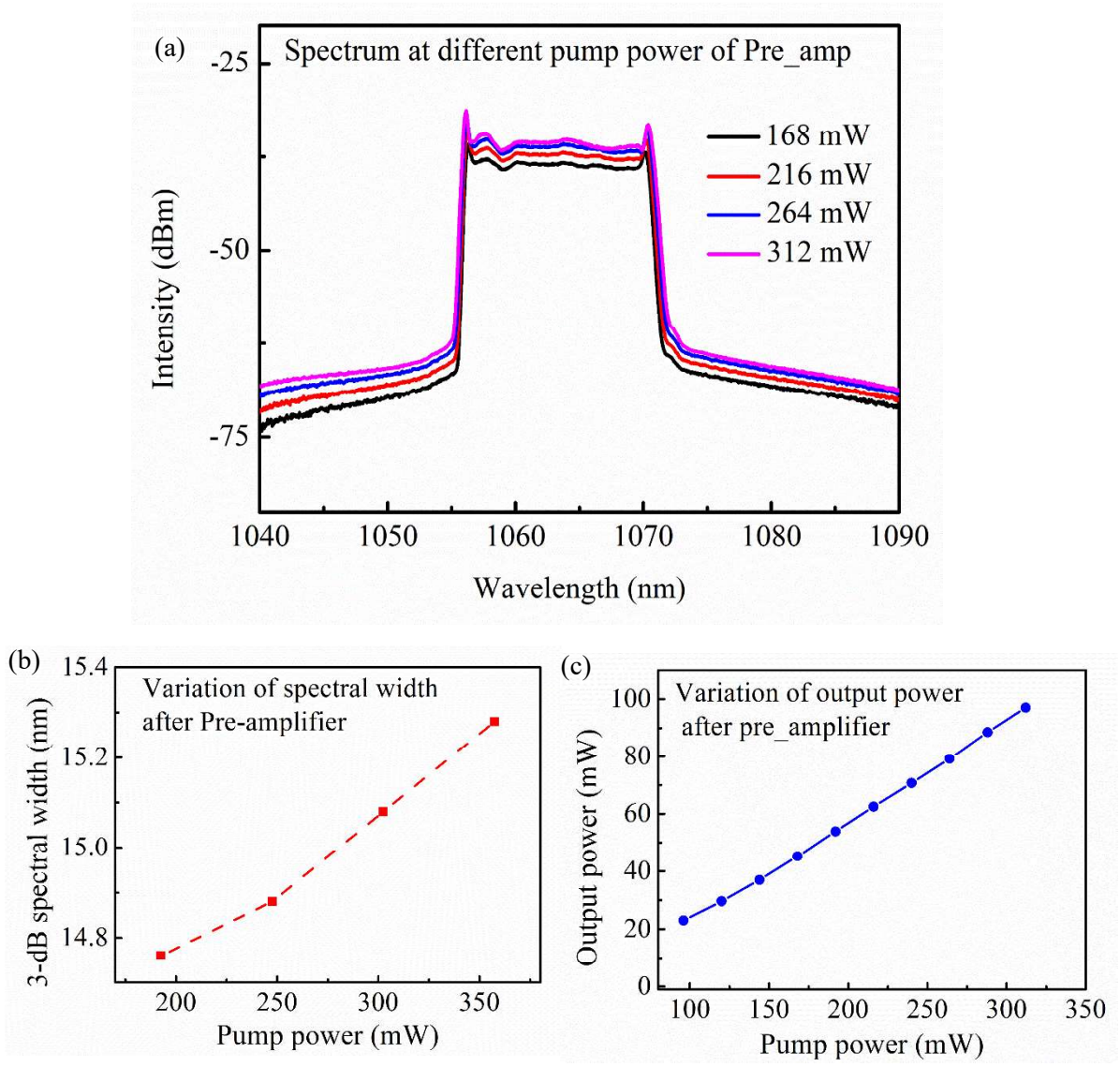

Figure: 6.3: (a)Spectral evolution after pre_amplifier with pump power (b) Variation of 3-dB spectral width (c) variation of average output power with pump power

pump power. The maximum power is limited by the growth of ASE pedestal. Figure 6.3(b) depicts the variation of 3-dB spectral width with pump power. The measured average output power is plotted in figure 6.3(c).

6.2.3: Stretcher: The stretcher fiber is spliced after the pre_amplifier keeping the pump power

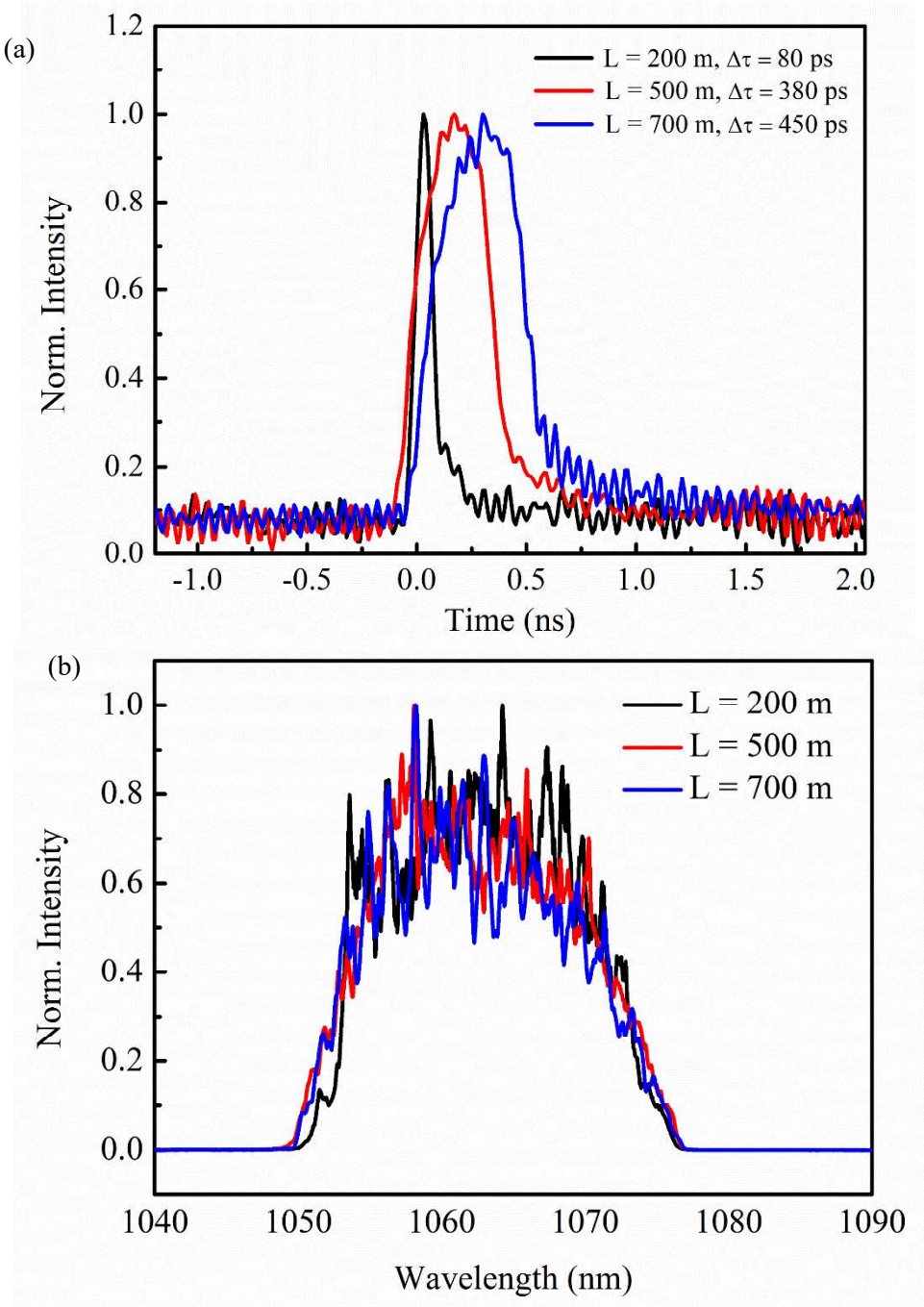

Figure 6.4: (a) Temporal & (b) spectral profile after the stretcher of different fiber length

fixed at 312 mW. We have checked the temporal and spectral broadening after three different lengths of fiber which are 200 m, 500 m, 700 m. Figure 6.4(a) represents the single pulse temporal profile after each of those length. As the length of stretcher fiber increases, the pulse width also broadens. Because of the temporal broadening the peak power reduces and as a results no significant non-linearity induced spectral broadening is observed after the stretcher. Figure 6.4(b) depicts the normalized spectrum after each length and no such

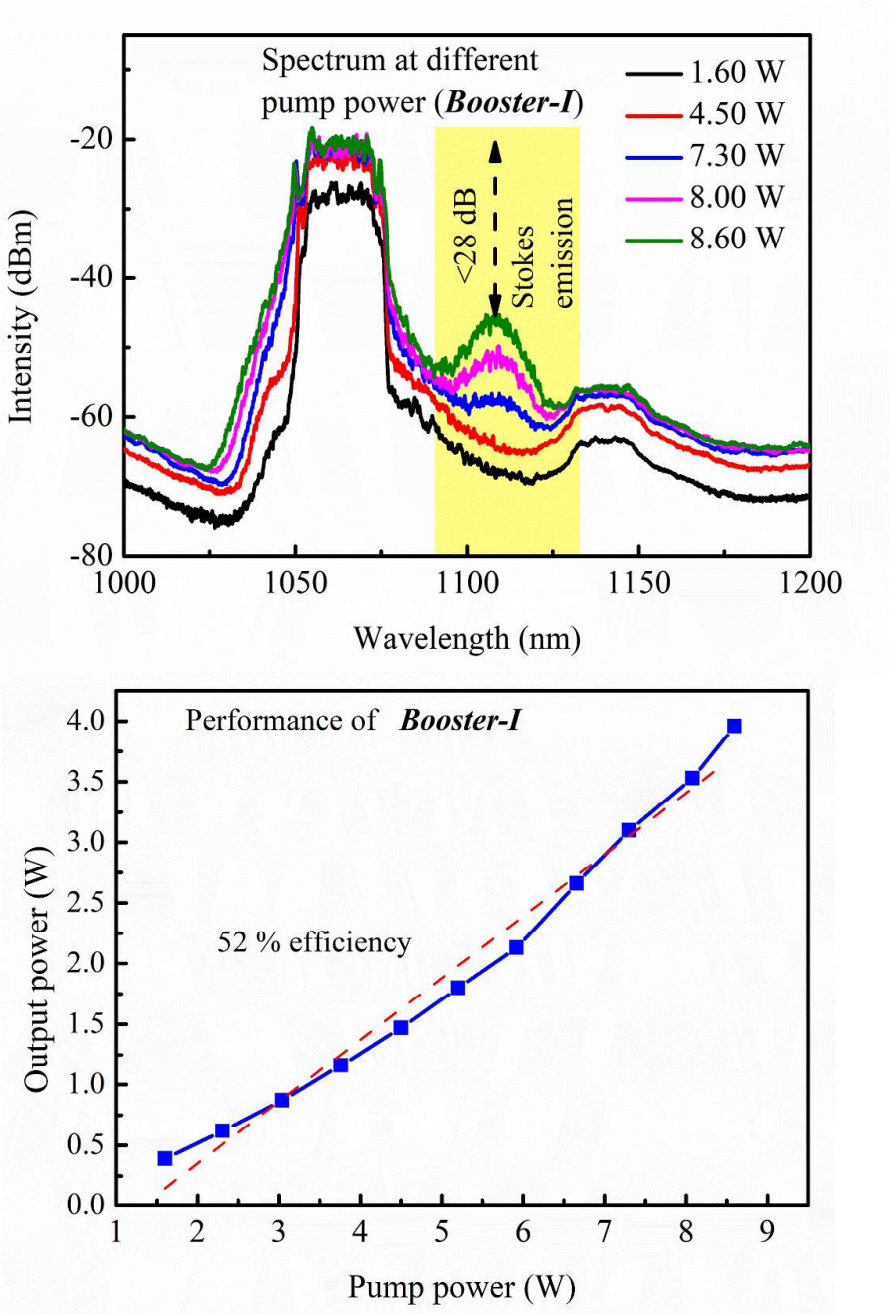

Figure 6.5: (a) Spectrum after booster at different pump power (b) Variation of output power

difference is noticed. For the final configuration, stretcher of 200 m length is chosen. The pulse duration and spectral width are 80 ps and 18 nm respectively after the stretcher.

6.2.4: Booster-1: Spectrum at different pump power is shown in Figure 6.5(a). Raman emission is noticed around 1120 nm just after pump power crosses 6 Watt. The pump power is increased to 8.6 W where the Raman peak is below 30 dB of the signal peak. Figure 6.5(b) shows the variation of output power with pump power of booster-1. The maximum average output power is 4 Watt, corresponding to pulse energy of 220 nJ.

6.2.5: Compression: The amplified pulse after booster-1 is compressed using two diffraction gratings in Littrow configuration [17,18]. Grating-1 diffracts the collimated beam spatially then the spatially diffracted beam is incident on Grating-2. Grating-2 makes the beam parallel again and directed to mirror-1. The reflected beam from the mirror is retraced back through the Grating-2 and Grating-1 respectively. In this path the beam is de-chirped and measured via auto-correlator. The intensity autocorrelation is shown in figure-6.6. Considering Gaussian shape of the pulse, the duration is about 295 fs. The average power becomes 2.8 W after compression providing 70 % efficiency. Finally, the pulse peak power becomes 540 kW corresponding to 160 nJ pulse energy.

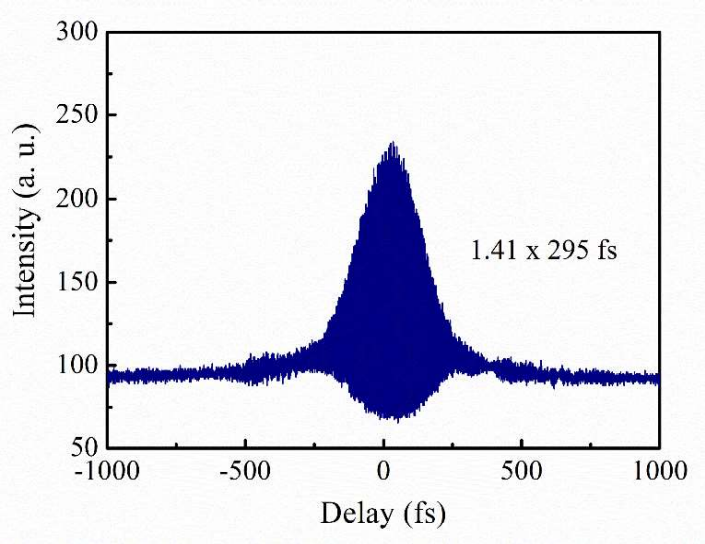

Figure 6.6: Intensity auto-correlation of the final pulse.

6.3: Architecture -2: 2 µJ pulse energy,~150 ps duration, 1.09 MHz system

In this configuration, the setup is modified by implementing an AOM after the stretcher, which is controlled by an arbitrary waveform generator. The signal frequency is decreased gradually in the following order $f_{rep}/2$, $f_{rep}/4$, $f_{rep}/8$ and $f_{rep}/16$. $f_{rep}/16$ is around 1.09 MHz which is chosen for further amplification. Another amplifier stage is included after Booster-1 which comprises a 7 meter gain fiber of 30 micron core diameter and cladding diameter 125 micron. The NA of the gain fiber is 0.082 and it is pumped in cladding pump configuration via multi-mode laser diode. The complete set up is shown in figure 6.7.

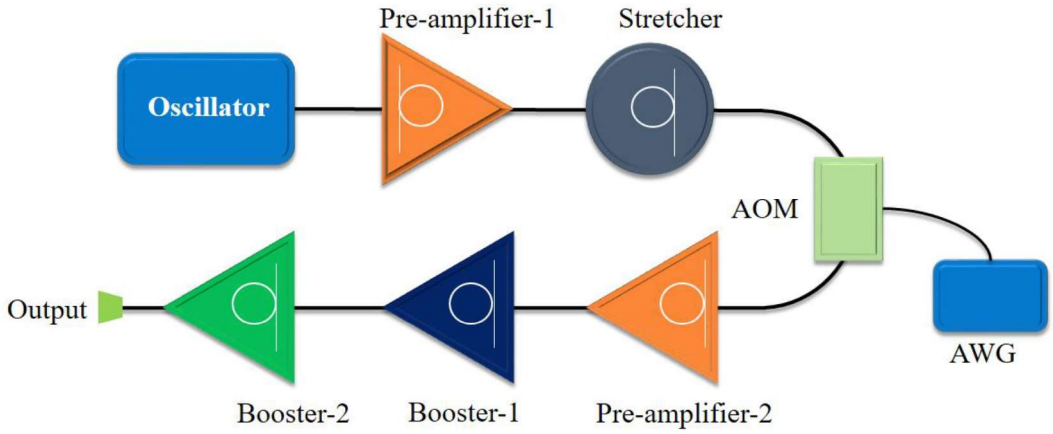

Figure 6.7: Pictorial representation of the architecture delivering 2 microjoule pulse energy

6.3.1: Pulse picking: This is a process to reduce the repetition rate outside main oscillator. The AOM acts as an optical shutter which allows pulses according to the signal frequency provided to it. An accurate pulse picking method comprises a digital delay pulse generator system (DDPG) which is synchronized to main oscillator. Here, as we did not have such system, the signal frequency is tuned to the desired value every time we turn on the system. Figure 6.8(a) shows the output after the AOM at different signal frequency. Figure 6.8(b) shows the variation of average output power with the signal frequency. The power loss is mainly due to the insertion loss of the AOM. The average power also reduces with the reduction of signal frequency as greater number of pulse is blocked. For this configuration, the signal frequency is fixed at $f_{rep}/16$. After the pulse picker, another amplifier in core pumping scheme is included. In this stage, the output power is scaled up from 0.72 mW to 4.5 mW. As the repetition rate and input power is low in this amplifying stage, performance of the amplifier is limited by the growth of ASE. The output spectrum at different pump power is shown in figure 6.9(a). The amplifier pump power is then kept fixed at 160 mW for further step.

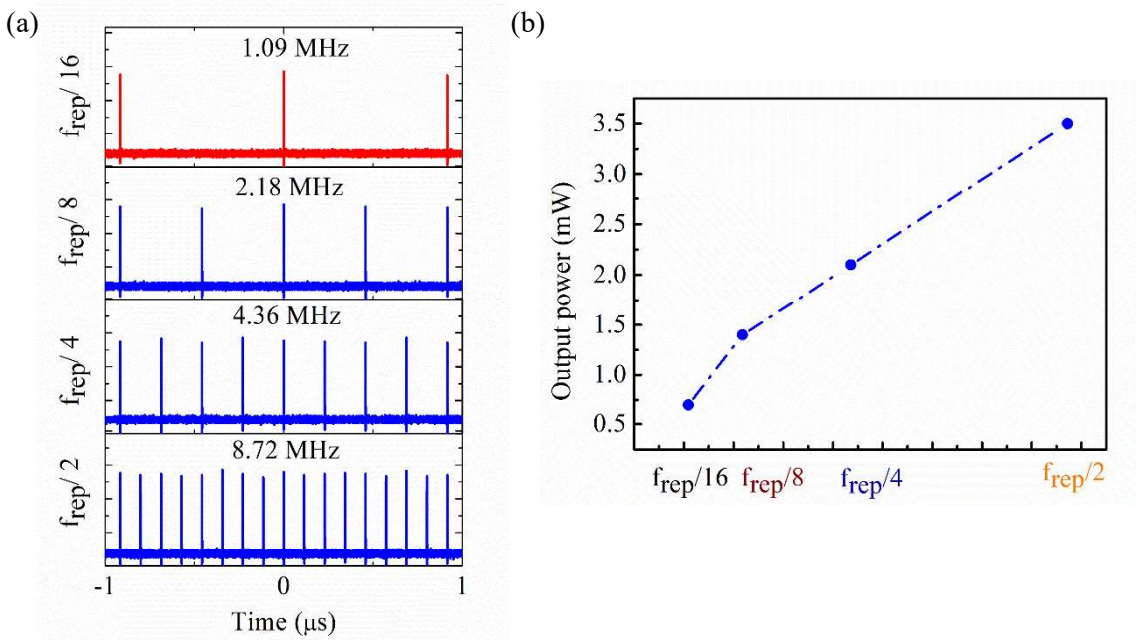

Figure 6.8: (a) output pulse train at different signal frequency (b) Average output power after pulse picking

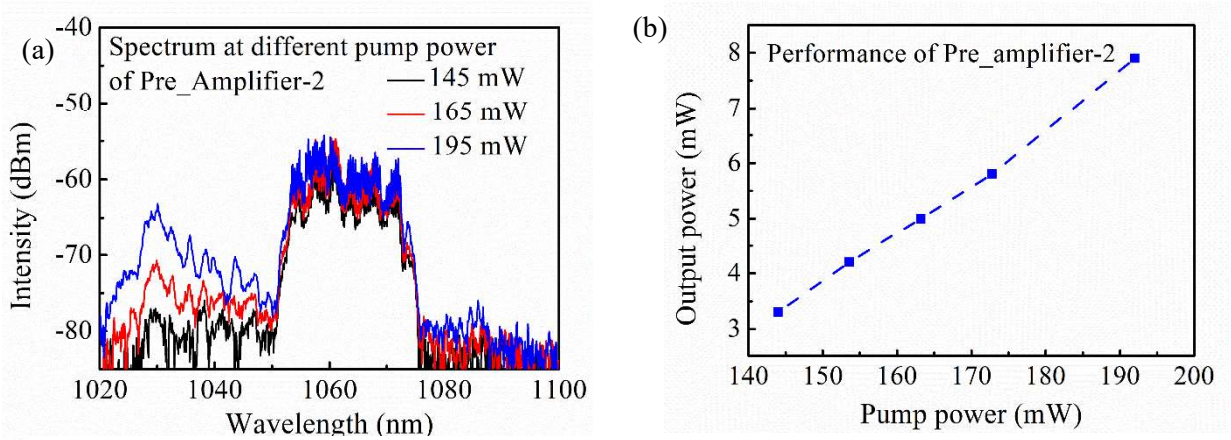

Figure 6.9: (a) Spectrum after the Pre_amplifier-2 at different pump power. (b) Variation of average output power at different pump power

6.3.2: Booster-1: The output spectrum at different pump power after the booster-1 is shown in figure 6.10(a). The variation of output power is also presented in figure 6.10(b). It is observed that, after 1 W of pump power, ASE levels start to grow significantly. To keep the SNR better, the pump power is kept fix at 1 W which corresponds to 67 mW of output power.

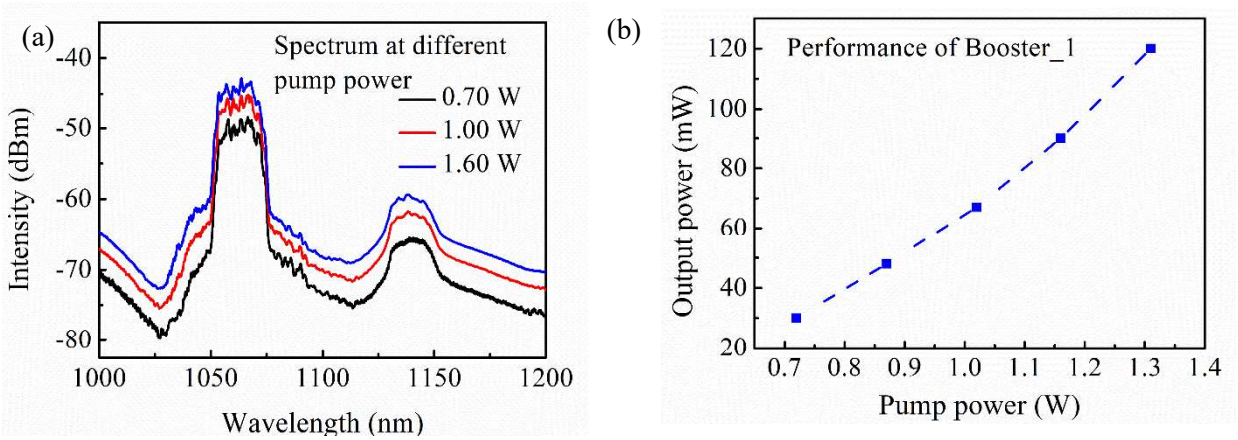

Figure 6.10: (a) Spectrum after the booster-1 at different pump power. (b) Variation of average output power at different pump power

6.3.3: Booster-2: Figure 6.11 depicts the performance of booster-2. In this stage, maximum average power of 2.2 W is obtained at the expense of 11.7 W of pump power. The spectrum at distinct pump power is shown in figure 6.11 (a). The 10-dB spectral width at the maximum pump power is 27 nm. The variation of average output power is shown in figure 6.11(b). The maximum pulse energy obtained is 2 μJ. Because of unavailability of grating pair suitable for high energy operation, compression part is not done.

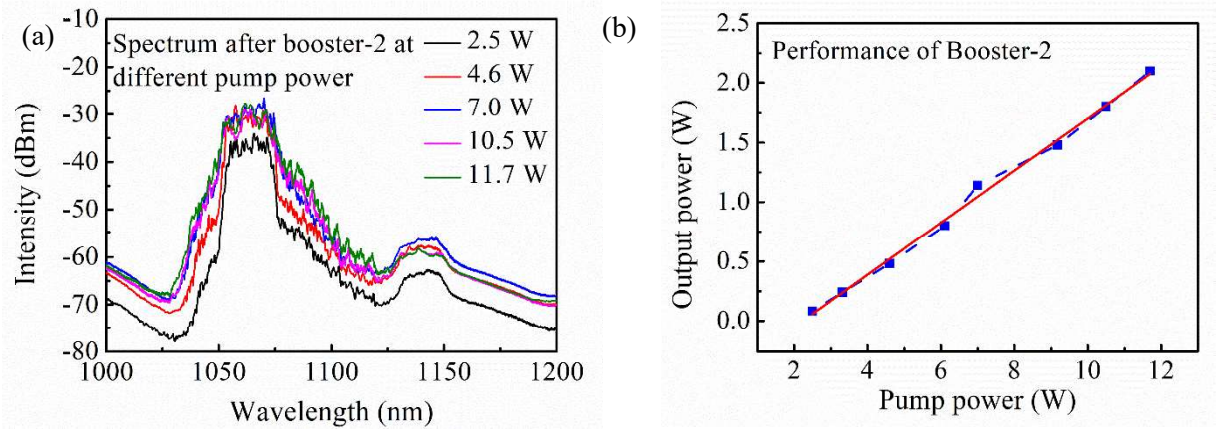

Figure 6.11: (a) Spectrum after the booster-2 at different pump power. (b) Variation of average output power at different pump power

The beam quality measurement is done after collimating the output through an aspheric lens. The value of M^2_X is 1.22 and M^2_Y is 1.25. Figure 6.12 depicts the M^2 measurement of the beam profile. The beam shape maintains 99 % circularity and the image is shown in figure 6.12_inset.

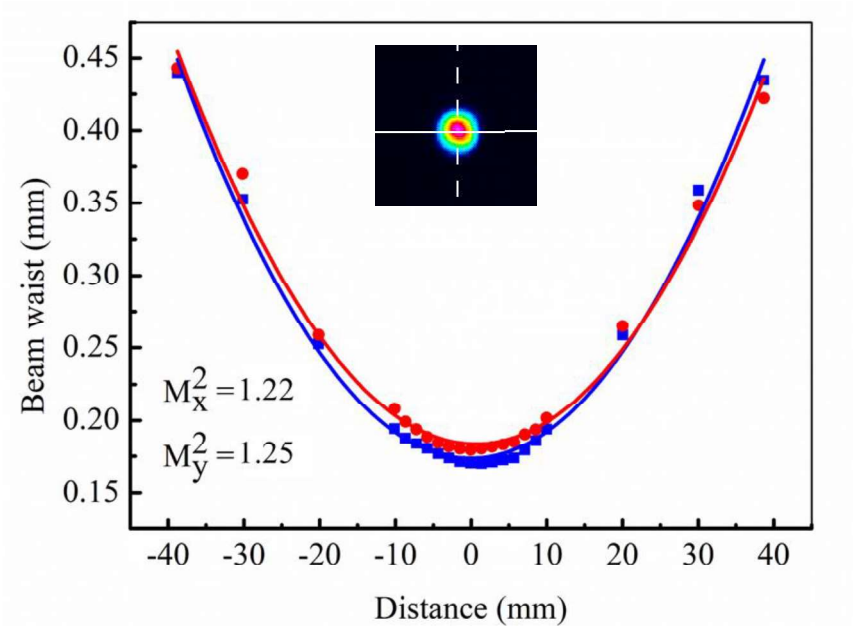

Figure 6.12: Beam quality measurement of the output

6.4. Conclusions: Two different setup is considered for the amplification of ultrashort pulses at 1064 nm. First architecture delivers pulses of 160 nJ energy with a peak power of almost 540 kW. The average power is limited by Raman emission after amplification. The second architecture delivers much more pulse energy as the repetition rate is reduced before the final stage of amplification. However, the maximum power is limited by ASE from the amplifier and excessive ASE degrades the pulse quality by adding phase noise. The maximum pulse energy achieved from this set up is 2.2 micro joule. The stretched pulse is not compressed and the duration is 150 ps approximately.

{Bibliography}

1. Chang, Hong, Zhaochen Cheng, Ruoyu Sun, Zhigang Peng, Miao Yu, Yu You, Min Wang, and Pu Wang. "172-fs, 27-μJ, Yb-doped all-fiber-integrated chirped pulse amplification system based on parabolic evolution by passive spectral amplitude shaping." *Optics Express* 27, no. 23 (2019): 34103-34112.

2. Imeshev, G., I. Hartl, and M. E. Fermann. "Chirped pulse amplification with a nonlinearly chirped fiber Bragg grating matched to the Treacy compressor." *Optics letters* 29, no. 7 (2004): 679-681.

3. Wan, Peng, Lih-Mei Yang, and Jian Liu. "High pulse energy 2 μm femtosecond fiber laser." *Optics Express* 21, no. 2 (2013): 1798-1803.

4. Limpert, J., T. Schreiber, S. Nolte, H. Zellmer, and A. E. D. Q. G. Tünnermann. "All fiber chirped-pulse amplification system based on compression in air-guiding photonic bandgap fiber." *Optics Express* 11, no. 24 (2003): 3332-3337.

5. Wei, Rongling, Mengmeng Wang, Zexiu Zhu, Weiyu Lai, Peiguang Yan, Shuangchen Ruan, Jinzhang Wang, Zhipei Sun, and Tawfique Hasan. "High-power femtosecond pulse generation from an all-fiber Er-doped chirped pulse amplification system." *IEEE Photonics Journal* 12, no. 2 (2020): 1-8.

6. Klenke, Arno, Michael Müller, Henning Stark, Marco Kienel, Cesar Jauregui, Andreas Tünnermann, and Jens Limpert. "Coherent beam combination of ultrafast fiber lasers." *IEEE Journal of Selected Topics in Quantum Electronics* 24, no. 5 (2018): 1-9.

7. Müller, M., C. Aleshire, L. H. Stark, J. Buldt, A. Steinkopff, E. Haddad, F. Legare, A. Klenke, A. Tünnermann, and J. Limpert. "10.4 kW 12-channel ultrafast fibre laser." In *Advanced Solid State Lasers*, pp. ATu4A-2. Optica Publishing Group, 2020.

8. Müller, Michael, Arno Klenke, Albrecht Steinkopff, Henning Stark, Andreas Tünnermann, and Jens Limpert. "3.5 kW coherently combined ultrafast fiber laser." *Optics letters* 43, no. 24 (2018): 6037-6040.

9. Zaytsev, Alexey, Yi-Jing You, Sheng-Wen Huang, and Ci-Ling Pan. "Spectrally shaped chirped pulse amplification of an all-normal dispersion Yb-doped fibre laser." *Laser Physics Letters* 15, no. 8 (2018): 085107.

10. Bartulevicius, T., L. Veselis, K. Madeikis, A. Michailovas, and N. Rusteika. "Compact femtosecond 10 μJ pulse energy fiber laser with a CFBG stretcher and CVBG compressor." *Optical Fiber Technology* 45 (2018): 77-80.

11. Veselis, Laurynas, Tadas Bartulevicius, Karolis Madeikis, Andrejus Michailovas, and Nerijus Rusteika. "Compact 20 W femtosecond laser system based on fiber laser seeder, Yb: YAG rod amplifier and chirped volume Bragg grating compressor." *Optics express* 26, no. 24 (2018): 31873-31879.

12. Yang, Peilong, Teng Hao, Zhongqi Hu, Shaobo Fang, Junli Wang, Jiangfeng Zhu, and Zhiyi Wei. "Highly stable Yb-fiber laser amplifier of delivering 32-μJ, 153-fs pulses at 1-MHz repetition rate." *Applied Physics B* 124 (2018): 1-6.

13. Röser, F., J. Rothhard, B. Ortac, A. Liem, O. Schmidt, T. Schreiber, J. Limpert, and Andreas Tünnermann. "131? W220? fs fiber laser system." *Optics Letters* 30, no. 20 (2005): 2754-2756.

14. Zhao, Zhigang, and Yohei Kobayashi. "Ytterbium fiber-based, 270 fs, 100 W chirped pulse amplification laser system with 1 MHz repetition rate." *Applied Physics Express* 9, no. 1 (2015): 012701.

15. Manchee, C. P. K., J. Möller, and R. J. D. Miller. "Highly stable, 100 W average power from fiber-based ultrafast laser system at 1030 nm based on single-pass photonic-crystal rod amplifier." *Optics Communications* 437 (2019): 6-10.

16. Thulasi, S., and S. Sivabalan. "High power chirped pulse Yb fiber amplifier seeded by mode-locked fiber laser oscillator with multimode interference based saturable absorber." *Optics & Laser Technology* 157 (2023): 108626.

17. Forget, Nicolas, Vincent Crozatier, and Pierre Tournois. "Transmission Bragg-grating grisms for pulse compression." *Applied Physics B* 109, no. 1 (2012): 121-125.

18. Treacy, Edmond. "Optical pulse compression with diffraction gratings." *IEEE Journal of quantum Electronics* 5, no. 9 (1969): 454-458.

Chapter: 07

Future outlooks

The whole work contributes to the following regions:

❖ Area of contribution

- Optical fiber fabrication & characterization
- Q-switched fiber laser with few-microsecond pulse duration
- Mode-locked fiber lasers delivering picosecond duration
- Multipulse state, Harmonic mode-locked state, Chaotic pulse dynamics; characterization and identification
- Features of Dissipative solitons, Dispersion managed solitons, Amplifier similaritons
- Novel pulse dynamics of Noise-like pulse state
- Novel architecture of all-fiber Mamyshev oscillator
- Ultra-short pulse amplification

The outcomes and associated observations of the performed experiments indicate to few directions which can be explored in future. Those possibilities are listed below:

- Although in this work, SESAM based laser has delivered the most stable fundamental mode-locked state, literature suggests that NALM could also be a good option maintaining an all-PM configuration. A long length of fiber is required in our case to obtain enough phase-shift between two counter-propagating electric fields in the amplifying loop. But a non-reciprocal phase-shifter can solve this problem. Its job is to provide an extra amount of phase to both the waves which satisfy the requirement of phase difference in obtaining fundamental mode-locked state.

- A double stage-Lyot filter can be constructed by using two segments of birefringent fiber which do have a large FSR compared to single-stage Lyot filter. A large FSR will solve the problem of interference of spectral

components after the spectral filter. Then stable smoothed spectrum will be attainable from both the output terminals of the laser.

- The output pulse energy from the CPA architecture can be scaled up further by adopting a LMA gain fiber such as rod-type fiber, RE-doped PCFs etc. Recently, LMA PCFs are also being used in CPA set up as the last stage of booster.

Appendix – I

Algorithm of converting time domain signal to DFT spectrogram

---

To perform DFT, the output of the laser is connected to long dispersive medium, in my work I have used commercial optical fiber G.652 of length 10 km. Then the output from it is captured as long pulse train via a high speed photodiode and bandwidth. After that the time signal is rearranged following some mathematical formulation. As the last step the time domain is mapped to wavelength domain to get the final spectrogram.

The spectral resolution depends on the GVD, bandwidth of photodiode and oscilloscope, sampling frequency of the digitizer.

$d\lambda_{Digitizer} = (f * D * Z)^{-1}$;

$d\lambda_{BW} = (B * D * Z)^{-1}$;

$d\lambda_{GVD} = (f * D * Z)^{-1}$;

D is the absolute value of dispersion in ps/nm-km, Z is the fiber length, f is the sampling frequency, B is the bandwidth of photodiode or oscilloscope (whichever has the lowest value). The algorithm is shown below.

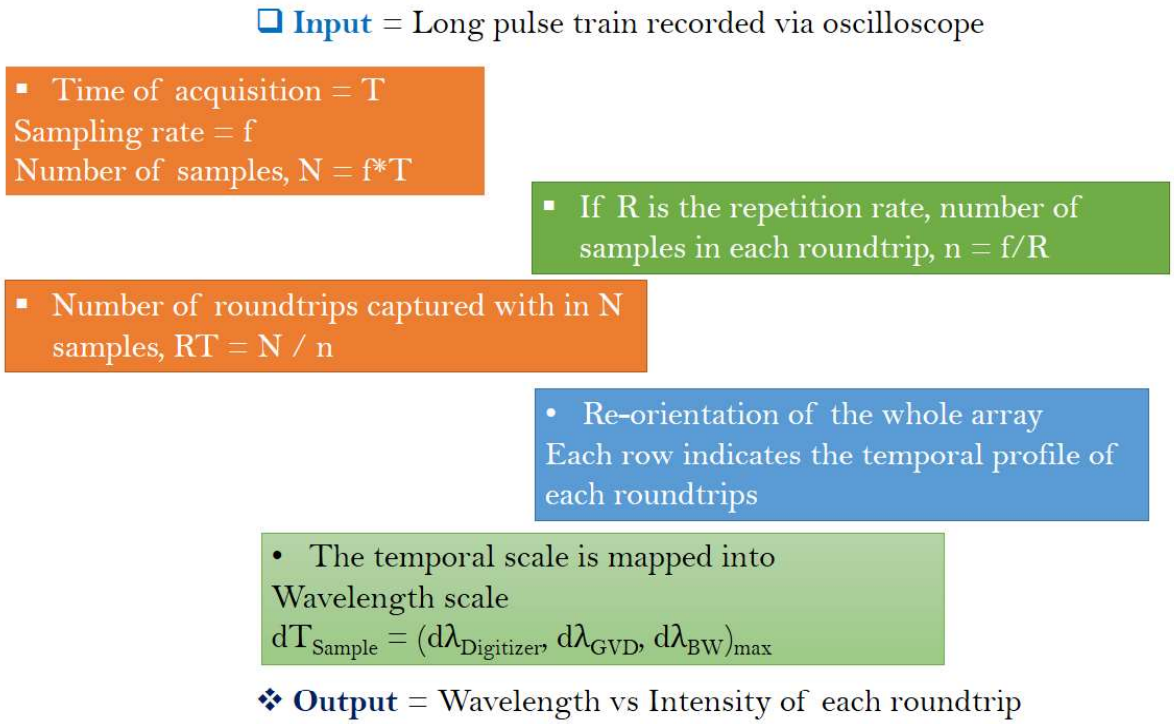

List of Publications

Journal (SCI) Papers:

1. **Uttam Kumar Samanta**, and Mukul Chandra Paul. "Peak-power and width tunable noise-like pulses from a figure-9 cavity with two separate gain segments." *Optik* (2024): 171836.
2. **Uttam Kumar Samanta**, Sourav Das Chowdhury, and Mukul Chandra Paul. "Modelling of a Lyot filter based Mamyshev oscillator." *Optical Fiber Technology* 83 (2024): 103650
3. **Uttam Kumar Samanta**, Sourav Das Chowdhury, and Mukul Ch Paul. "Pump power induced instability and hysteresis in an all-normal dispersion linear mode-locked fiber laser." *Laser Physics* 33, no. 7 (2023): 075101.
4. **Uttam Kumar Samanta**, Sourav Das Chowdhury, and Mukul Chandra Paul. "Generation of stable Q-switched pulses at 1566 nm by using a segment of erbium-doped fiber as saturable absorber." *Laser Physics* 32, no. 8 (2022): 085104.
5. A. Ghosh, H. N. A. Ali, N. Arsad, **U. K. Samanta**, S. Das, A. Dhar, A. H. A. Rosol, M. Yasin, S. W. Harun, and M. C. Paul. "Q-switched pulse generation by stimulated Brillouin scattering assisted four-wave mixing effect in erbium–bismuth co-doped multi-elements silica glass based optical fiber laser." Laser Physics 33, no. 12 (2023): 125103.
6. Shailendra Kr. Singh, **Uttam Kr Samanta**, Anirban Dhar, and Mukul Chandra Paul. "Structural, Morphological, and Optical Properties of Ag-Doped TiO2 Thin-Film over Fiber Optic Substrate for Sensing Applications." *physica status solidi (a)* 218, no. 22 (2021): 2100447.
7. Shailendra Kr. Singh, **Uttam Kr Samanta**, Anirban Dhar, Mrinmay Pal, and Mukul Chandra Paul. "Preparation of Bi-Doped ZnO Thin Film over Optical Fiber and Their Application as Detection of Ethylenediamine in an Aqueous Medium Based on the Evanescent Field Technique." *Physica status solidi (a)* 217, no. 24 (2020): 2000537.

Conference presentations:

1. Poster presentation on **Workshop on recent advances of photonics (WRAP)**, IIIT Allahabad, India, 2023;
2. Poster presentation on **National laser symposium (NLS-32)**, IIT-Kharagpur, India, 2022
3. Poster presentation on **Conference on Optics, Photonics & Quantum Optics (CoPaQ)**, IIT-Roorkee, India, 2022